NASA/CR—2011-217323

Constitutive Soil Properties for Mason Sand and Kennedy Space Center

Michael A. Thomas and Daniel E. Chitty
Applied Research Associates, Inc., Albuquerque, New Mexico

December 2011

NASA STI Program . . . in Profile

Since its founding, NASA has been dedicated to the advancement of aeronautics and space science. The NASA scientific and technical information (STI) program plays a key part in helping NASA maintain this important role.

The NASA STI program operates under the auspices of the Agency Chief Information Officer. It collects, organizes, provides for archiving, and disseminates NASA's STI. The NASA STI program provides access to the NASA Aeronautics and Space Database and its public interface, the NASA Technical Report Server, thus providing one of the largest collections of aeronautical and space science STI in the world. Results are published in both non-NASA channels and by NASA in the NASA STI Report Series, which includes the following report types:

- TECHNICAL PUBLICATION. Reports of completed research or a major significant phase of research that present the results of NASA programs and include extensive data or theoretical analysis. Includes compilations of significant scientific and technical data and information deemed to be of continuing reference value. NASA counterpart of peer-reviewed formal professional papers, but having less stringent limitations on manuscript length and extent of graphic presentations.

- TECHNICAL MEMORANDUM. Scientific and technical findings that are preliminary or of specialized interest, e.g., quick release reports, working papers, and bibliographies that contain minimal annotation. Does not contain extensive analysis.

- CONTRACTOR REPORT. Scientific and technical findings by NASA-sponsored contractors and grantees.

- CONFERENCE PUBLICATION. Collected papers from scientific and technical conferences, symposia, seminars, or other meetings sponsored or co-sponsored by NASA.

- SPECIAL PUBLICATION. Scientific, technical, or historical information from NASA programs, projects, and missions, often concerned with subjects having substantial public interest.

- TECHNICAL TRANSLATION. English-language translations of foreign scientific and technical material pertinent to NASA's mission.

Specialized services also include creating custom thesauri, building customized databases, and organizing and publishing research results.

For more information about the NASA STI program, see the following:

- Access the NASA STI program home page at *http://www.sti.nasa.gov*

- E-mail your question via the Internet to help@sti.nasa.gov

- Fax your question to the NASA STI Help Desk at 443-757-5803

- Phone the NASA STI Help Desk at 443-757-5802

- Write to:
  NASA STI Help Desk
  NASA Center for AeroSpace Information
  7115 Standard Drive
  Hanover, MD 21076-1320

NASA/CR—2011-217323

Constitutive Soil Properties for Mason Sand and Kennedy Space Center

Michael A. Thomas and Daniel E. Chitty
Applied Research Associates, Inc., Albuquerque, New Mexico

National Aeronautics and
Space Administration

Langley Research Center
Hampton, Virginia 23681-2199

Prepared for Langley Research Center
under Contract NNL07AA00B

December 2011

Acknowledgments

Applied Research Associates, Inc (ARA) conducted this soil study under contract to NASA Langley Research Center's (LaRC) prime contractor for engineering support, ATK Space. ATK Space is the Technology Engineering and Aerospace Mission Support (TEAMS) prime contractor. The study was conducted for LaRC's Landing Systems ADP group, charged with evaluating the new Orion launch abort scenario at Kennedy Space Center (KSC). Dr. Edwin Fasanella, LaRC, sponsored the study. ARA developed soil models for LaRC use in modeling an Orion impact on KSC sand and a surrogate test sand, Mason Sand. This report provides constitutive soil properties for landing simulations. The primary author is Michael A. Thomas, with contributions from Daniel E. Chitty, Martin L. Gildea, and Stephen R. Quenneville. All are engineers with ARA.

Available from:

NASA Center for AeroSpace Information
7115 Standard Drive
Hanover, MD 21076-1320
443-757-5802

Abstract

Accurate soil models are required for numerical simulations of land landings for the Orion Crew Exploration Vehicle (CEV). This report provides constitutive material models for two soil conditions at Kennedy Space Center (KSC) and four conditions of Mason Sand. The Mason Sand is the test sand for LaRC's drop tests and swing tests of the Orion. The soil models are based on mechanical and compressive behavior observed during geotechnical laboratory testing of remolded soil samples. The test specimens were reconstituted to measured in situ density and moisture content. Tests included: triaxial compression, hydrostatic compression, and uniaxial strain. A fit to the triaxial test results defines the strength envelope. Hydrostatic and uniaxial tests define the compressibility. The constitutive properties are presented in the format of *LS-DYNA Material Model 5: Soil and Foam*. However, the laboratory test data provided can be used to construct other material models.

The soil models are intended to be specific to the soil conditions they were tested at. The two KSC models represent two conditions at KSC: low density dry sand and high density in-situ moisture sand. The Mason Sand model was tested at four conditions which encompass measured conditions at LaRC's drop test site.

Table of Contents

1 Introduction

Langley Research Center (LaRC) was tasked with modeling the interaction between the Orion spacecraft and soil. The principle site of interest is Kennedy Space Center (KSC). The scenario is a launch abort event where the Orion impacts the sands surrounding the launch pad. LaRC is approximating the KSC sand with Mason Sand, locally available at LaRC. The drop test site is LaRC's gantry facility. An Orion boilerplate was dropped on Mason Sand, the surrogate replacement for KSC sand. LaRC is interested in determining soil factors influence Orion's safety during impact.

This report quantifies soil conditions and provides constitutive soil properties to support LaRC's numerical modeling of Orion boilerplate tests. For this modeling, LaRC is using LS-DYNA, a 3-dimensional finite element software program. Applied Research Associates, Inc. (ARA) performed soil sampling on field visits to each site. The soil samples were shipped to ARA's geotechnical laboratory for a series of laboratory tests. The tests were designed to yield the required constitutive inputs for LS-DYNA's Material Model 5: Soil and Foam.

This document is intended as a stand-alone report. It supplements the 1 Feb 2008 report titled "Constitutive Soil Properties for Cuddeback Lake, CA and Carson Sink, NV." The KSC models replace those from "Constitutive Soil Properties for Unwashed Sand and Kennedy Space Center" dated 13 May 2008. Comparisons between the new and old models are made throughout the report.

2 LS-DYNA Material Model 5 Description

LS-DYNA Material Model 5 was identified by LaRC for modeling the soils in preliminary calculations. The constitutive properties derived in this report are tailored for constructing this type of model. This section describes the physical meaning of each of the model inputs. Section 3 addresses how each of the model inputs were obtained from material testing.

Because soil strength is pressure dependent, a pressure dependent material model is necessary for constitutive modeling. In LS-DYNA, Material Model 5: Soil and Foam is the most basic of the pressure dependent strength models available. It is also the oldest LS-DYNA pressure dependent model and therefore has accumulated a considerable amount of user experience and feedback. As a result, the model is quite robust given its simple inputs.

Defining the model requires shear and unloading bulk moduli, three coefficients that define the quadratic shear failure surface, a pressure cutoff value that defines the maximum tension allowed, and 10 points on a pressure-volume strain curve to define compressibility. Table 2-1 defines these inputs. Based on LaRC preference for their numerical modeling, the material model inputs are provided in pounds and inches.

The elastic shear modulus, *G*, describes shear deformation when the soil is initially loaded. The bulk unloading modulus, BULK, describes the expansion of the soil when the load is reduced. These two parameters are necessary because the loading and unloading behavior of soil is not equal due to permanent deformations.

The a_0, a_1, and a_2 inputs define a quadratic fit to a strength curve. The strength curve is defined as a yield surface plotted in J_2' versus pressure space. Pressure is the mean stress, the average of all the principle stresses on the material. Pressure is positive in compression. J_2' is the second invariant of the stress deviator. Material tests define points on the yield surface, and the quadratic fit is LS-DYNA's approximation of material strength. In the LS-DYNA manual, the second invariant of the stress deviator is denoted J_2. In this report, the more common notation, J_2', is used to represent the same quantity.

Volumetric strain behavior is defined by the natural log of the relative volume and is negative in compression. Relative volume is the ratio of the current soil cell volume to the initial volume at the start of the calculation. The volumetric strain is represented as a 10 point curve in pressure versus volume strain space. Each point on the curve is obtained from material testing at the given pressure.

The LS-DYNA Theory Manual describes Material Model 5 in more detail. Appendix A contains excerpts from the manual.

Table 2-1. LS-DYNA Material Model 5 Inputs.

Input	Obtained from soil test:	Description
MID	N/A	LS-DYNA's material identification number. A unique number identifying an input set of material properties. A number must be assigned.
RO	Nuclear density field test	Mass density. Obtained from dividing weight density (mass/unit volume) by gravity.
G	Uniaxial strain	Elastic shear modulus. The slope of the shear stress vs. shear strain curve. Can be computed from constrained modulus and Poisson's ratio from a uniaxial test.
BULK	Hydrostatic compression	Unloading bulk modulus. It is the slope of the mean stress vs. strain curve when the pressure is reduced (unloaded) from a higher pressure load. Can also be obtained from uniaxial strain unloading.
A0	Triaxial compression	A quadratic fit coefficient. In a J_2' vs. p (second invariant of stress difference vs. pressure) plot, a_0 represents the intersection of the shear failure envelope's (or yield surface) quadratic fit and the J_2' axis. a_0 coefficient is the Y-intercept. The J_2' vs. p plot is derived from stress difference vs. normal stress.
A1	Triaxial compression	a_1 is a quadratic fit coefficient. It is the initial slope coefficient of the shear failure envelope's quadratic fit.
A2	Triaxial compression	a_2 is a quadratic fit coefficient. It is the curvature coefficient of the shear failure envelope's quadratic fit.
PC	Triaxial compression	"Pressure cut-off." Maximum tension stress allowed, representing tensile fracture. It is the mean stress intercept of the shear failure envelope.
VCR	This is a flag variable. VCR=0	VCR=0 turns on volumetric crushing, defined by the 10 points on the pressure-volume curve. VCR=1 turns off. The pressure-volume curve defines the deformation of the material at 10 pressures.
REF	This is a flag variable. REF=0	This option controls the use of reference geometry to initialize the pressure. REF=0 is recommended. This option does not initialize the deviatoric stress state.
EPS1, P1	EPS1=0, P1=0	This is the first point on the pressure volume curve; at zero loading there is zero volume change. EPS is the natural logarithmic volume strain = (ln [1 - ε_{volume}]), where ε_{volume} = (initial volume – current volume)/initial volume
EPS2, P2	Uniaxial strain	2nd pressure-volume point
EPS3, P3	Uniaxial strain	3rd pressure-volume point
EPS4, P4	Uniaxial strain	4th pressure-volume point
EPS5, P5	Uniaxial strain	5th pressure-volume point
EPS6, P6	Uniaxial strain	6th pressure-volume point
EPS7, P7	Uniaxial strain	7th pressure-volume point
EPS8, P8	Uniaxial strain	8th pressure-volume point
EPS9, P9	Uniaxial strain	9th pressure-volume point
EPS10, P10	Uniaxial strain	10th pressure-volume point

3 Methodology for Obtaining Constitutive Soil Properties

This section describes the methodology for deriving LS-DYNA material model inputs from laboratory test data.

3.1 Geotechnical Laboratory Tests

ARA operates a specialized geotechnical laboratory in South Royalton, VT where the soil samples were shipped for testing. The types of tests conducted for this effort are listed and explained below:

- Grain density
- Grain size distribution
- Moisture content
- Hydrostatic compression
- Uniaxial strain
- Triaxial compression

The Atterberg limits test does not apply here because the soils are sands.

3.1.1 Grain Density

A given volume of soil is comprised of solid particles and void space. The grain density (ρ_g) of a soil is the density of the solid particles. Knowing the grain density of a soil allows one to perform accurate saturation and void volume calculations. Soils typically have a grain density of 2.7 +/- 0.1 g/cm^3. Although not specifically used in constitutive modeling, the grain density is a basic piece of information useful for characterizing the soil as a whole.

The grain density is measured according to the procedures defined by ASTM D854-83. This test is performed using a pycnometer, a special-purpose glass flask with a drilled ground glass stopper that allows it to be filled with the same volume of water with density ρ_w. First, the weight of a 100-ml pycnometer is determined. Second, the pycnometer is filled with distilled, de-aired water to its fill point and re-weighed, (m_a). Then, the water is dumped, and an oven dried soil sample is placed in the dried pycnometer and weighed to determine the mass of the oven-dried sand sample (m_o). Distilled, de-aired water is added to the pycnometer again to slightly above the soil sample. The air entrapped in the sample soil is removed by vacuum. More de-aired, distilled water is added to the pycnometer until reaching the same fill point, and the mass of pycnometer, soil, and water (m_b) is recorded. Finally, the grain density of the soil is computed, including temperature corrections, which are not shown, by the following:

$$\rho_g = \frac{\rho_w m_0}{\left[m_0 + \left(m_a - m_b\right)\right]}$$ **Equation 3-1**

3.1.2 Grain size distribution

A given soil contains a variety of particle sizes. The relative proportions of all particle sizes is captured by defining grain size distribution. The distribution is a good indicator of general soil behavior. A soil with mostly fine grains will have poor drainage, retain water for long periods of time, exhibit cohesive strength, and have very low shear strengths at high moisture contents. The low shear strength in fine grained soils is due to pore pressures building up during loading because of the poor drainage. This pore pressure reduces the effective shear stress, carried by grain-to-grain contact in the soil. Grain size distribution is also essential in recommending surrogate soils to replace a soil of interest. Soils with similar grain size distributions tend to have similar behavior. The grain size distribution is not specifically used in LS-DYNA, but it offers great insight into what the soil is comprised of, and how it will behave with varying moisture levels.

Wet or dry sieve analysis can be used to obtain grain size distribution, also a basic test. Dry grain size distribution tests on soils are performed with the material in the oven-dried condition. The sample is broken up and shaken through a stack of sieves that are graduated from coarse at the top to fine at the bottom. The material retained on each sieve is then weighed, and the results are presented in terms of the percent passing (or percent finer than) each sieve size as a function of the logarithm of the grain size. The sieves used for this characterization effort were US standard meshes of No. 5, 10, 20, 30, 40, 70, 100, 140, and 200. Wet sieving flushes the soil with water, further breaking up cohesive particles that would otherwise not pass through a sieve. Once flushed, the retained soil is dried and weighed. Dry sieving is less reliable because cohesive blocks of soil grains can distort the distribution. However, wet sieving is much more time consuming because the retained soil must be completely dried.

3.1.3 Moisture content

The moisture content of a soil is another basic test and key property. It is the gravimetric ratio of water to dry soil material. Although not a direct input to LS-DYNA's Material Model 5, water plays an important role in soil strength and knowing the moisture content in conjunction with grain density allows one to compute saturation and air void volumes in the soil. Soils have an optimum moisture content, at which soil strength is maximized. Any moisture content lower or above this optimum value will reduce the soil strength. At lower values, removing water also removes some cohesion strength. At higher values, the extra water causes pore pressures to build up in the soil, reducing its effective strength. Approximate moisture content (w%) can be obtained through field testing with a nuclear density gage, and verified through laboratory testing. Laboratory testing to obtain moisture content is performed by first weighing a set of soil samples. Then the samples are oven dried and weighed again to measure the difference caused by the loss of water. The difference in weight is m_w. The oven dried weight is m_s. Individual moisture content is calculated for each sample, and the results are averaged. The formula for calculating water content is:

$$w\% = \frac{m_w}{m_s} \qquad \textbf{Equation 3-2}$$

3.1.4 Triaxial compression

The results of triaxial compression tests are used to define the strength envelope, or yield surface as it's referred to in LS-DYNA, of the soil. The following paragraphs describe the triaxial testing machine, how the sample is tested, and how the coefficients of the shear failure surface, a_0, a_1, and a_2 are derived from laboratory test data.

3.1.4.1. Triaxial test apparatus

All of the mechanical property tests were performed in a triaxial compression test apparatus, which is illustrated schematically in Figure 3-1. For each test, a cylindrical specimen of soil is first prepared inside a fluid-tight membrane to prevent infiltration of the confining fluid (air). In the triaxial apparatus, it is possible to apply two independently controlled components of load to the test specimen, as appropriate to each individual test. Pressurized fluid (air) in the vessel is used to impose a hydrostatic stress, simulating the effect of adjacent soil in the field. The other component of load is derived from a piston, which extends through a seal in the top of the pressure vessel, loading the cylindrical specimen in the axial direction. Electronic instrumentation is used to measure both the applied loads and the resulting deformations of the soil specimens. The following paragraphs describe in more detail how the test specimens were prepared, instrumented, and tested.

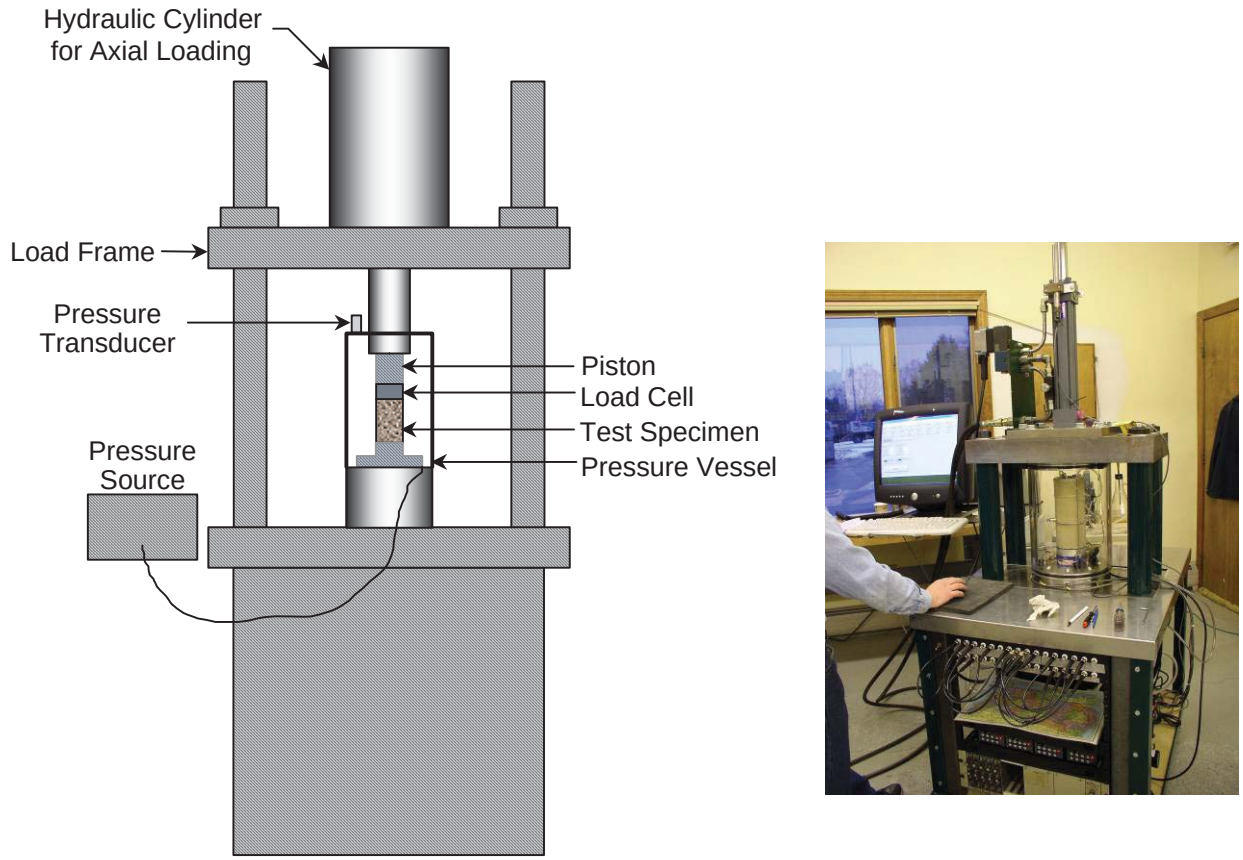

Figure 3-1: Schematic and photograph of a triaxial compression test apparatus.

3.1.4.2. Soil specimen preparation

The first step in the test process is to pack the soil to the measured field density inside the latex rubber membrane that separates the specimen material from the confining fluid. The membrane lines the inside of a steel cylinder mold, which can be removed by splitting in half. The soil is placed in the mold in measured lifts and compacted to the field density. The soil sample reconstitution is described in more detail in the individual material chapters. Once the mold is filled, the top cap is installed in the same manner as the bottom cap, and final measurements of the specimen dimensions and mass are made. The sample is then placed in the triaxial apparatus. Figure 3-2 illustrates how the membranes are sealed on each end to hardened steel endcaps through which the axial load was applied. The membrane was then sealed to the bottom cap using sealant and O-rings. Figure 3-3 is a "ready to test" photograph.

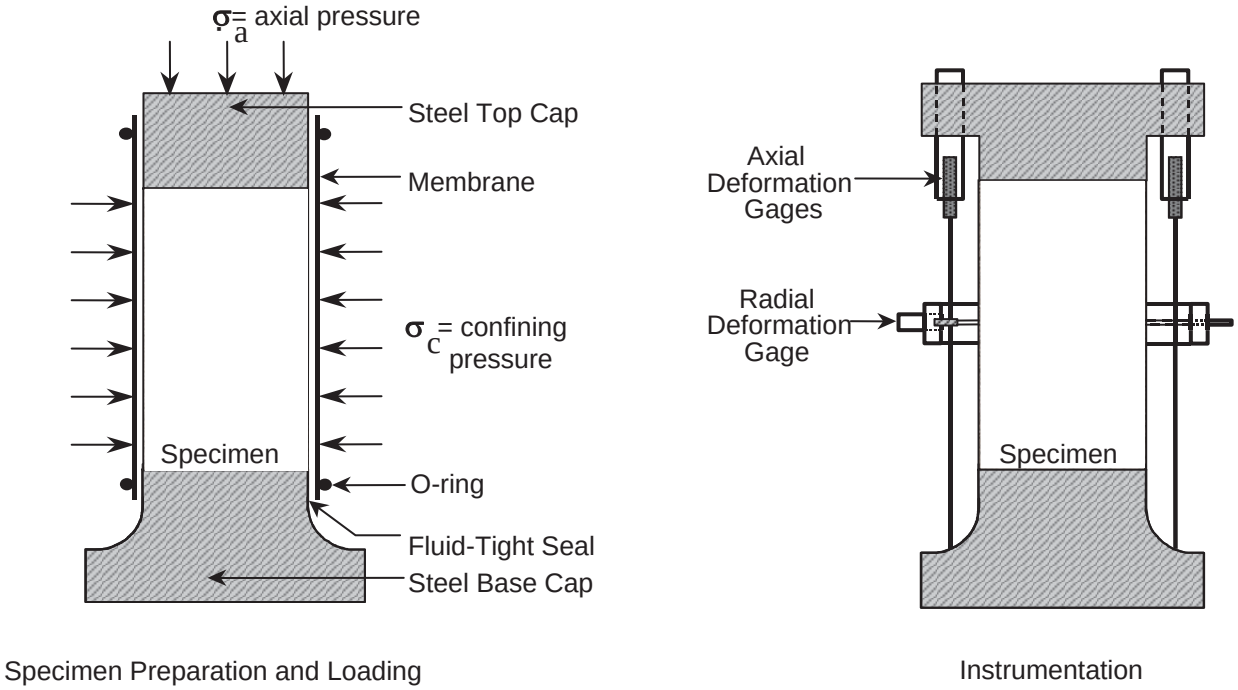

Figure 3-2: Schematic of an instrumented soil specimen.

Figure 3-3: Specimen photo.

Electronic instruments were used to monitor the applied loads and specimen responses during the tests. Three linear variable differential transformer (LVDT) type displacement transducers were installed as illustrated in Figure 3-2 to provide measurements of specimen deformations under load. A pressure transducer was used to monitor the confining pressure, which is equal to the radial stress on the on the specimen, and a load cell measured the axial load. The load cell was located inside the pressure vessel to eliminate errors that would result from seal friction if it were outside the vessel. The necessary corrections were made to eliminate the effects of confining pressure on the load cell output. All of the instruments were calibrated against standards traceable to the National Institute of Standards Technology (NIST) and adjusted to provide the necessary measurement resolution over the expected range of each test. A microcomputer based digital data acquisition system was used to record the transducer output at equally-spaced discrete intervals in time.

3.1.4.3. Deriving constitutive parameters from triaxial test results

In the triaxial compression, or strength test, the specimen is loaded hydrostatically to a pre-selected confining pressure. The confining pressure is then held constant while a compressive axial strain is imposed. The imposed axial strain induces an increment of axial stress above the confining pressure level, and that stress difference results in shear stresses on all planes except the principal directions parallel and perpendicular to the specimen axis. The shear strength of

earth materials is strongly dependent on the normal stress level. By performing strength tests at a range of confining pressure levels, the strength envelope (yield surface) of the material can be defined. The measured specimen deformations provide additional information on the material's volumetric response to shear loading. For this effort, confining pressures of 2, 5, 10, 20, and 50 psi were selected. Each test corresponds to a point on the strength (yield surface) curve, and the maximum shear stresses achieved at these pressures define the strength of the materials over the stress range of interest. The lower confining pressures simulate the near surface soil conditions.

Two components of load are measured in the triaxial compression test. The measured confining pressure is equal to the radial stress on the specimen. Force is also measured in the axial direction, from which the axial stress is determined. The strength data in this report are presented in terms of true axial stress, σ_a. True axial stress is computed at each evenly spaced time interval. It is defined as the total axial load divided by the current cross sectional area of the specimen as derived from the radial deformation measurement. True stress difference, σ_Δ, is the difference between the true axial stress and the confining pressure. Because the confining pressure is always applied to the current area, it is naturally a measure of true radial stress, σ_c. For presentation of strength results, the true stress difference is plotted against true mean stress, $\bar{\sigma}$, which is the average of the stresses in three perpendicular directions. True mean stress is equal to pressure p in LS-DYNA, as explained in the following derivation. The triaxial test outputs are:

$$\sigma_\Delta = \sigma_a - \sigma_c = \text{true stress difference} \qquad \textbf{Equation 3-3}$$

$$\bar{\sigma} = (\sigma_a + 2\sigma_c) / 3 = \text{true mean stress} \qquad \textbf{Equation 3-4}$$

where: σ_a = true axial stress
σ_c = true radial stress = confining pressure
$\bar{\sigma} = p$ = pressure, as explained in the following derivation

To relate the triaxial test data to LS-DYNA's yield surface, one must use Equation 19.5.1 in LS-DYNA's user manual (see Appendix A) to describe the shear failure surface in Material Model 5 format:

$$\frac{1}{2} s_{ij} s_{ij} = a_0 + a_1 p + a_2 p^2 \qquad \textbf{Equation 3-5}$$

LS-DYNA Equation 2.10 specifies s_{ij} as the deviatoric stress tensor defined by:

$$s_{ij} = \sigma_{ij} + (p + q)\delta_{ij} \qquad \textbf{Equation 3-6}$$

Where p is the pressure and q is the bulk viscosity. Because viscosity is not used in Material Model 5, $q = 0$. LS-DYNA Equation 2.11 defines p as:

$$p = -\frac{1}{3}\sigma_{ij}\delta_{ij} = -\frac{1}{3}\sigma_{kk} \qquad \textbf{Equation 3-7}$$

where: σ_{ij} = the stress tensor
δ_{ij} = the Kronecker delta, which is one if the subscripts are the same and zero otherwise

Equation 3-5 and Equation 3-7 are written using indicial notation, in which summation over the repeated subscripts in each term is implied. Thus, *p* is simply the mean (average) of the three diagonal components of the stress tensor, shown in Equation 3-4.

In the special case of the triaxial compression test, the measured stresses are principal stresses and the intermediate principal stress is equal to the minimum principal stress. Specifically, the axial stress, σ_a, is the maximum principal stress and the other two principal stresses are equal to the confining pressure, σ_c. In triaxial testing, one of the most important data outputs is principal stress difference, σ_Δ, given in Equation 3-3. σ_Δ is also referred to as the stress deviator.

Because the stresses measured with respect to the axial and radial directions on the test specimen are principal stresses, the stress tensor expressed relative to those axes has no off-diagonal components, and is given by:

$$\sigma = \begin{bmatrix} \sigma_a & 0 & 0 \\ 0 & \sigma_c & 0 \\ 0 & 0 & \sigma_c \end{bmatrix} \qquad \textbf{Equation 3-8}$$

Returning to Equation 3-6, the expanded version of the stress deviator tensor, *s*, is given by:

$$s = \begin{bmatrix} \sigma_a - p & 0 & 0 \\ 0 & \sigma_c - p & 0 \\ 0 & 0 & \sigma_c - p \end{bmatrix} \qquad \textbf{Equation 3-9}$$

In a triaxial compression test, *p* is given by:

$$p = \frac{\sigma_a + 2\sigma_c}{3} \qquad \textbf{Equation 3-10}$$

and:

$$\sigma_a - p = \frac{3\sigma_a - \sigma_a - 2\sigma_c}{3} = \frac{2(\sigma_a - \sigma_3)}{3} = \frac{2\sigma_\Delta}{3} \qquad \textbf{Equation 3-11}$$

$$\sigma_c - p = \frac{3\sigma_c - \sigma_a - 2\sigma_c}{3} = \frac{\sigma_c - \sigma_a}{3} = \frac{-\sigma_\Delta}{3} \qquad \textbf{Equation 3-12}$$

Thus, Equation 3-9, still for the special case of triaxial compression loading, can be re-written:

$$s = \begin{bmatrix} \frac{2\sigma_\Delta}{3} & 0 & 0 \\ 0 & \frac{-\sigma_\Delta}{3} & 0 \\ 0 & 0 & \frac{-\sigma_\Delta}{3} \end{bmatrix} \qquad \textbf{Equation 3-13}$$

The left hand side (LHS) of Equation 3-5 is the second invariant of the stress deviator tensor, defined as J_2':

$$J_2' = \frac{1}{2} s_{ij} s_{ij} \qquad \textbf{Equation 3-14}$$

When the stress tensor is a diagonal, the indicial notation of Equation 3-14 expands to:

$$J_2' = \frac{1}{2}\left[\left(s_{11}\right)^2 + \left(s_{22}\right)^2 + \left(s_{33}\right)^2 \right] \qquad \textbf{Equation 3-15}$$

Further, for the triaxial compression deviator stress tensor given by Equation 3-13, we have:

$$J_2' = \frac{1}{2}\left(\frac{\sigma_\Delta}{3} \right)^2 \left(2^2 + \left(-1\right)^2 + \left(-1\right)^2 \right) = \frac{\sigma_\Delta^2}{3} \qquad \textbf{Equation 3-16}$$

The foregoing development details the methods for computing J_2' (the LHS of Equation 3-5) and p from the stresses measured in the triaxial compression tests at the strength limit (or elastic limit). Once triaxial data are converted to J_2' and p, one can plot the resulting of values of J_2' against p and perform a quadratic fit to define the required Material Model 5 coefficients, a_0, a_1, and a_2.

An example strength envelope based on triaxial compression tests is presented in terms of mean stress and stress difference in Figure 3-4. Also shown is the linear fit to the triaxial compression test data that corresponds to reasonable values of cohesion and friction angle. To derive the coefficients for input to LS-DYNA, it is necessary to fit the square of the stress difference, as defined by Equation 3-16. The strength data is re-plotted in terms of J_2' versus pressure p, and is shown in Figure 3-5. Material Model 5 uses a quadratic fit to describe this yield surface, given in Equation 3-17.

$$J_2 = 0.490 + 1.386\,p + 0.979\,p^2 \qquad \textbf{Equation 3-17}$$

Therefore, the Material Model 5 strength coefficients are:

$$A0 = 0.490$$
$$A1 = 1.386$$
$$A2 = 0.979$$

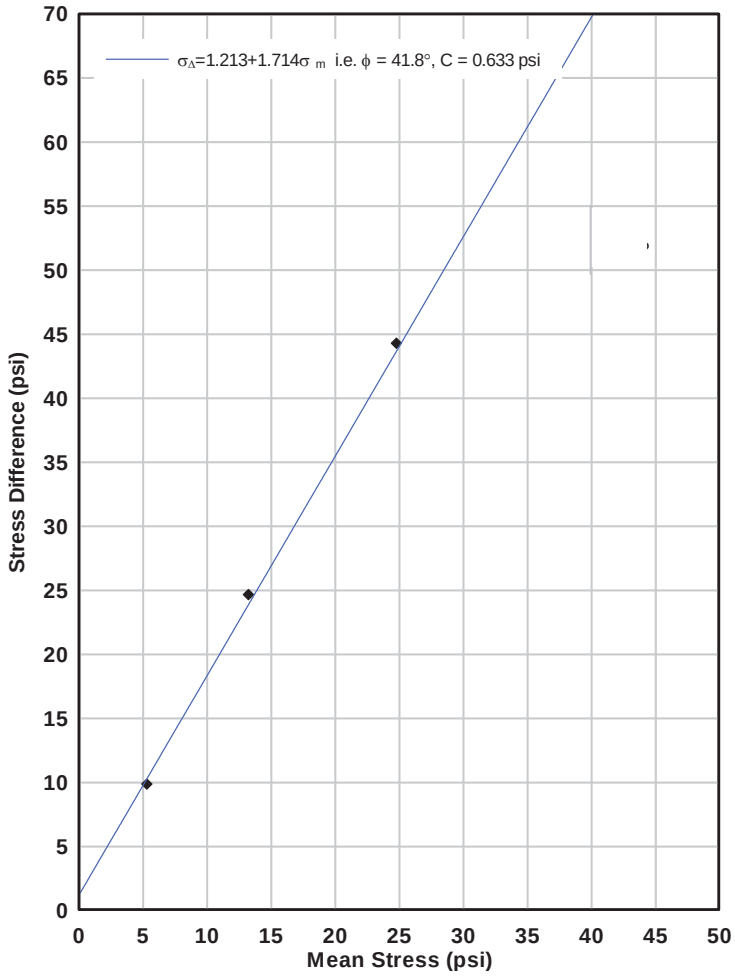

Figure 3-4: Example strength envelope. Black points represent peak strengths from triaxial tests. Blue line is a strength fit.

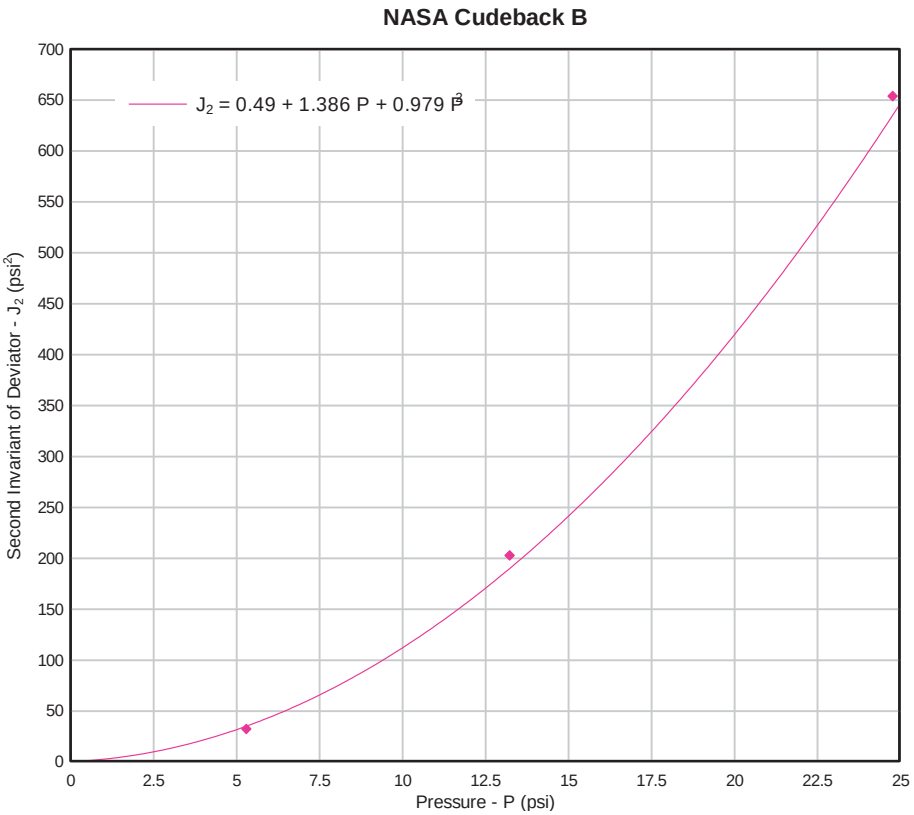

Figure 3-5: Strength envelope in terms of LS-DYNA's yield surface, J_2' vs. *p*. Black points from Figure 3-4 are converted to J_2' and plotted as pink points.

3.1.5 Hydrostatic compression

Hydrostatic compression tests are also conducted using the triaxial device. In the hydrostatic compression test, the cylindrical soil specimens are loaded only by fluid (air) pressure, without any piston loading. The stresses on the specimen are the same in all directions and there is no shear stress on any plane. This is referred to as the hydrostatic state of compression. Material Model 5's pressure *p* is equal to the fluid pressure. The results of these tests are used to define the volumetric deformation behavior of the material for modeling. The stress state is completely defined by the confining pressure. When confining pressure is reduced, the soil expands at a different rate than compression. This expanding rate yields the bulk unload modulus (BULK, see Table 2-1).

In the laboratory, LVDT measurements are used to define axial and radial deformations which, in turn, are used to compute the current volume of the specimen at each time step. The volumetric strain, ε_v, can be computed using the following equation:

$$\varepsilon_v = \frac{V_o - V_d}{V_o}$$ **Equation 3-18**

Where V_d = current (deformed) volume of the specimen
and V_o = initial specimen volume (including grains and void space)

3.1.5.1. Deriving constitutive parameters from hydrostatic compression

The axial and radial specimen strains are recorded as the fluid pressure increases inside the vessel. The recorded data forms a pressure versus volumetric strain curve. The test typically starts with an initial rate of compression, denoted as I in Figure 3-6.

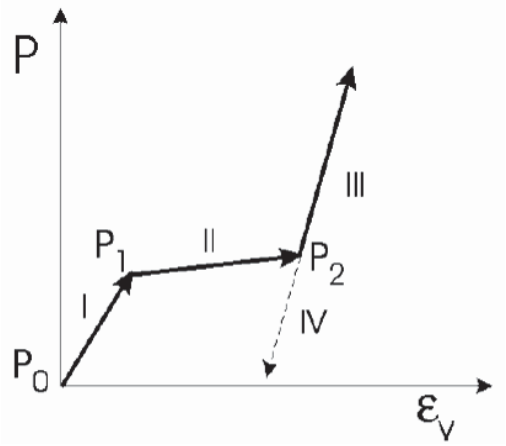

Figure 3-6: Theoretical hydrostatic compression curve. Pressure *p* vs. volumetric strain ε_v. The slope of Segment IV, the unloading portion, corresponds to the bulk unloading modulus. (Figure © Leonard Schwer, LSTC class material)

3.1.6 Uniaxial strain

The uniaxial strain test also utilizes the triaxial device, albeit differently. In a uniaxial strain test, the axial stress and confining pressure are applied in such a way that the specimen undergoes compressive axial strain with no strain in the radial direction. The uniaxial strain loading is accomplished with an automated loading control system using the radial deformation measurement as feedback in the control loop. If the radial strain increases, the confining pressure is increased to return the radial strain to zero. Because no radial strain is allowed in a uniaxial strain test, the axial strain is equal to the volumetric strain in the specimen. There is a difference between axial and radial stress, and hence shear stresses exist in the specimen. However, the uniaxial strain constraint typically prevents the stress state from reaching the strength envelope, and failure of the specimen does not occur. The Material Model 5 shear modulus G and the pressure-volume curve can be derived from uniaxial strain data, as described in the following section.

3.1.6.1. Deriving constitutive parameters from uniaxial strain

The elastic constants to calculate shear modulus G are derived from a uniaxial strain test. First, Poisson's ratio can be obtained from an axial stress versus confining pressure plot, a uniaxial test output. There are two independent components of loading applied, confining pressure and axial load. Other linear combinations of these two independent components can yield other properties. For example, the mean stress and stress difference are invariants of the stress tensor and deviatoric stress tensor, respectively. To assure consistency, two different derivations of Poisson's ratio are presented below. As an aid, example plots are provided.

The first derivation is based on a relationship between axial stress and confining pressure. The elastic Poisson's ratio value can be derived from the initial portion of the axial stress versus confining pressure curve. A fitted line is drawn over the initial curve portion. The inverse slope of the fitted line is commonly called lateral earth pressure, k_0. Poisson's ratio, ν, is related to k_0 by:

$$\nu = \frac{k_0}{1 + k_0} \qquad \textbf{Equation 3-19}$$

Figure 3-7 is an example application of the first method of obtaining ν from uniaxial test results. Commonly, there is a very small region at the beginning of the test where the data look somewhat incoherent because the loading piston is just making contact with the specimen. Usually, uniaxial strain control cannot maintained in this region because of sample "seating," when the loading piston closes the tiny gaps between test hardware contact points. Because it occurs at very low stress only, it is ignored for this analysis. The Poisson ratio ν is derived from the initial linear portion of the test. In Figure 3-7, the initial linear portion reaches 35 psi axial stress. By fitting a line to that region, we find that it has a slope of 4.406. So k_0 = 1/4.406. From Equation 3-19, k_0 = 0.227 and ν = 0.185.

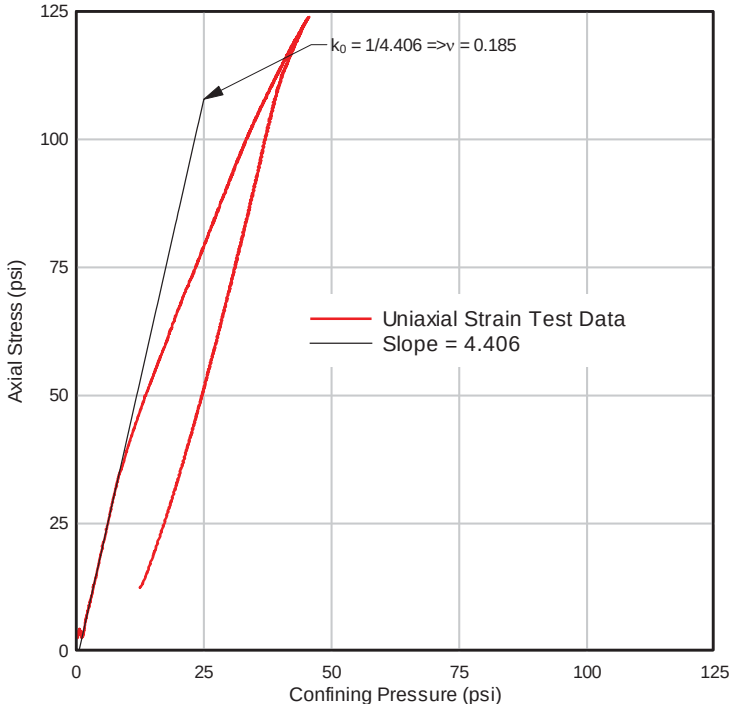

Figure 3-7: Example of axial stress vs. confining pressure plot from uniaxial test.

The second method of deriving ν is to examine the stress path in terms of mean stress and stress difference. Uniaxial test data can be used to plot mean stress versus stress difference, as shown in Figure 3-8. The definitions of mean stress and stress difference are shown in Equation 3-3 and Equation 3-4. The slope of this different curve can also be used to calculate ν.

In Figure 3-8, the slope does not have a commonly used name or symbol. For convenience, call the slope of the line k^*. It is seen that $k^* = 1.598$. Poisson's ratio is related to k^* by:

$$\nu = \frac{3 - k^*}{6 + k^*} \qquad \textbf{Equation 3-20}$$

Thus, ν = 0.185, which agrees with the first derivation.

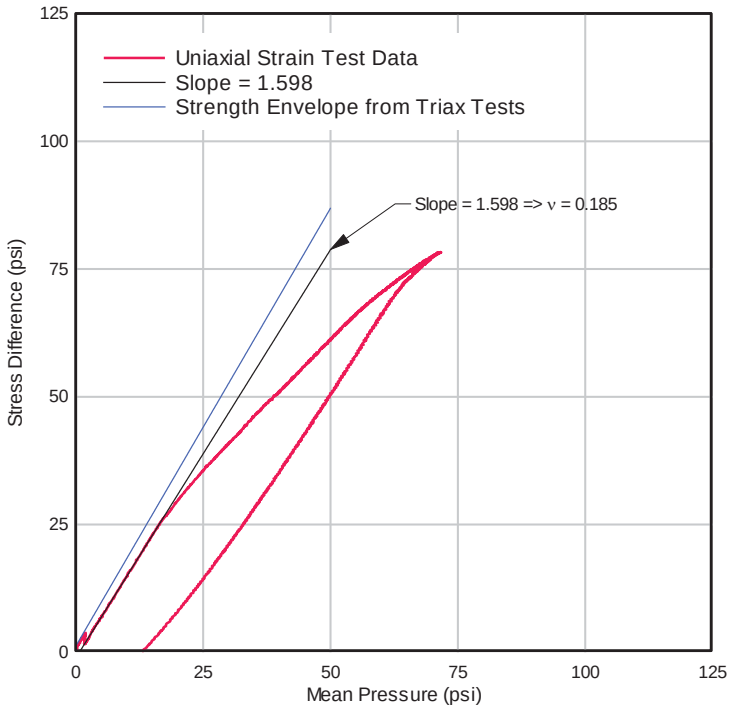

Figure 3-8: Example of stress difference vs. mean stress plot from uniaxial test.

The preceding paragraphs present two approaches to defining Poisson's ratio, which is one elastic constant. It is necessary to have one more elastic constant for a complete set. Consider the stress-strain curves plotted in Figure 3-9. In a uniaxial strain test, the radial strain is constrained to be zero, and the axial strain is the same as the volume strain. In Figure 3-9, axial strain is plotted against both axial stress and mean stress. As with the definition of Poisson's ratio, for the purpose of defining elastic constants, attention is confined to the initial linear regions of the curves. First, consider the axial stress curve in Figure 3-9. The initial slope of the axial stress curve is the constrained modulus, *M*, of the material. It is defined as the ratio of axial stress to axial strain under uniaxial strain conditions. From Figure 3-9, it is seen that M = 6950 psi.

Similarly, the slope of the mean stress-volume strain curve is defined as the bulk *loading* modulus, *K*. Actually, bulk modulus is defined as the ratio of pressure to volumetric strain under hydrostatic loading, but as long as the material behaves elastically, this definition is equivalent. From Figure 3-9, K = 3370 psi. It is of interest to know how these values relate to other elastic constants. Recall that Young's modulus, *E*, is the ratio of axial stress to axial strain under unconfined compression (or tensile) loading. The relations between *E* and the constrained and bulk moduli are:

$$M = \frac{E(1-\nu)}{(1+\nu)(1-2\nu)} \qquad \textbf{Equation 3-21}$$

$$K = \frac{E}{3(1-2\nu)} \qquad \textbf{Equation 3-22}$$

From those two equations, it is straightforward to find the relationship between M and K:

$$\frac{M}{K} = \frac{3(1-\nu)}{(1+\nu)}$$ **Equation 3-23**

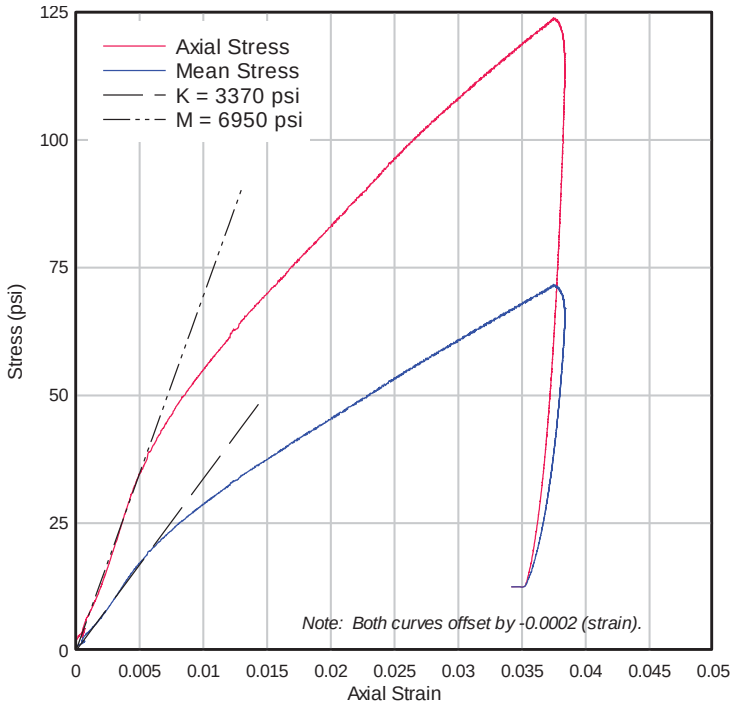

Figure 3-9: Example stress vs. strain curves from uniaxial test.

If the right hand side (RHS) of Equation 3-23 is computed from the values of M and K determined above and the left hand side (LHS) is computed from ν, it is found that both are equal to 2.06. Thus, we have a consistent set of elastic constants. During Material Model 5 input derivation, slight fit adjustments for constrained and bulk moduli were made to ensure Equation 3-23's consistency. The final elastic constant of interest is the shear modulus, G, which is related to E and ν by:

$$G = \frac{E}{2(1+\nu)}$$ **Equation 3-24**

In summary, for the initial linear loading phase, the elastic constants for the example case are:

Table 3-1: Example summary of elastic constants from uniaxial strain testing

Young's Modulus E	6370	psi
Poisson's Ratio ν	0.185	
Shear Modulus G	2690	psi
Bulk Loading Modulus K	3370	psi
Constrained Modulus M	6950	psi

The unload bulk modulus is derived from the same uniaxial strain test data as shown in Figure 3-9. Because bulk modulus is required, attention is restricted to the mean stress vs. volume strain curve. Figure 3-10 is an expanded view of the unload region. As the unloading behavior is not very linear, geotechnical expertise is used to approximate the curve with a single line. The portion shown as a heavy blue line was considered in the linear fit. The resulting value of unload modulus is K_u = 17,000 psi.

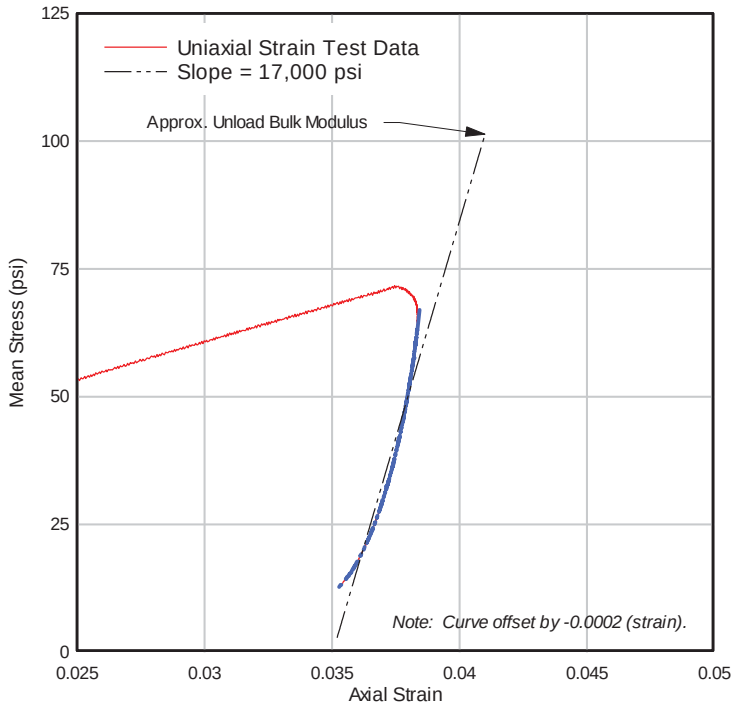

Figure 3-10: Expanded view of the unload region of the uniaxial strain test.

According to the LS-DYNA documentation, the compressibility curve used for Material Mode 5 is defined in terms of logarithmic strain, which is defined as:

$$\varepsilon_{\log} = \ln\left(\frac{V}{V_0}\right) \qquad \textbf{Equation 3-25}$$

where: V = current volume
V_0 = initial unstressed volume

Because there is no radial strain in the uniaxial strain test, the cross sectional area remains constant and the logarithmic strain can be computed from the initial length and change in length of the specimen as:

$$\varepsilon_{\log} = \ln\left(\frac{L_0 - \Delta L}{L_0}\right) \qquad \textbf{Equation 3-26}$$

where: L_0 = initial specimen length
ΔL = change in length (positive in compression)

The logarithmic strain is negative in compression. The pressure-logarithmic strain curve from the uniaxial strain test is presented in Figure 3-11 along with the ten-point idealization for input to LS-DYNA. The tabulated points are:

Table 3-2: Example pressure-volume points from uniaxial strain test.

Pressure (psi)	Logarithmic Strain
0	0.0000
16.39	-0.0050
18.24	-0.0056
20.44	-0.0064
22.48	-0.0072
24.31	-0.0080
28.42	-0.0100
36.81	-0.0149
52.42	-0.0250
70.6	-0.0378

The ten points are chosen in such a way to best characterize the shape of the compressibility curve.

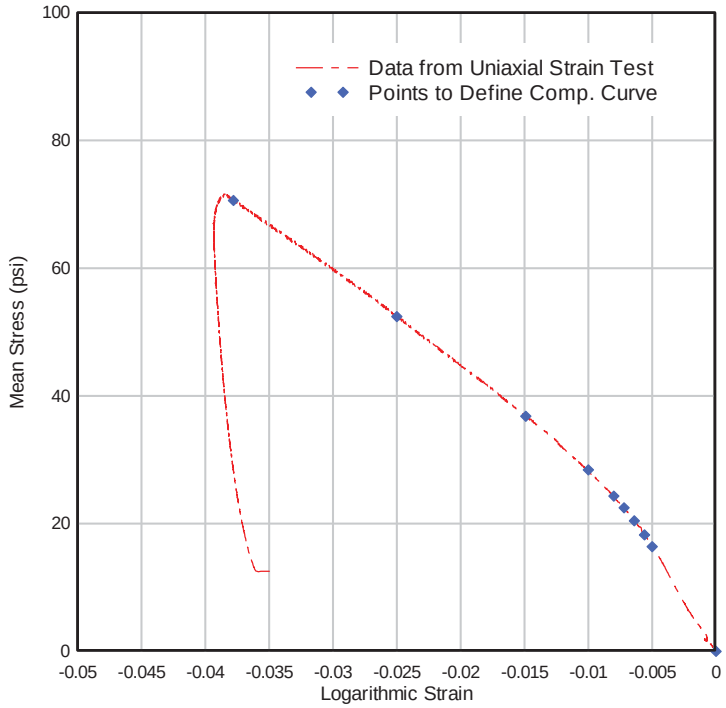

Figure 3-11: Example of ten points on the pressure-volume compressibility curve in terms of logarithmic strain.

4 KSC Low Density Dry Sand

The general description, field observations, test data, and Material Model 5 inputs for KSC Low Density Dry (LDD) Sand is discussed in this chapter. KSC LDD Sand comprises the soft shoreline near the beach dunes. It is above the waterline and almost completely dry. It is a fine sand deposited under low density conditions, making it the weakest and most compressible KSC sand.

4.1 Location

KSC lies on a sand bar deposit from the Eocene era (Ref. 9). Most of the surface sands were deposited within the last 7000 years, making all sands closely related in terms of origin. The sands near the KSC Pads have common parent material constituents and similar grain size distributions. Figure 4-1 is an aerial view of Launch Pads 39A and 39B.

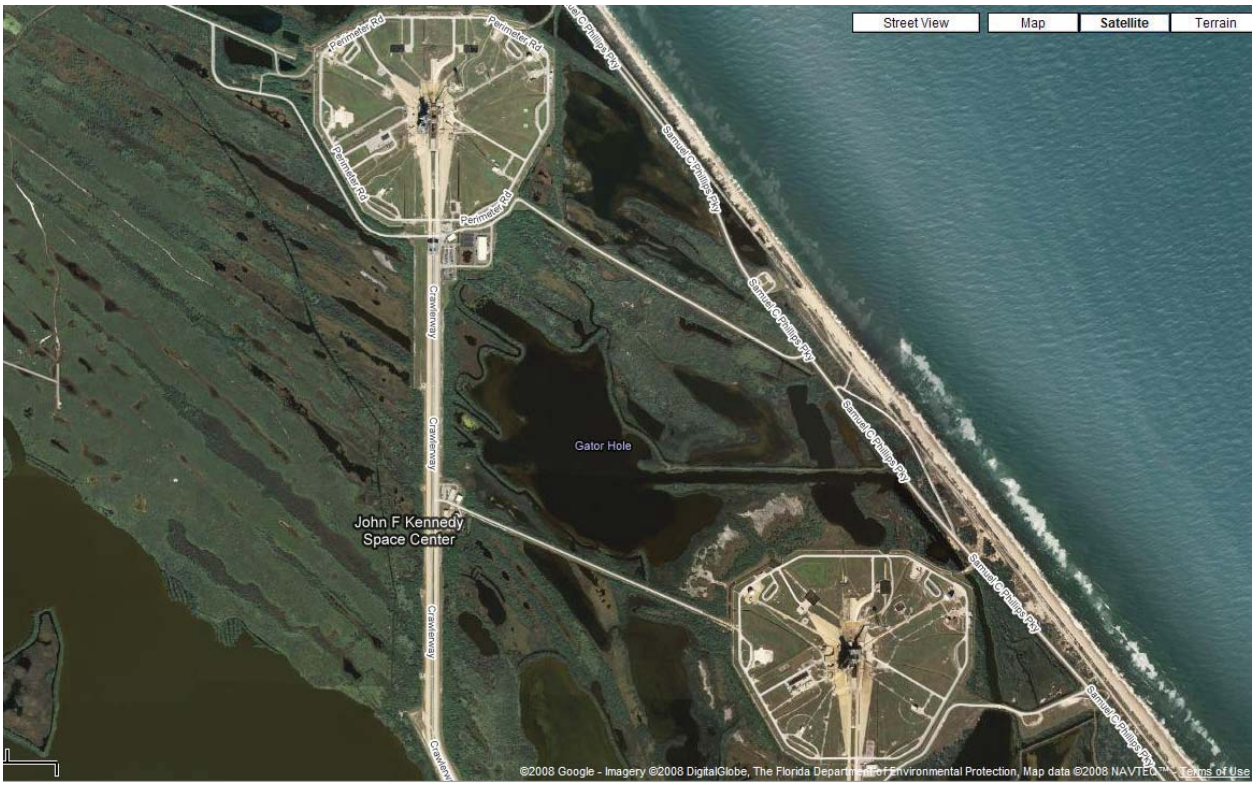

Figure 4-1: Aerial view of Kennedy Space Center. Pad A is the southernmost. Pad B is the northernmost (top of figure)

KSC LDD Sand lies along the coastal dunes. The KSC LDD Sand can reasonably represent any KSC sand deposit that falls under these conditions: fine sand, ~80 lbs/ft^3 surface density and < 5% moisture content. Figure 4-2 displays a soil map and sands under similar conditions.

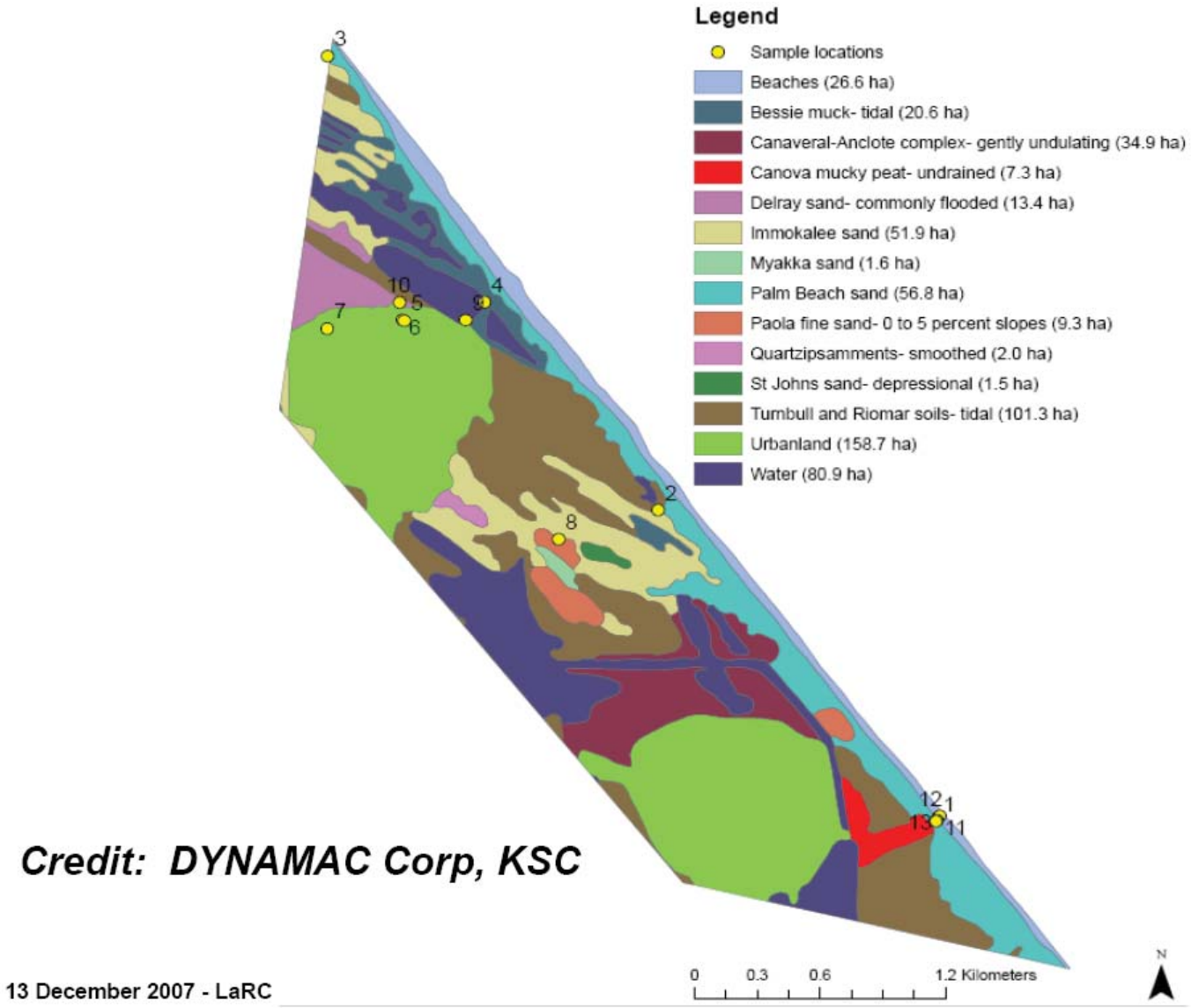

Figure 4-2: KSC soil map, sourced from Dynamac (Ref. 9). "Palm Beach Sand" was the sampling source for KSC Low Density Dry Sand. Immokalee and Paola sand also fall under similar conditions. The areas labeled urbanland are Pads 39 A and B.

4.2 General description

KSC LDD Sand was the softest soil observed at KSC. It is a fine sand deposited by wind and ocean movements thousands of years. The sand type was observed to remain consistent to a depth of 30 inches. It is highly likely that the sand is uniform with depth across the entire KSC coastline. A small portion of the sand attributes its source to organic particle accumulation. The surf zone sand, KSC High Density Flooded Sand, contains higher organic particle content, such

as shell fragments. The natural methods of deposition add very little compaction to the soil. As a result, the soil surface deforms several percent strain when loaded with even small pressures. This is because LDD sand is cohesionless and very dependent upon confining pressure for strength. The sand's ability to highly compress is due to the granular nature of sand when it is very dry. In the lack of moisture, there is no cohesive force to resist shear stress, and without significant confining pressure, the low density soil responds by compressing to a stronger density to support load.

Most coastal terrain had less than a 5% slope except for the dunes. LDD sand's surface is essentially barren of vegetation except for the dunes. Table 4-1 shows Dynamac's field density measurements that were typically sampled up to 3 inches depth. A steel ring is driven to a shallow depth and the soil mass is recovered from inside the ring. Notice the very low field minimum density. This is due to very shallow sampling. The field minimum value of 56.2 lbs/ft^3 appears to be very low, and may not be a realistic minimum value. It is also extremely difficult to handle a specimen below 80 lbs/ft^3, so all KSC LDD Sand tests were conducted at the minimum feasible density (Table 4-2).

Table 4-1: Field density measurements from Dynamac 2000 report (Ref. 9)

KSC coastal sand	Samples N	Field Min	Field Max	Mean
Wet Density (lbs/ft^3)	23	56.2	87.4	74.3

Table 4-2: Absolute density minimum and maximum from ARA laboratory's 4"x8" specimen cylinder mold

	Absolute Lab Min	Absolute Lab Max	Min Feasible for Testing
Wet Density (lbs/ft^3)	64	99	80

Figure 4-3: KSC LDD Sand sampling site (left). Uniformity with depth apparent (right).

4.2.1 Soil classification

KSC Low Density Dry Sand is classified as SP in the Unified Soil Classification System, a poorly graded fine sand. The poor gradation indicates that most particle sizes are about the same. Classification was based on standard sieve analysis.

Table 4-3: KSC Low Density Dry Sand soil classification. Source – Dynamac 2000.

Soil Class	Mean Grain Size (mm)	USCS Class
Coastal (includes KSC Low Density Dry Sand and High Density In Situ w% Sand)	0.31	SP, fine sand

4.3 Laboratory test data

Laboratory tests conducted on KSC LDD Sand are presented in this section. The test log summarizes the tests using the triaxial apparatus.

Table 4-4: Test log for KSC LDD Sand.

Test ID	Sample ID	Type	Confining Pressure (psi)	Moisture content	Wet Density (lbs/ft^3)	Dry Density (lbs/ft^3)	Grain Density G_s (g/cm^3)	Porosity n
M10B08	Pad A	Triax	2	3.05%	80.00	77.51	2.67	53.4%
M10D08	Pad A	Triax	5	3.04%	80.00	77.49	2.67	53.4%
M11E08	Pad A	Triax	10	2.78%	80.00	77.83	2.67	53.3%
M11H08	Pad A	Triax	20	2.78%	80.00	77.83	2.67	53.3%
M12B08	Pad A	Triax	50	2.89%	80.00	77.74	2.67	53.4%
M12I08	Pad A	Uniax	50	2.70%	80.00	77.84	2.67	53.3%
A29C08	Pad A	Uniax	50	3.20%	80.00	77.52	2.67	53.5%
U24D09	Pad A	Triax	75	3.28%	80.00	77.46	2.67	53.5%
U26B09	Pad A	Triax	100	3.06%	80.00	77.62	2.67	53.4%
U29B09	Pad A	Triax	75	2.96%	80.00	77.70	2.67	53.4%
L10A09	Pad A	Uniax	100	3.03%	80.00	77.65	2.67	53.4%

4.3.1 Grain density and grain size analysis

Figure 4-4 displays the dry sieve results for KSC LDD Sand. Dry sieve analysis was provided from the Dynamac report (Reference 9). ARA also performed sieve analysis on samples from the dunes near Pad A. These samples were used to construct specimens for KSC LDD testing. The Pad A samples have fewer course particles than the averaged coastal class sand. The flooded sand samples from the surf zone contain shell fragments, which increase the coarse grain count. From the "percent finer by weight", the coefficient of uniformity (C_u) can be calculated by dividing the 60^{th} percentile diameter by the 10^{th} percentile. Sands with similar C_u have a similar ratio of large particles to small particles. The Pad A samples are a reasonable

representation of the averaged coastal area because of the similar distribution of particle sizes in the fine region.

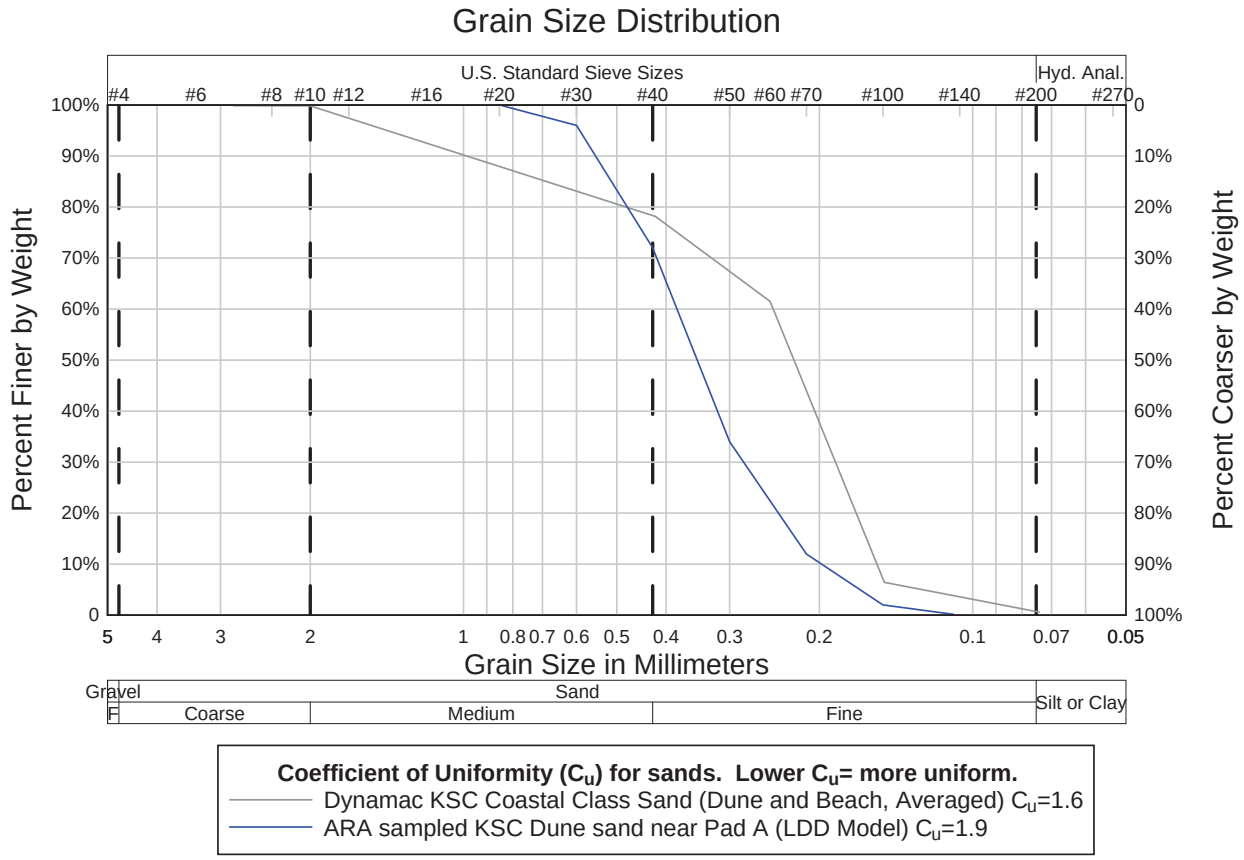

Figure 4-4: KSC LDD Sand grain size distribution and coefficient of uniformity, and comparison with Dynamac average for coastal class sand.

4.3.2 Triaxial compression

The triaxial compression test results for KSC LDD Sand are shown in Figure 4-5 through Figure 4-9. The notable difference between the new and old KSC LDD Sand model is the introduction of cohesion. The old model assumed no cohesion. The new model assumes a very small amount of cohesion, 0.25 psi. This cohesion produces a small intercept coefficient in the linear strength fit in Figure 4-7. The slope coefficient has barely changed in the new model, from 1.230 to 1.222. The failure surface is essentially the same.

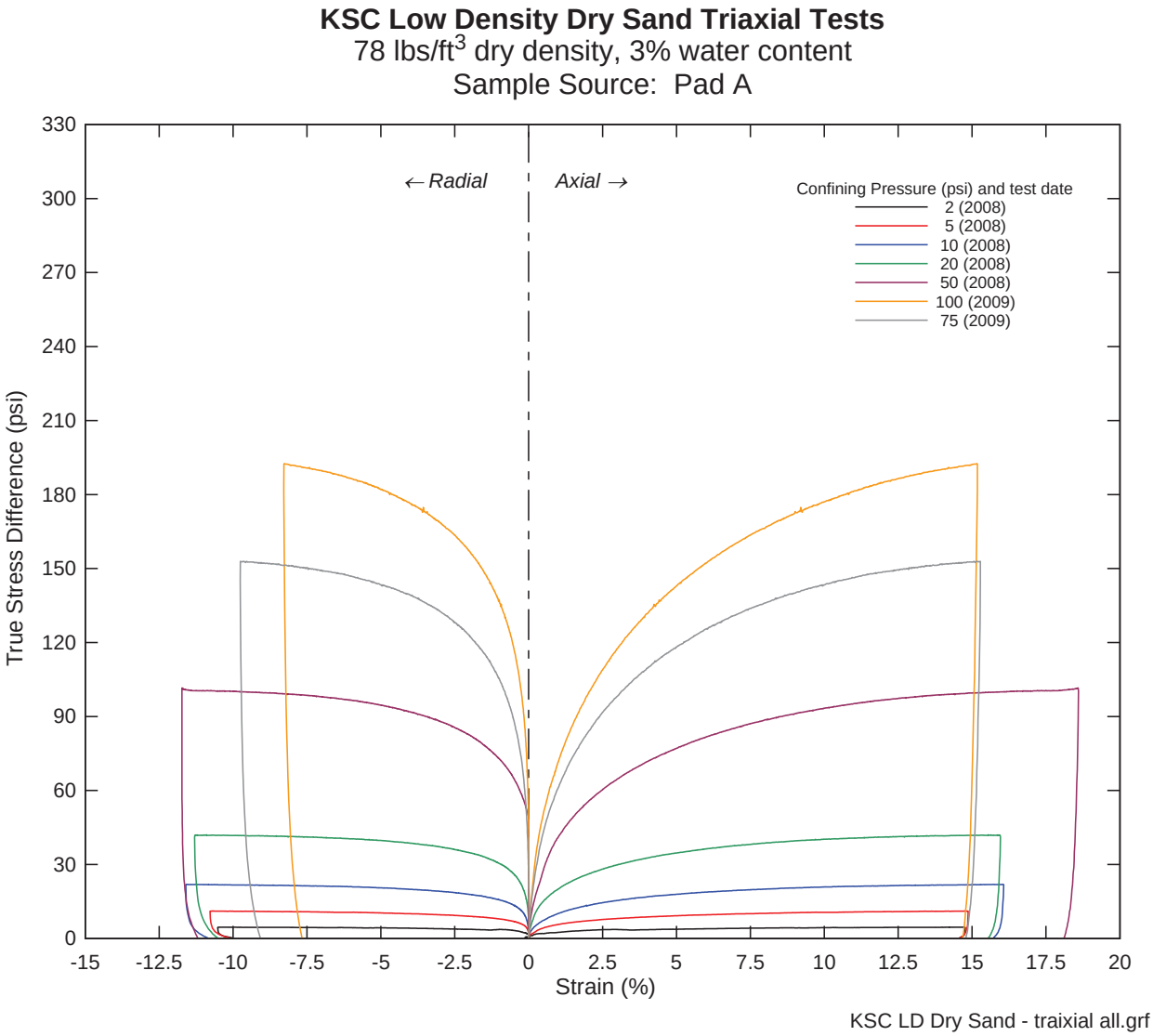

Figure 4-5: KSC LDD Sand triaxial test results.

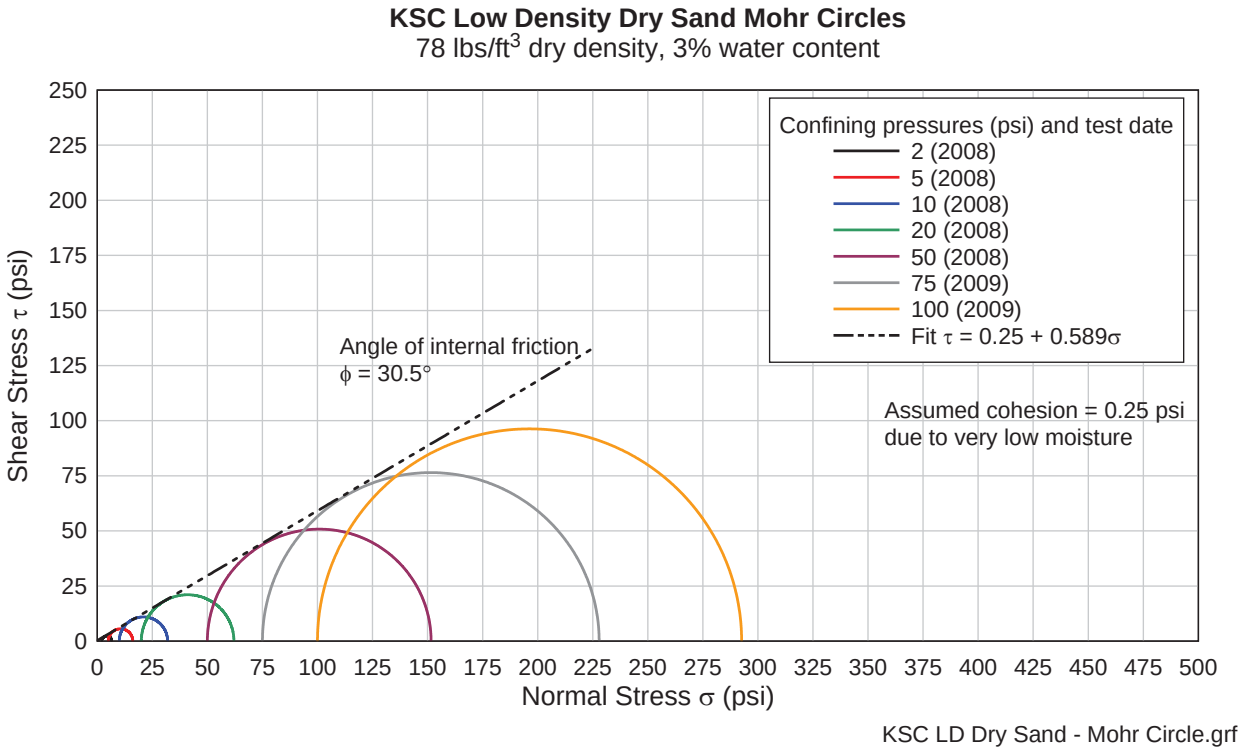

Figure 4-6: Mohr circles based on KSC LDD Sand's triaxial tests

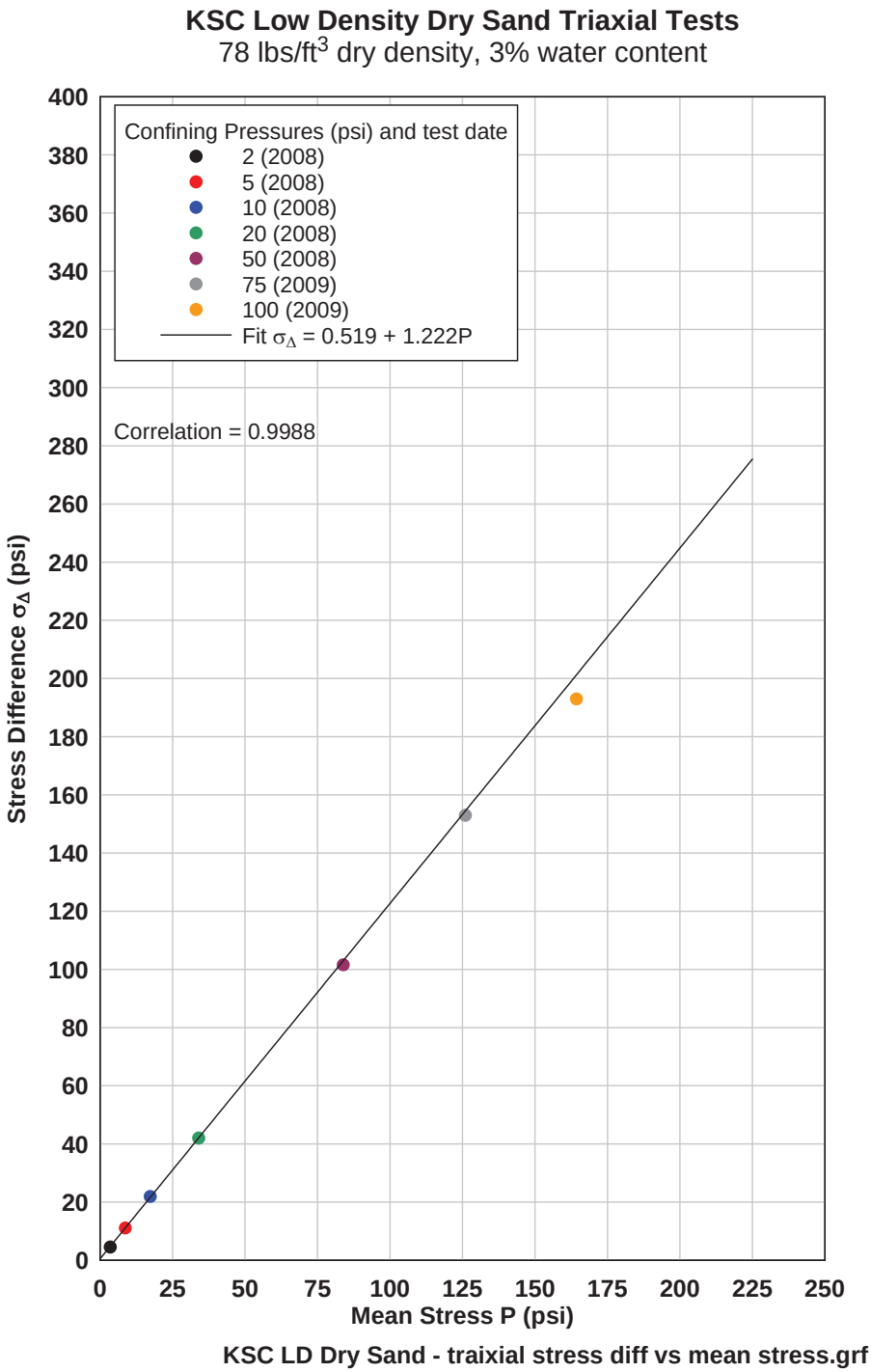

Figure 4-7: KSC LDD Sand's strength envelope from triaxial data.

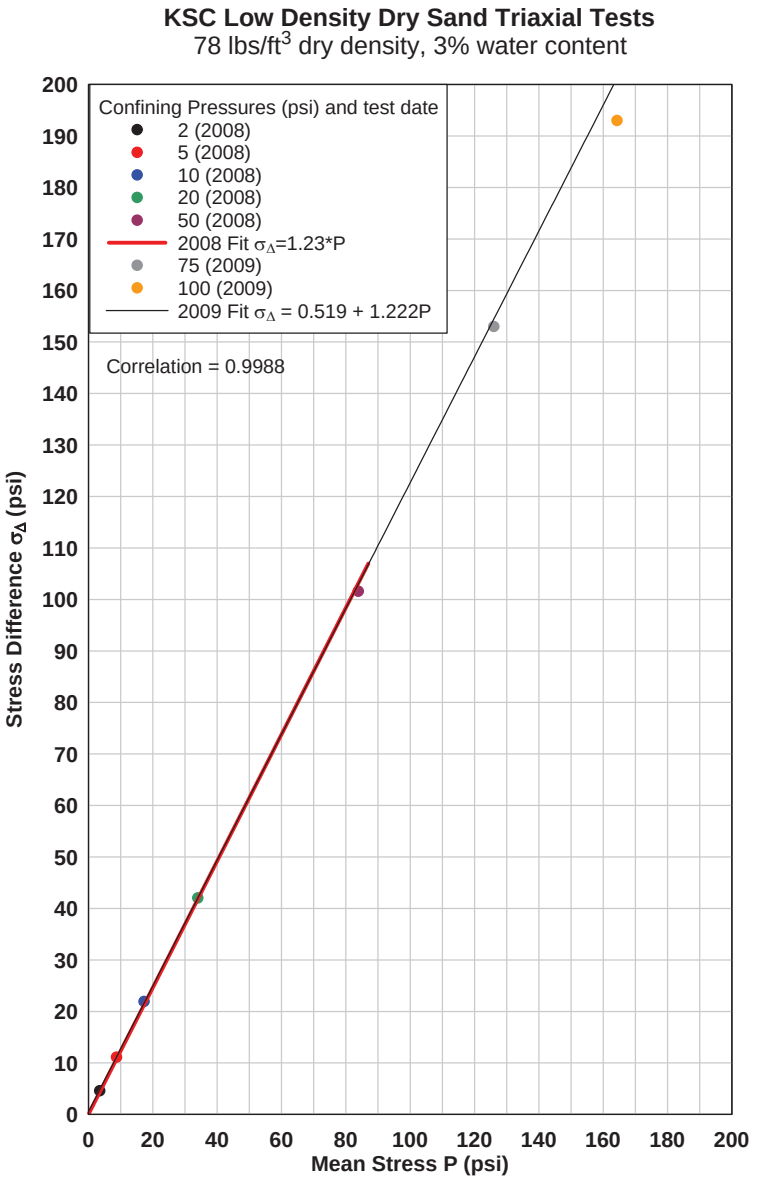

Figure 4-8: Old versus new KSC LDD linear strength fit.

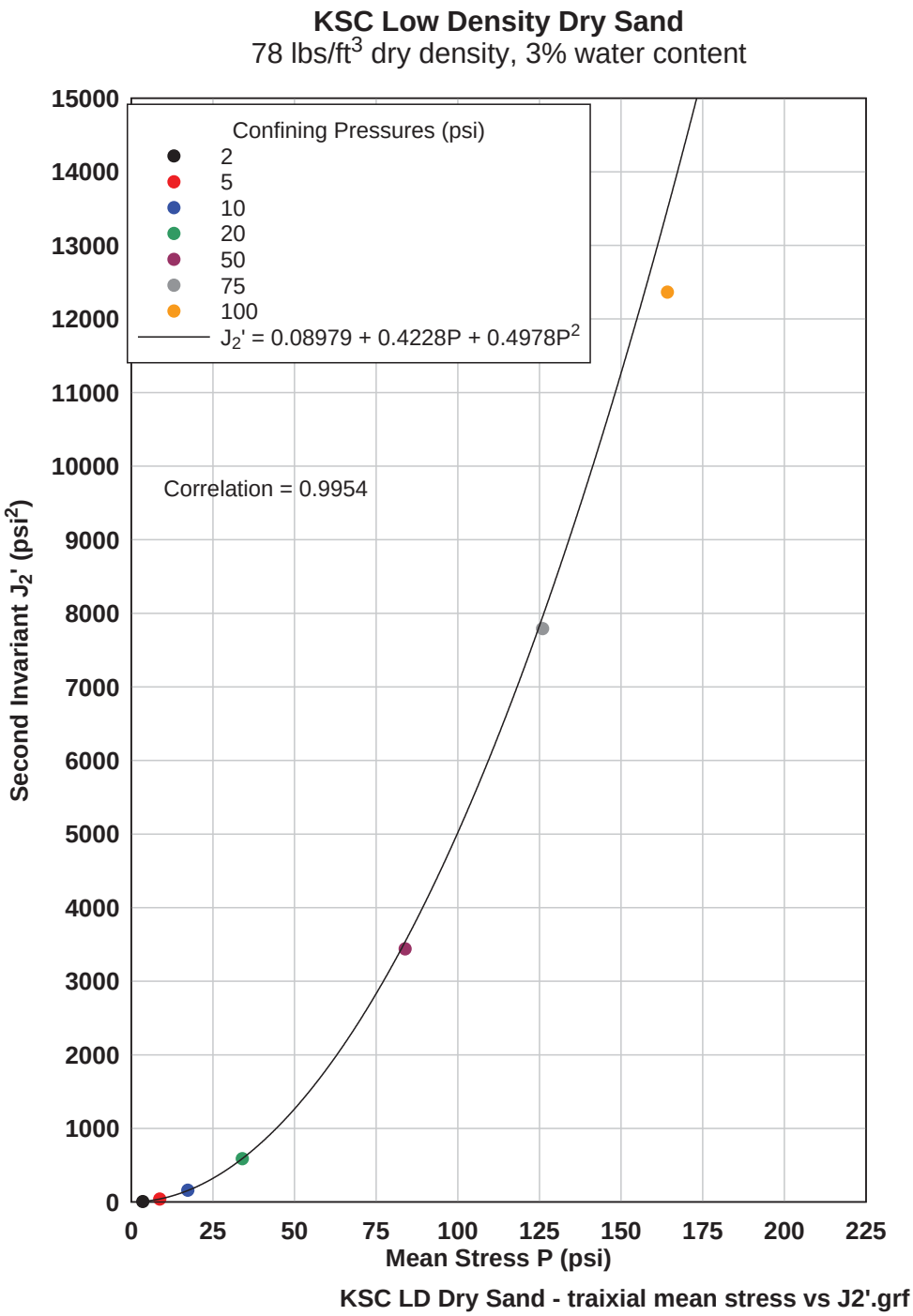

Figure 4-9: KSC LDD Sand, Material Model 5 yield surface fit from triaxial test data.

4.3.3 Hydrostatic compression

A hydrostatic test was conducted prior to each triaxial test. The 100 psi hydrostatic test is shown in Figure 4-10. Midway through the hydrostatic test, the specimen was unloaded and reloaded. When 50 psi is reached for the first time, the specimen is unloaded to zero, then reloaded again until 100 psi is reached. Then the specimen is reloaded to 100 psi again, and the triaxial test is performed.

The flat portions of the curve represent large deformations that occur very quickly. The low density sand is collapsing into a denser structure as more pressure is applied. When starting at this low density, the sand "jumps" to a higher density in discrete steps. This behavior stops after 2.9% strain during the hydrostatic test. The uniaxial tests also show this behavior.

The initial bulk modulus fit is drawn between zero and 1% strain, consistent with the modulus fits from the uniaxial tests. The bulk unload fits are drawn to the initial unloading portion of the curve, also consistent with the uniaxial fit. These fits reflect the hydrostatic test's compression loading. It is important to note that uniaxial tests have shear and compression, and the peak mean stress is greater than the 100 psi confining pressure. The hydrostatic fits are not used to define the model, but they do provide additional insight.

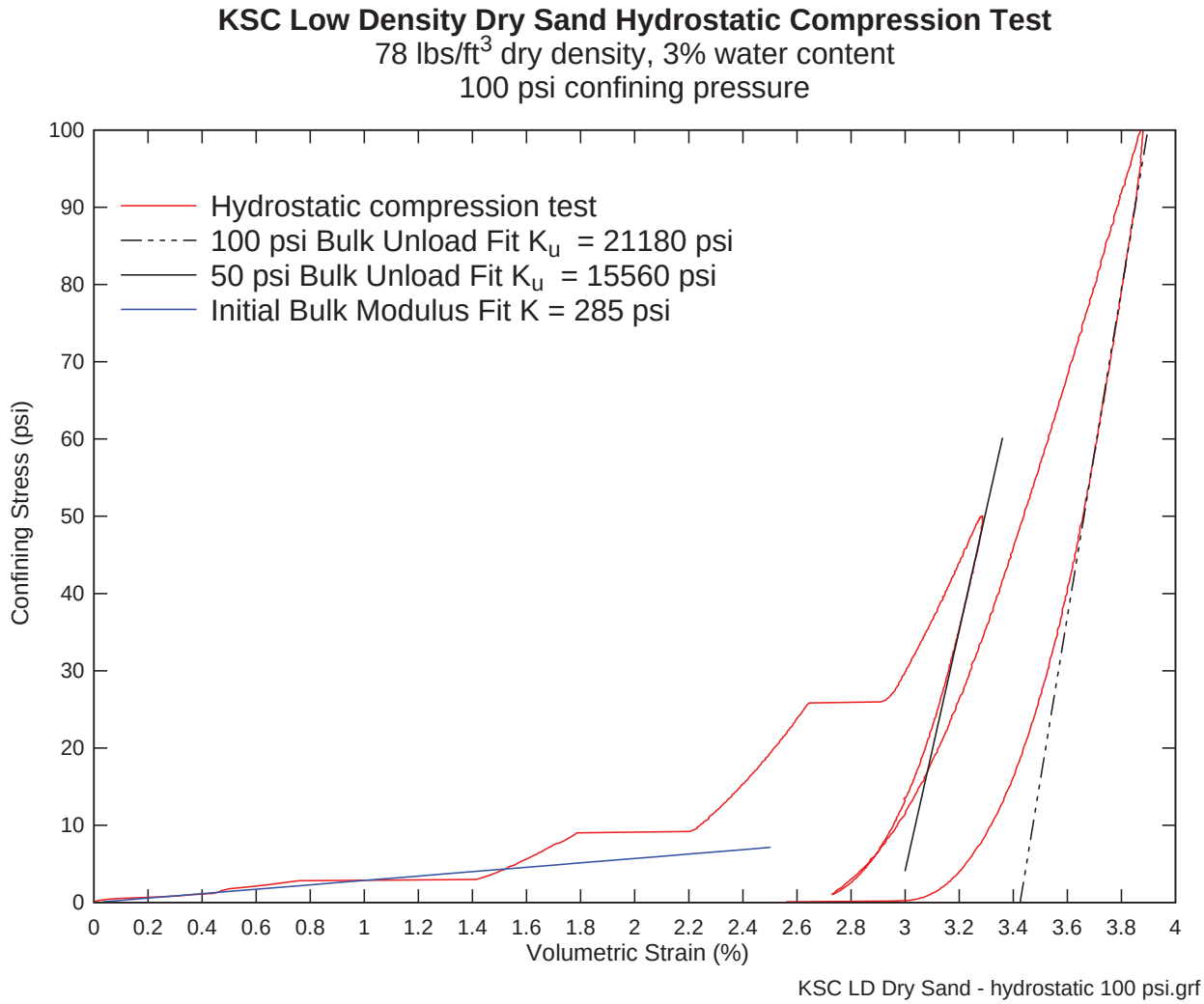

Figure 4-10: 100 psi hydrostatic compression test on KSC LDD Sand. Hydrostatic fits are drawn to initial loading and unloading portions of the curve.

4.3.4 Uniaxial strain

Three uniaxial strain tests were run on KSC LDD Sand, two at 50 psi and one at 100 psi. The 100 psi uniaxial strain data for KSC LDD Sand is shown in Figure 4-11. Comparisons to the 50 psi tests are show in Figure 4-12. Is it important to note the flat portion of all three tests. The flat portion physically represents the loading piston pressing into the specimen, but no additional load is seen by the load cell at the bottom of the specimen. This means the downward movement of the piston is compressing the sand, but the sand is collapsing without taking additional load. Void space within the sand is being closed, but without the soil skeleton transmitting additional load to the load cell at the bottom. This phenomenon is attributed to testing at such low densities. The skeleton collapses by forcing sand grains into void spaces until enough grain contacts have formed to carry additional load.

The flat portion occurs at different strains in each test. Despite all three tests having the same target density ($80 lbs/ft^3$), the specimen density can change when placed into the vessel. This is because low density cohesionless sands are very sensitive to movement. The sands will compact under slight vibration, resulting in slightly higher density. The change in axial length is known because the axial LVDT readings can be compared to the original specimen mold height. However, the radial change is not fully known due to vacuum and membrane. The sand's density is not high enough to stretch the membrane to make uniform, full contact with the inner walls of the mold. Also, the specimen is placed under 0.5 psi vacuum to stabilize the sand for movement into the vessel. These factors slightly increase the specimen density before the test begins. This problem is only unique to testing KSC LDD Sand, as the other models have sufficient density to avoid these sensitivities.

The stress-strains below 2% in Figure 4-12 show two uniaxial tests (red and blue curves) have very similar initial loading. The third (black curve) is higher. Also, once the skeleton collapse (flat portion) is complete, the slopes of all three tests appear parallel. The third test is suspected to have started at a higher density than the other two. The specimen most likely settled to higher density during handling. The higher density created an initial modulus much higher than the other two. Yet after the skeleton collapse, the parallel slopes suggest remarkably uniform behavior, even for the suspected higher density specimen. The KSC LDD model uses fits drawn to the red and blue curves because these specimens were closer to the target density when the test began, and the two tests were very similar during initial loading. The Poisson ratio and shear modulus G are derived from this initial loading.

The ten selected pressure-volume points are based on the 100 psi uniaxial test. The comparison to the 2008 KSC HDD Sand model is shown in Figure 4-16. The new model experiences 1% more strain before stress load increases again, which occurs at 3.8% versus 2.8%.

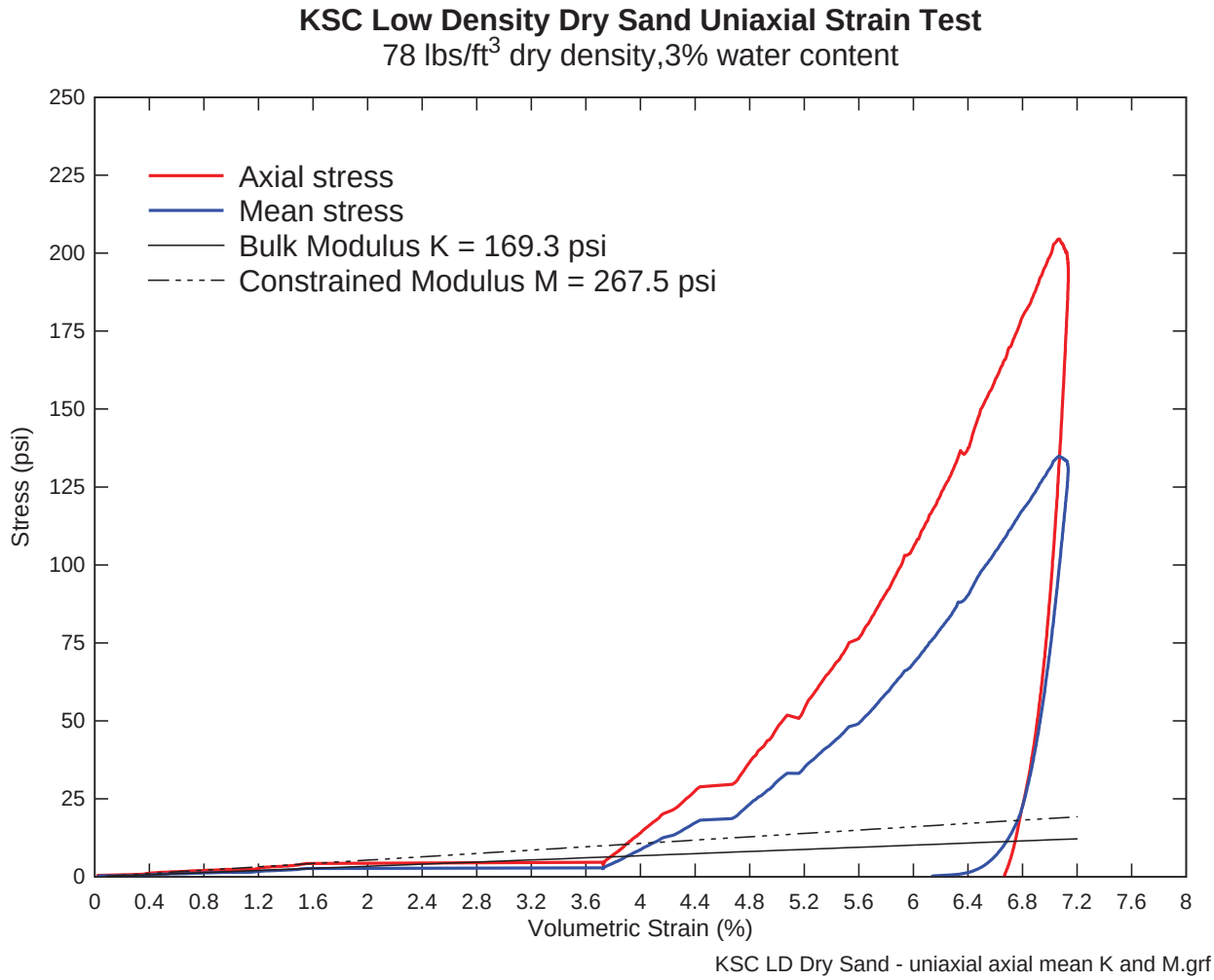

Figure 4-11: KSC LDD Sand 100 psi uniaxial strain test results. Constrained and bulk moduli fits shown.

-

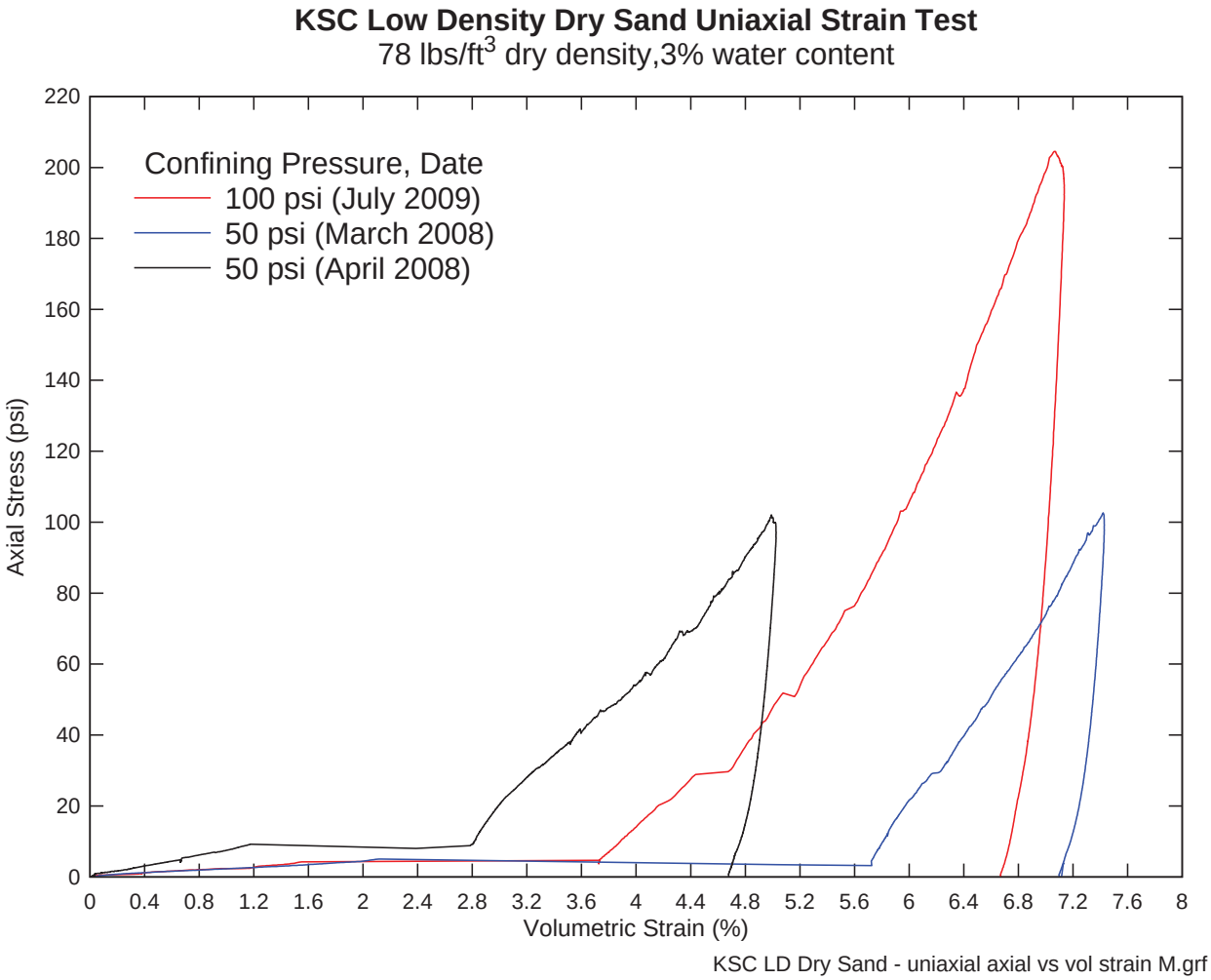

Figure 4-12: Comparison of all three KSC LDD Sand uniaxial strain tests. One 100 psi test and two 50 psi tests. Axial stress vs. strain shown.

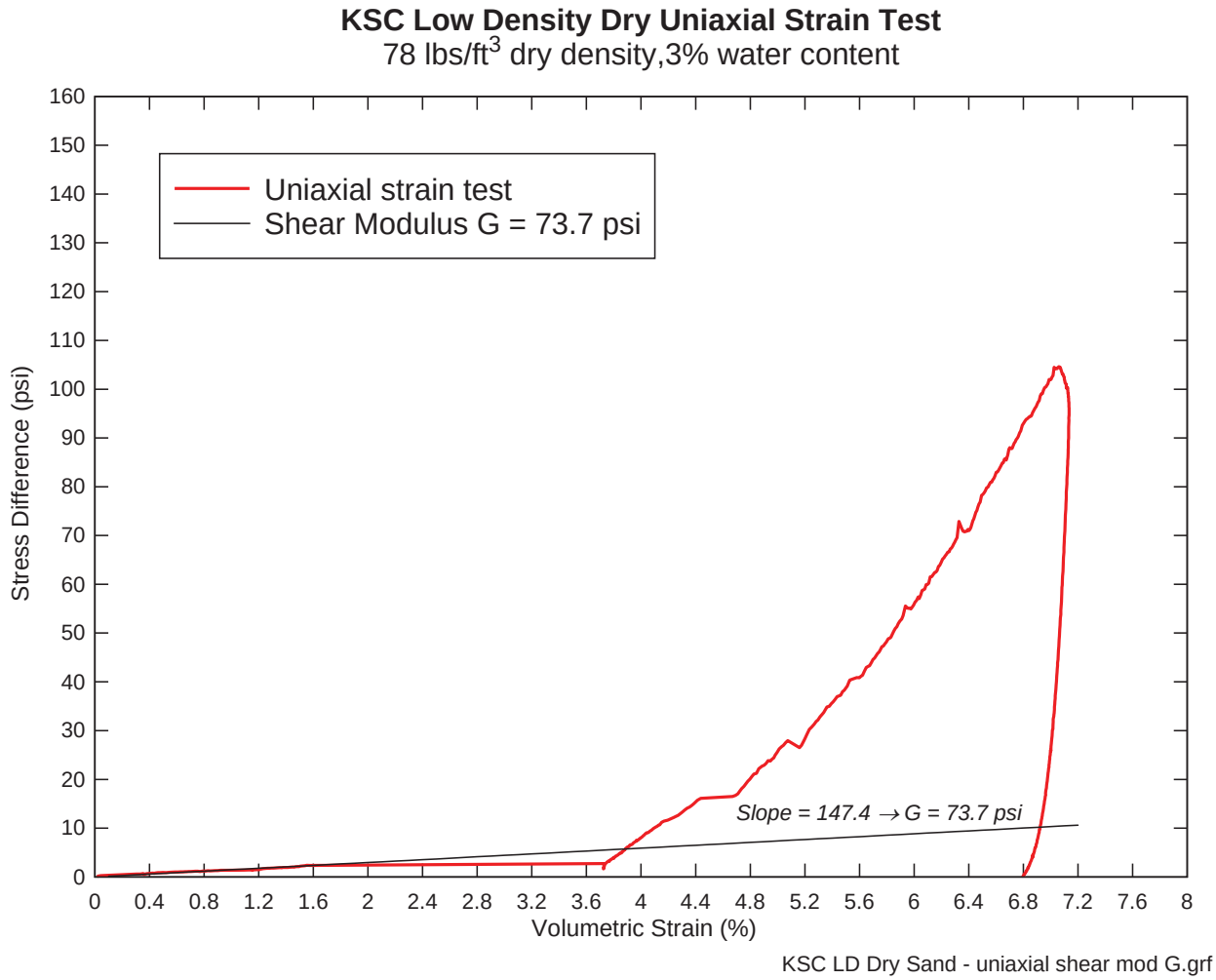

Figure 4-13: KSC LDD Sand 100 psi uniaxial strain test results plotted as stress difference vs. strain. Shear modulus G fit shown. Shear stress is half of stress difference. Uniaxial strain is equal to shear strain.

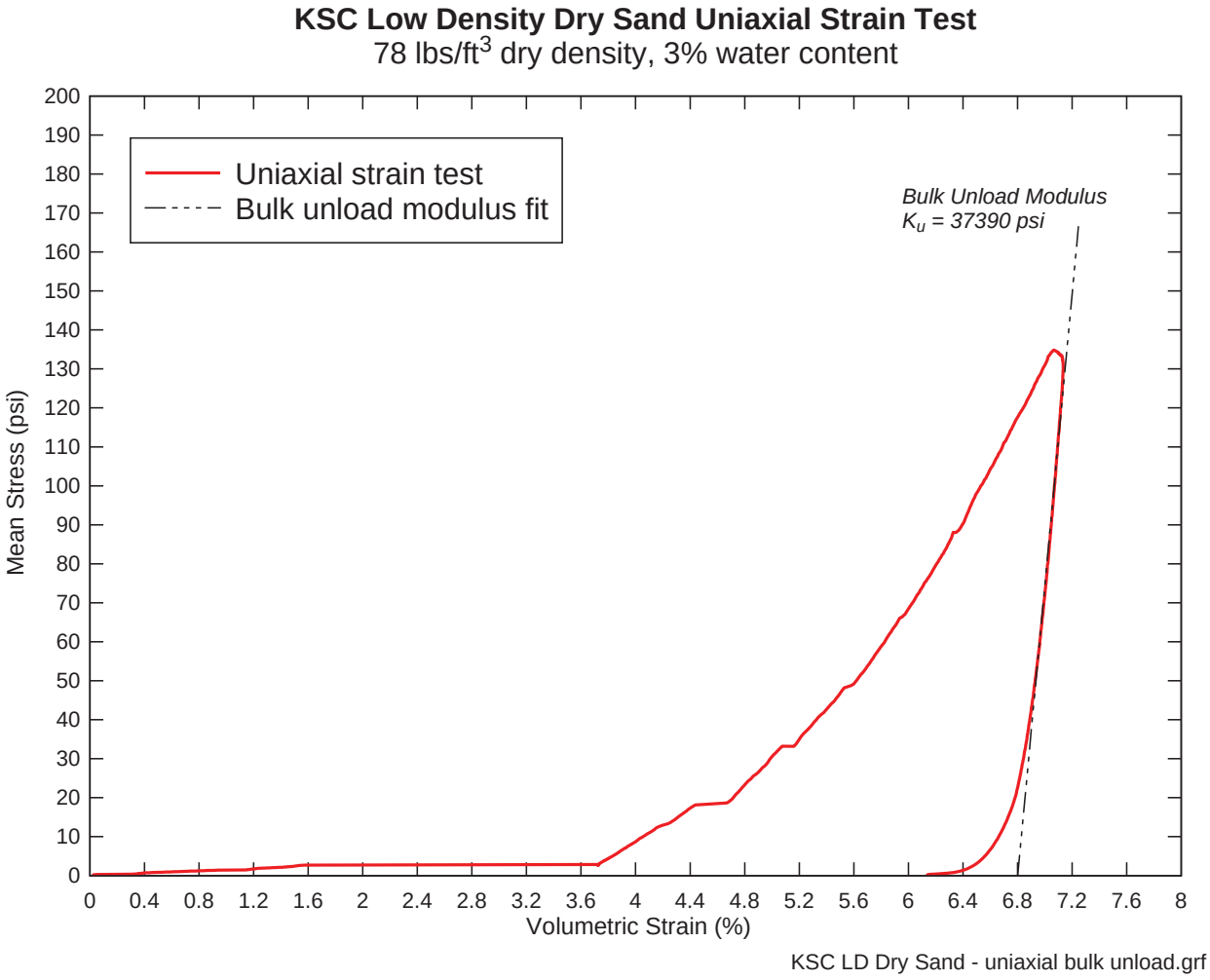

Figure 4-14: KSC LDD Sand 100 psi uniaxial strain unloading portion. Determination of bulk unloading modulus K_u (BULK) by linear fit to initial unloading.

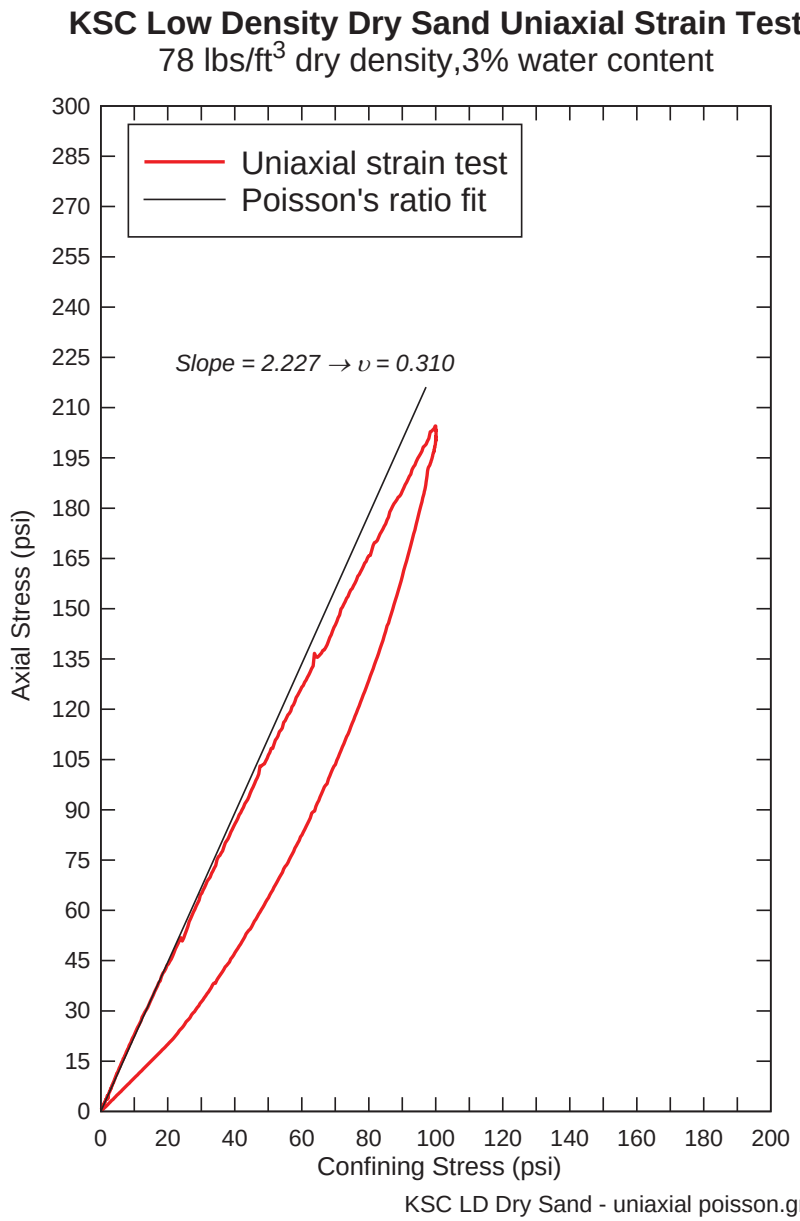

Figure 4-15: KSC LDD Sand 100 psi uniaxial strain test. Determination of Poisson's ratio via uniaxial strain test.

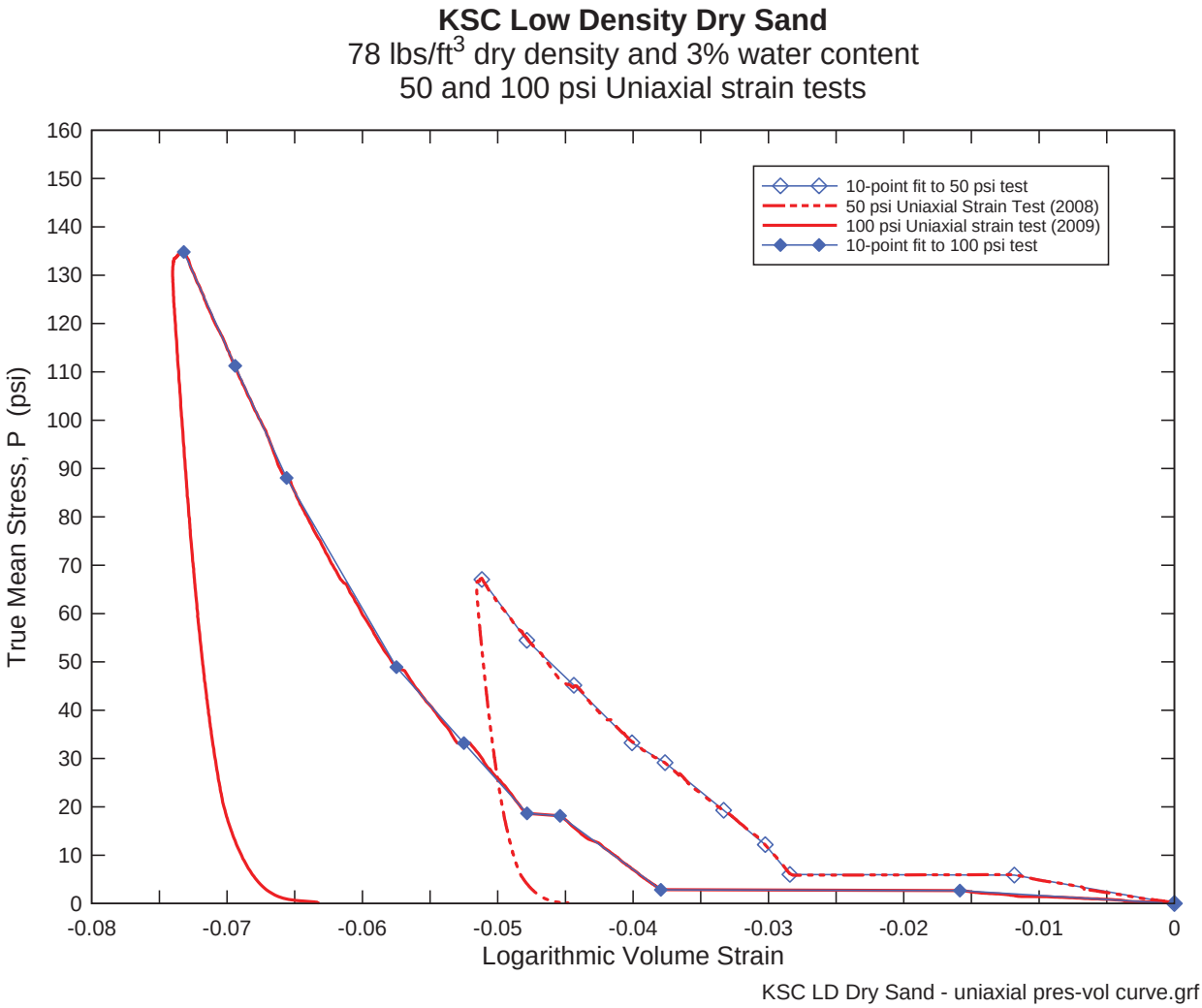

Figure 4-16: KSC LDD Sand Material Model 5 pressure-logarithmic volume curve with 10 input points. New (100 psi) and old (50 psi) models shown.

4.4 LS-DYNA Material Model 5 inputs

The recommended set of inputs for modeling KSC LDD Sand at 78 lbs/ft^3 dry density and 3% water content in LS-DYNA Material Model 5: Soil and Foam is shown in the table below.

Table 4-5: Material Model 5 inputs for KSC LDD Sand

	Input	Value	Units
Mass density	**RO**	0.000120	lb s^2/in^4
Shear modulus	**G**	73.7	psi
Bulk unloading modulus	**K**	37390	psi
Yield surface coefficient	**A0**	0.08979	psi^2
Yield surface coefficient	**A1**	0.4228	psi
Yield surface coefficient	**A2**	0.4978	-
Pressure cutoff	**PC**	-0.5	psi

	Input	Value	Input	Value	Units
Pressure-volume point	**EPS1**	0.0000	**P1**	0	psi
Pressure-volume point	**EPS2**	-0.01586	**P2**	2.685	psi
Pressure-volume point	**EPS3**	-0.03794	**P3**	2.85	psi
Pressure-volume point	**EPS4**	-0.04539	**P4**	18.14	psi
Pressure-volume point	**EPS5**	-0.04783	**P5**	18.66	psi
Pressure-volume point	**EPS6**	-0.05250	**P6**	33.2	psi
Pressure-volume point	**EPS7**	-0.05748	**P7**	48.9	psi
Pressure-volume point	**EPS8**	-0.06560	**P8**	88.05	psi
Pressure-volume point	**EPS9**	-0.06940	**P9**	111.24	psi
Pressure-volume point	**EPS10**	-0.07320	**P10**	134.8	psi

Table 4-6: Summary of elastic constants

Young's Modulus E	193	psi
Poisson's Ratio ν	0.310	
Shear Modulus G	73.7	psi
Initial Bulk Modulus K	169.3	psi
Constrained Modulus M	267.5	psi

5 KSC High Density In Situ Moisture Sand

This chapter describes the KSC High Density In situ moisture (HDI) Sand model. High density means the tested density reflects the more compacted areas around KSC. These include launch pads, road embankments, and other man-made areas. In situ moisture means that the sand was tested as sampled from the site. No changes in moisture content were made. The KSC HDI Sand model's purpose is to simulate the denser, stiffer areas around Pads 39 A and B. These areas are denser than any naturally deposited sand.

5.1 Location

The KSC HDI Sand was sampled from man-made areas. Most notable was within the ring road of Pad 39 B. It represents the "Urbanland" zones marked in Figure 4-2. According to local KSC experts, the fill material was taken from nearby sources. The sands from man made areas are very similar to sands from other areas. It is not uncommon for coastal areas to have uniform sand deposits.

5.2 General description

Nearly all man-made areas are topped with grass-like vegetation. A sandy topsoil layer 1-2 inches thick covers the surface. The topsoil can be described as a sandy organic mix. This thin layer was ignored for modeling purposes in favor of the underlying sand. The underlying sand was the sample source for the KSC HDI Sand model.

The sands underlying man-made areas were also consistent with depth. The sand remained uniform to a depth of at least 30 inches. This is indicative of the geologically uniform sand deposits that created Merritt Island. The sand was also damp due to moisture being trapped underneath the topsoil. Topsoil prevents the sand from drying out. No bodies of water were nearby, and the pads are elevated above the waterline. Because no recent rains occurred, the moisture content obtained from samples is believed to be representative of most man-made areas. Figure 5-1 illustrates the topsoil layer.

The unrealistic minimum density shown in Table 5-1 suggests the surface density measurements performed by Dynamac are not suitable for use in Orion impact modeling. The mean of 69.3 lbs/ft^3 is extremely low and may represent the first inch of depth, but certainly not the range of interest for impact modeling. ARA ran exploratory tests at 90 lbs/ft^3 wet density, but these were almost as soft as the KSC LDD sand model. Because the urban areas are mechanically flattened and compacted, ARA assumed a wet density of 100.3 lbs/ft^3 to represent a higher than natural relative density.

Table 5-1: Density measurements of surface sands from Dynamac 2000 report

KSC disturbed sand (man-made areas)	Samples N	Field Min	Field Max	Mean
Wet Density (lbs/ft^3)	22	37.4	87.4	69.3

Table 5-2: KSC HDI Sand soil classification. Source – Dynamac 2000.

Soil Class	Mean Grain Size (mm)	USCS Class
Disturbed (man-made areas)	0.18	SP, fine sand

Figure 5-1: Excavation at Pad 39 B, inside ring road. Topsoil is brown. Underlying sand is tan.

5.3 Laboratory data

The KSC HDI Sand is classified as poorly graded fine sand (USCS - SP). The Dynamac grain size distribution indicates that it is 75% fine sand, 10% medium sand, 5% coarse sand, and 10% organic fines. The organic fines come from the topsoil, and are not present at depth. The test log is shown in Table 5-3. ARA performed grain size distribution on samples extracted from within Pad B. The samples purposely do not contain topsoil because the sand itself is the focus of the model. These results are shown in Figure 5-2, and the fines are absent in ARA's grain size distribution. This leads to the difference in the coefficient of uniformity.

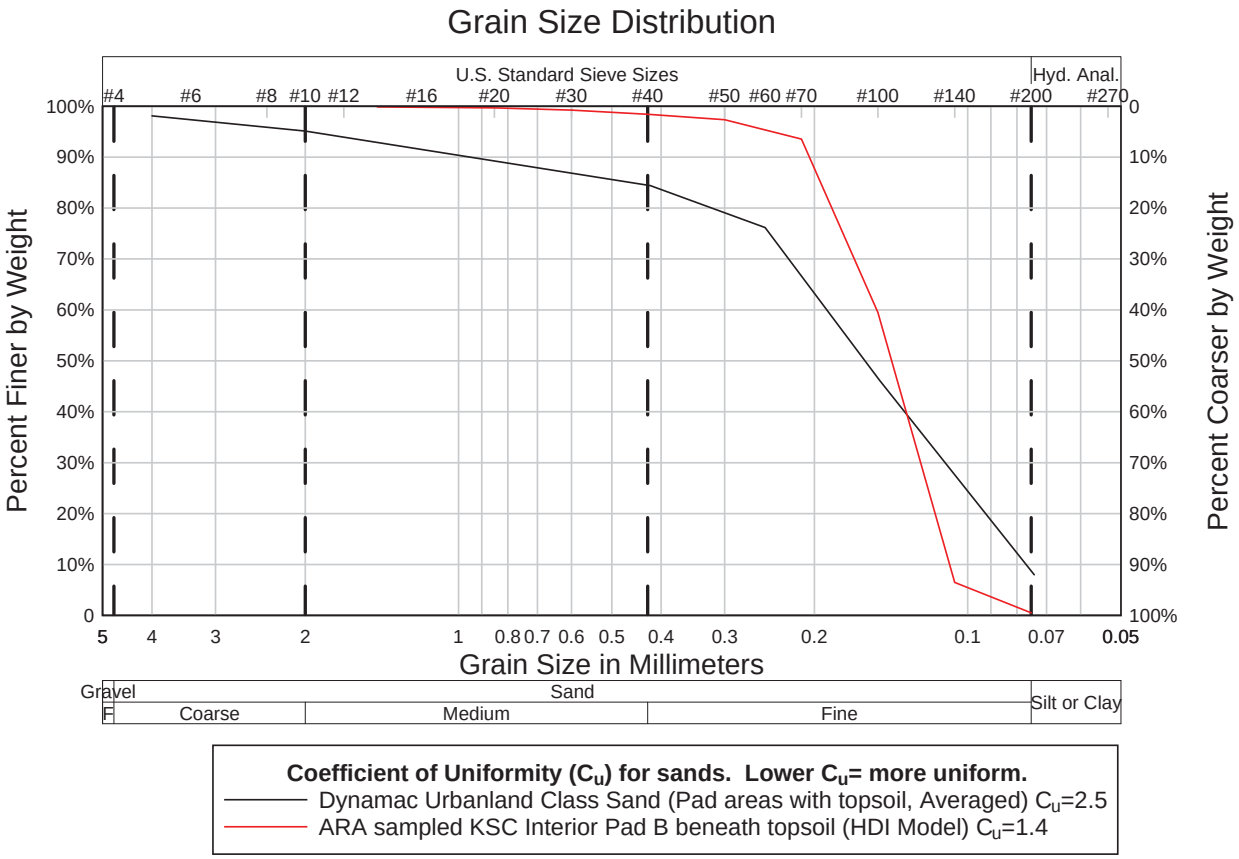

Figure 5-2: Grain size distribution for KSC HDI Sand, compared to Dynamac average.

Table 5-3: Test log for KSC HDI Sand. * The italicized tests were not used to create the KSC HDI model.

Test ID	Sample ID	Type	Confining Pressure (psi)	Moisture content	Wet Density (lbs/ft^3)	Dry Density (lbs/ft^3)	Grain Density G_s (g/cm^3)	Porosity n
*M28A08**	*Pad B*	*Uniax*	*50*	*15.32%*	***90***	*78.04*	*2.67*	*53.2%*
*M31C08**	*Pad B*	*Triax*	*2*	*16.96%*	***90***	*76.95*	*2.67*	*53.9%*
*M31E08**	*Pad B*	*Triax*	*5*	*16.60%*	***90***	*77.19*	*2.67*	*53.8%*
*A1C08**	*Pad B*	*Triax*	*10*	*17.25%*	***90***	*76.76*	*2.67*	*54.0%*
A2A08	Pad B	Triax	2	15.75%	100.3	86.62	2.67	48.0%
A8B08	Pad B	Triax	2	15.69%	100.3	86.42	2.67	48.0%
A7E08	Pad B	Triax	5	18.37%	100.3	84.43	2.67	49.2%
A7C08	Pad B	Triax	10	17.65%	100.3	84.93	2.67	48.9%
A3A08	Pad B	Triax	20	16.31%	100.3	85.94	2.67	48.3%
A4A08	Pad B	Triax	50	16.27%	100.3	85.98	2.67	48.3%
A10B08	Pad B	Uniax	50	15.76%	100.3	86.41	2.67	48.0%
Y12B09	Pad B	Triax	75	N/A	100.3	N/A	2.67	N/A
Y13D09	Pad B	Triax	75	13.71%	100.3	88.18	2.67	47.1%
Y14B09	Pad B	Triax	100	14.81%	100.3	87.34	2.67	47.6%
L9A09	Pad B	Uniax	100	16.52%	100.3	86.05	2.67	48.3%
G13B09	Pad B	Triax	50	16.10%	100.3	86.36	2.67	48.0%

5.3.1 Triaxial compression

The KSC HDI model was extended to higher pressures via three additional triaxial tests. The 50 psi triaxial was repeated, and an additional 75 and 100 psi tests were performed. In total, the triaxial strength envelope is based on 8 triaxial tests at 2, 5, 10, 20, 50, 75, and 100 psi confining pressures (50 psi ran twice). The 50 psi test was repeated because it was truncated at 10% strain in 2008. Although truncated, it was already well past the peak strength and did not affect the model. In 2009, testing resumed at 50 psi to confirm the same peak strength. After testing, the peak strength differed only by 1 psi. The 2008 test peaked at 108.7 psi, and the 2009 test peaked at 109.7 psi. The results are shown Figure 5-3. Strength envelope analysis and LS-DYNA yield surface fits are shown in Figure 5-5 and Figure 5-7.

The new model's strength parameters are similar to the old, but weaker. The linear fit coefficients in Figure 5-5 have a reduced slope coefficient. The new 75 and 100 psi data points fall short of a linear extension of the old model, but do not stray far. The 50 psi test was ignored in the old model; it is included in the new model due to the new focus on higher stress behavior. The slope coefficient was reduced to fit the 50, 75, and 100 psi points. Overall, the model's strength did not change significantly.

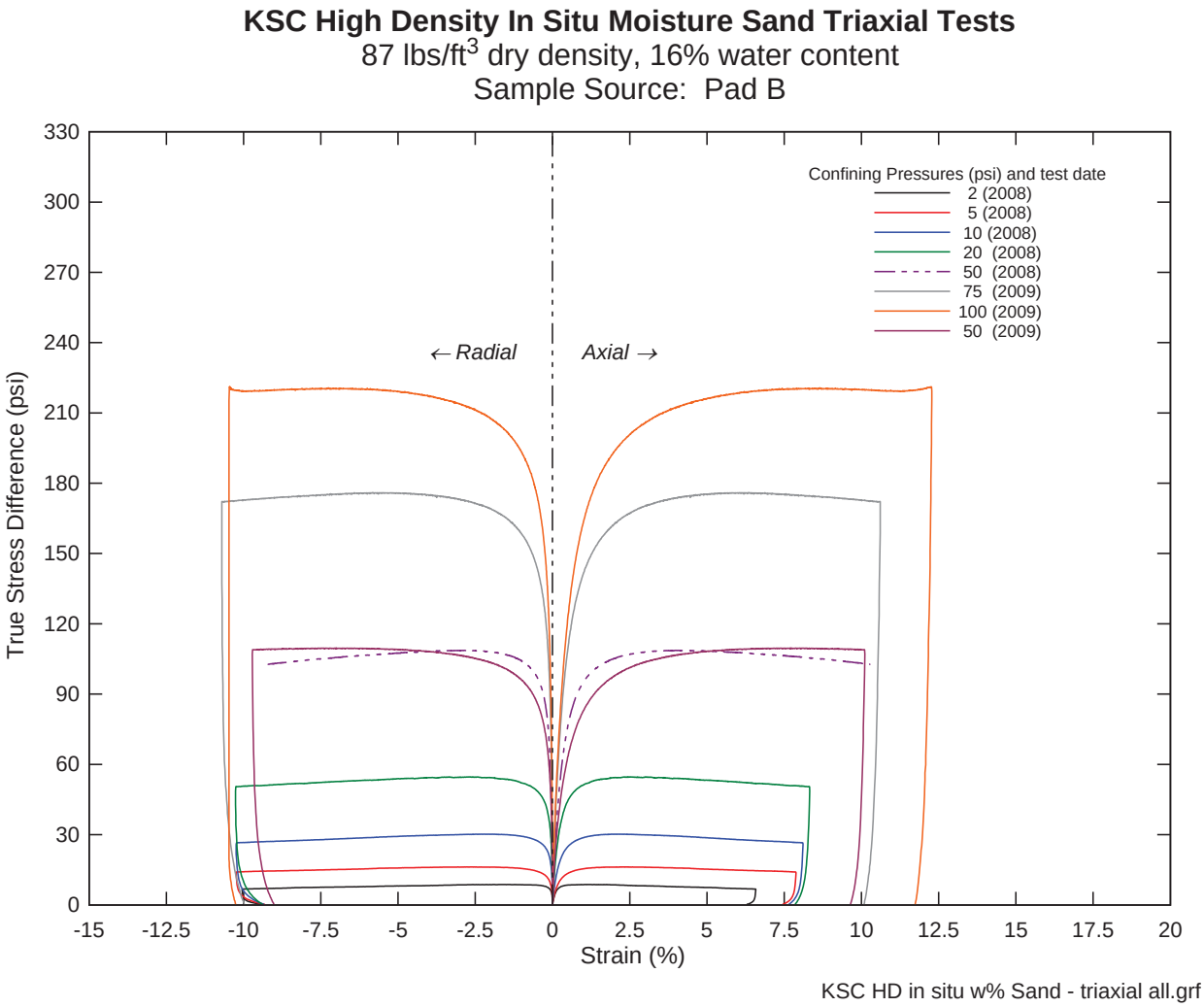

Figure 5-3: KSC HDI Sand model's triaxial compression test results. Performed 50 psi test twice.

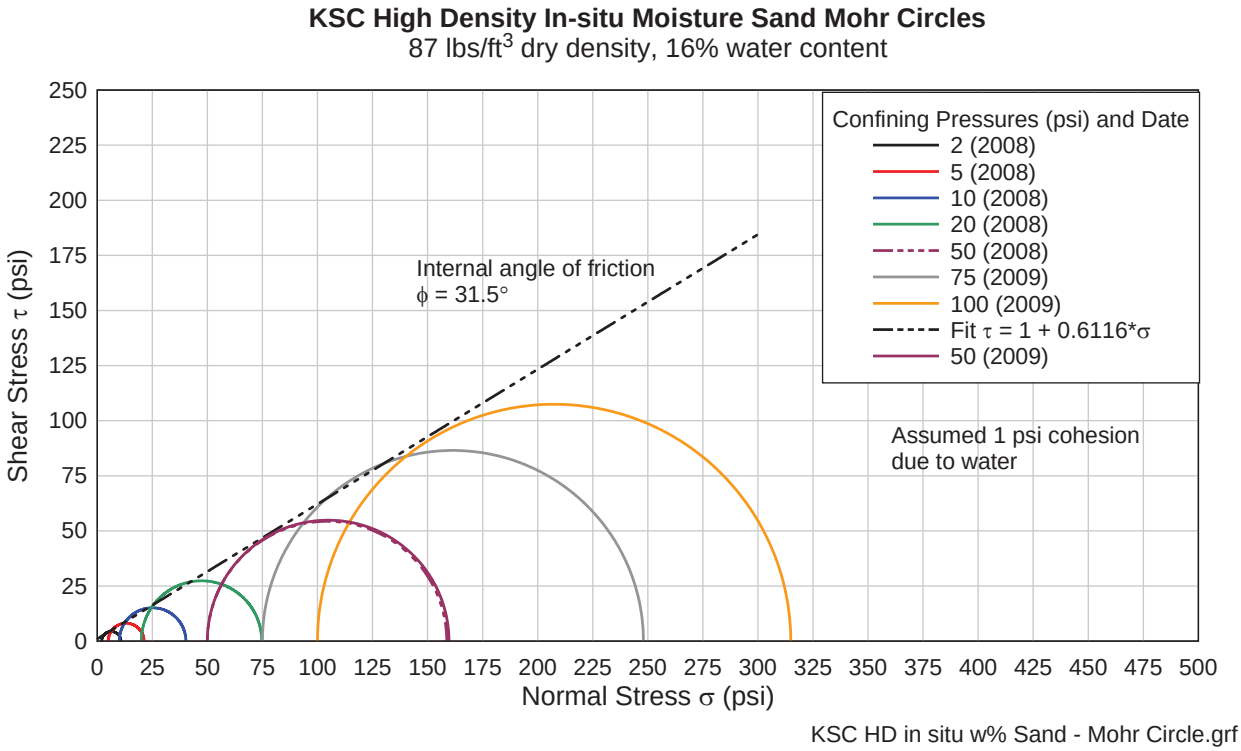

Figure 5-4: Mohr circles for KSC HDI Sand. Mohr circles for 50 psi tests plot essentially on top of each other.

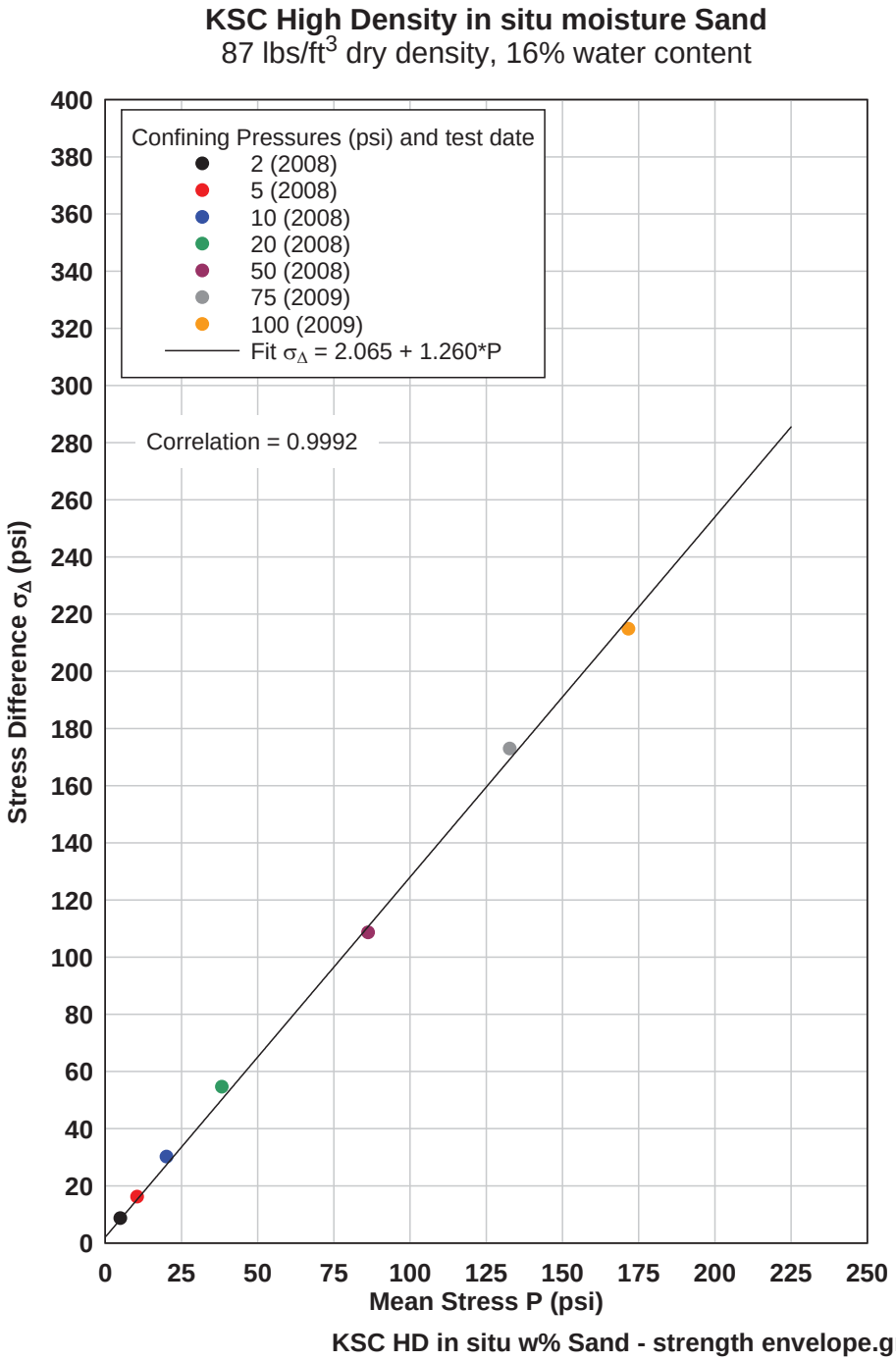

Figure 5-5: KSC HDI Sand model's strength envelope. The two 50 psi peak strengths were combined into one value.

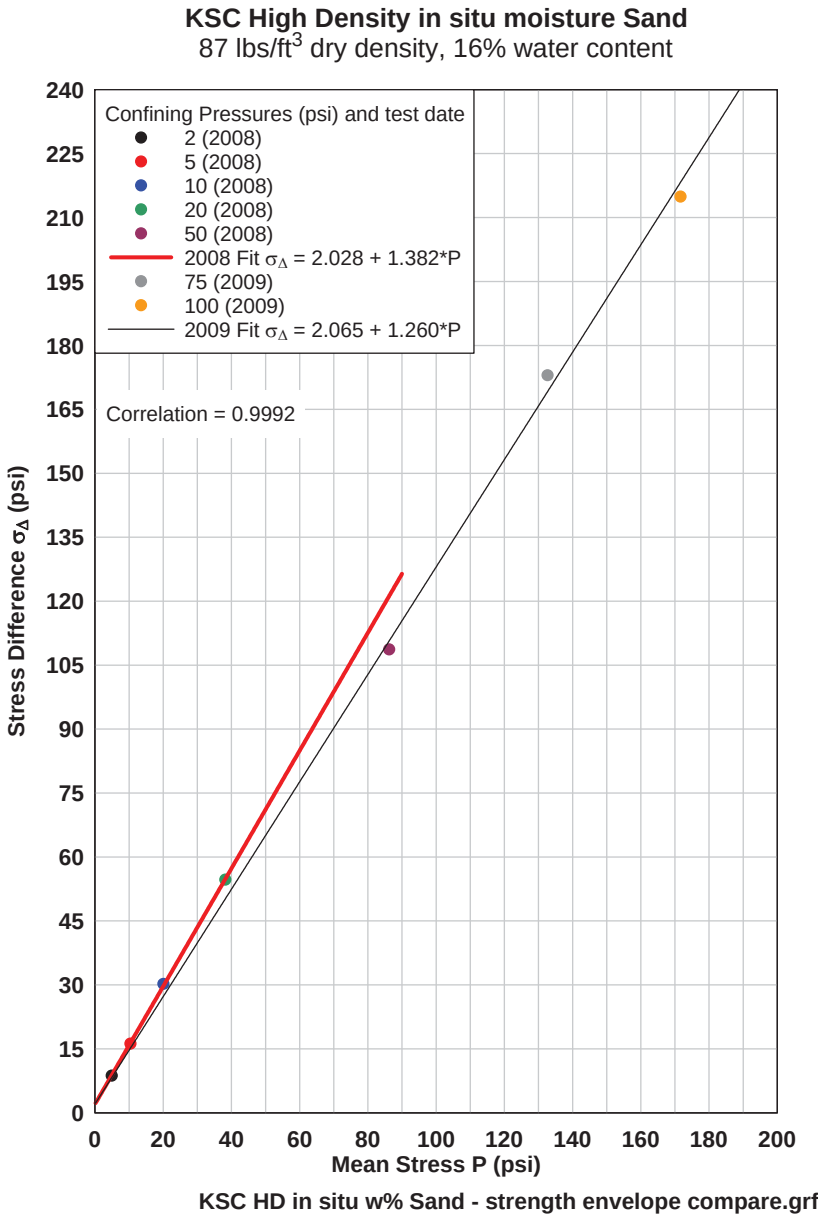

Figure 5-6: Old versus new KSC HDI linear strength fit.

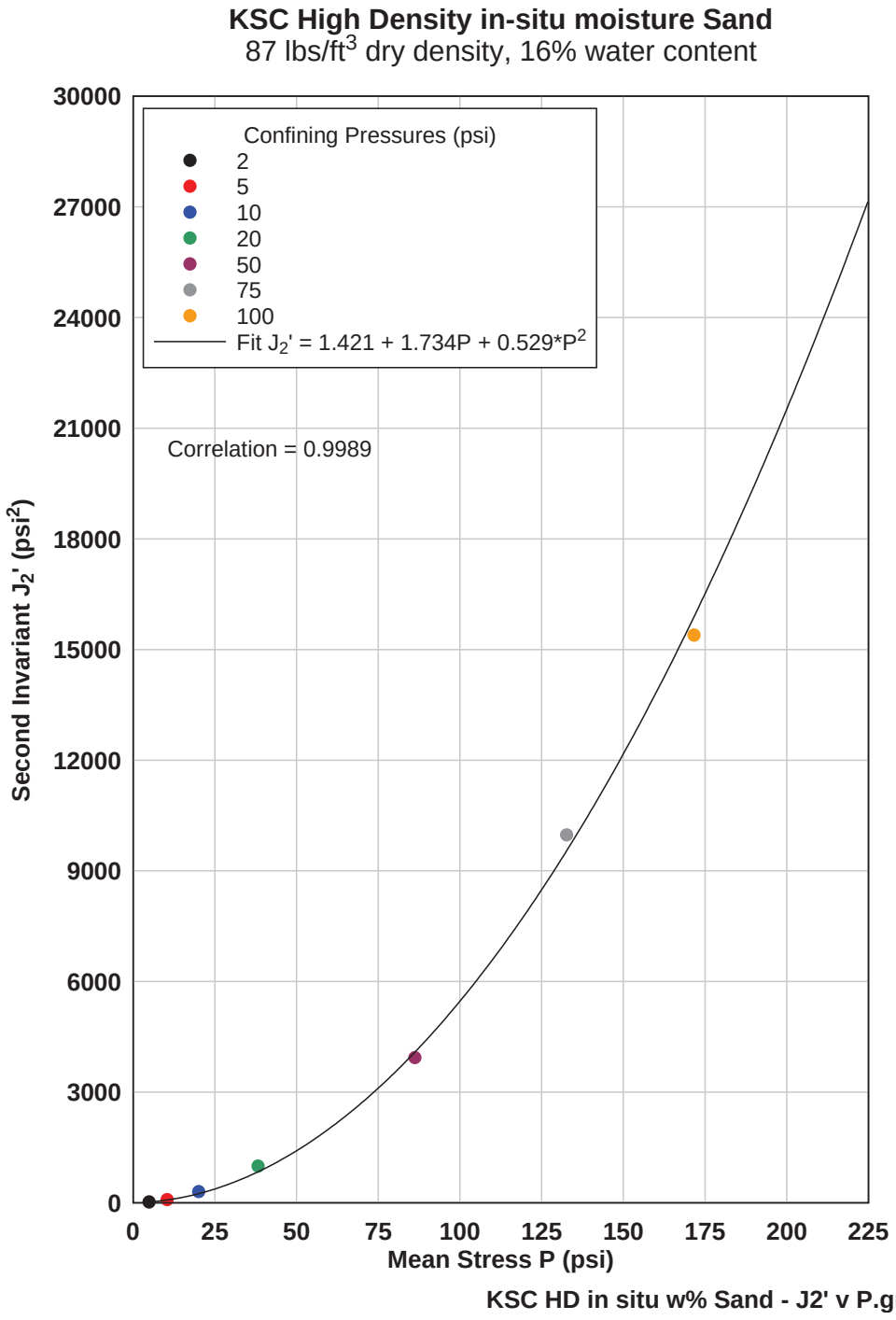

Figure 5-7: KSC HDI Sand Material Model 5 yield surface fit from triaxial data. The two 50 psi peak strengths were combined into one value.

5.3.2 Hydrostatic compression

The hydrostatic test loads the specimen to 50 psi, then unloads, then reloads to 100 psi. These two cycles are shown in Figure 5-8, plotted on the same scale as KSC LDD Sand in Figure 4-10 to illustrate the relative stiffness between the two. The fits shown below are not used in the KSC HDI model, but shown for comparison to the uniaxial data in the next section.

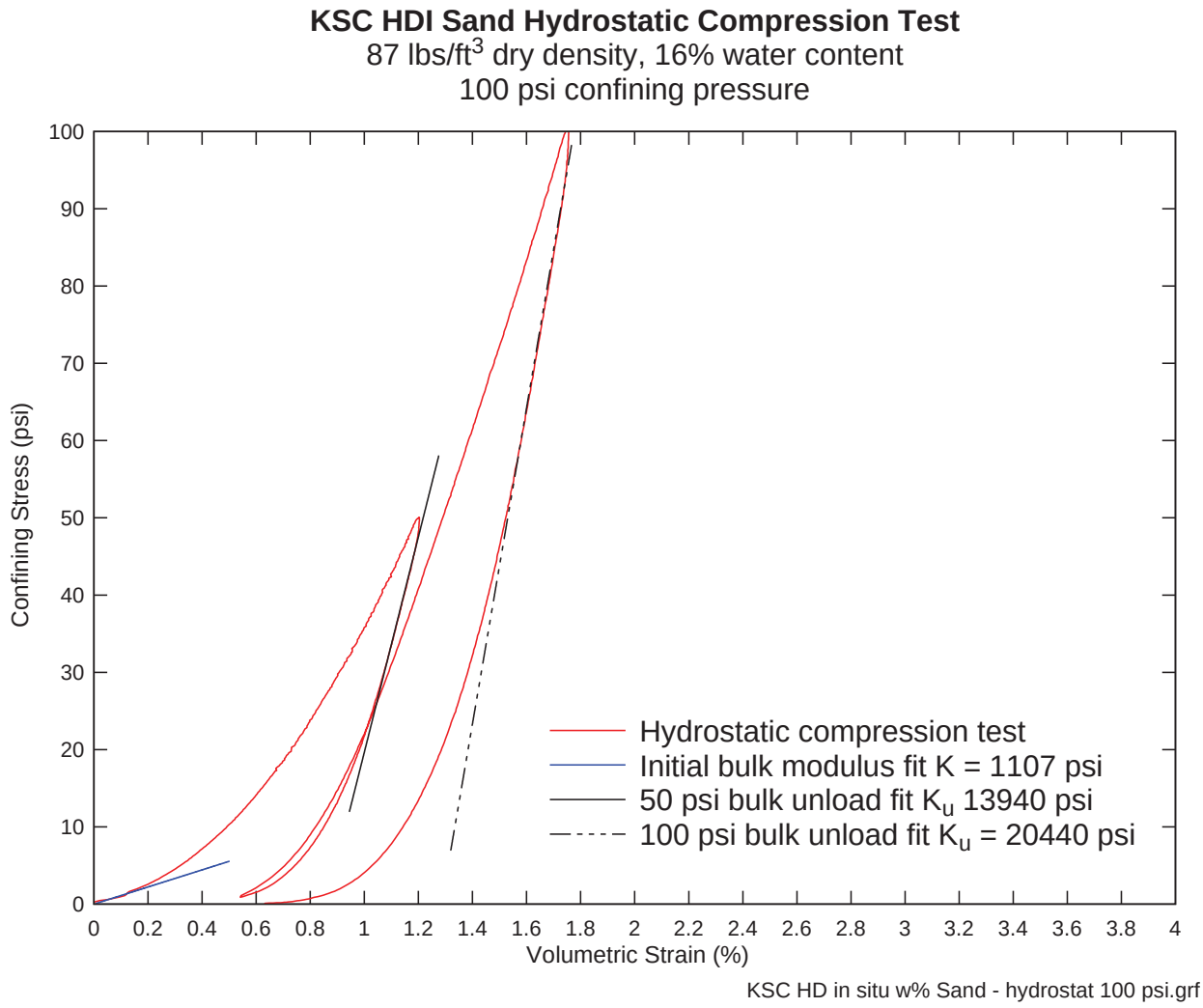

Figure 5-8: 100 psi hydrostatic compression test for KSC HDI Sand.

5.3.3 Uniaxial strain

KSC HDI Sand model's uniaxial strain test results are shown in Figure 5-9 through Figure 5-13. The 100 psi uniaxial strain test compares very favorably with the previous 50 psi test. The 100 psi test essentially extends where the 50 psi test terminated. The new model is a higher pressure extension of the old model with very similar properties.

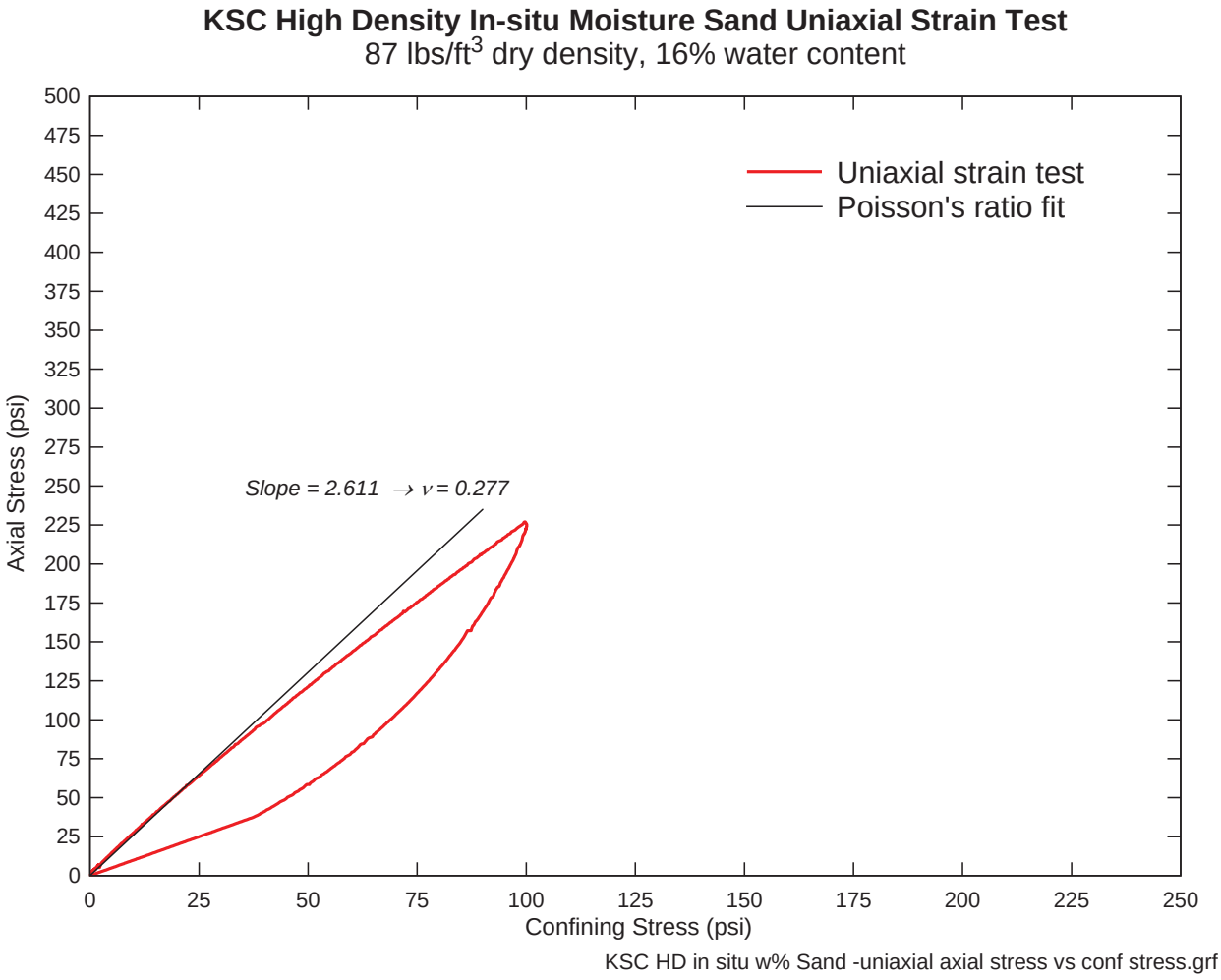

Figure 5-9: KSC HDI Sand model's uniaxial strain test. Axial stress vs. confining stress plotted to calculate Poisson's ratio from slopes.

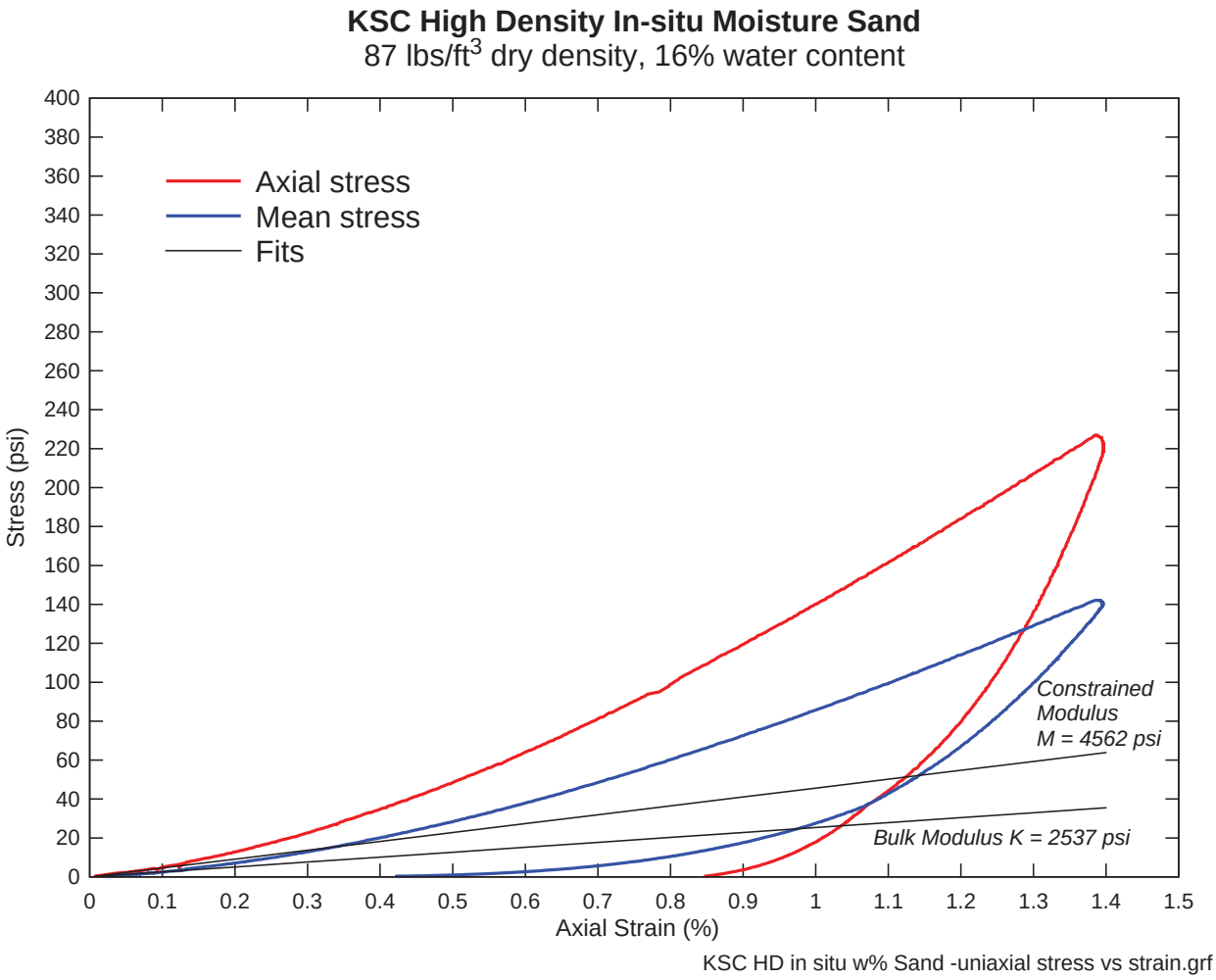

Figure 5-10: KSC HDI Sand model's uniaxial strain test. Stress vs. axial strain plotted to obtain constrained modulus from axial stress and Initial Bulk Modulus from mean stress.

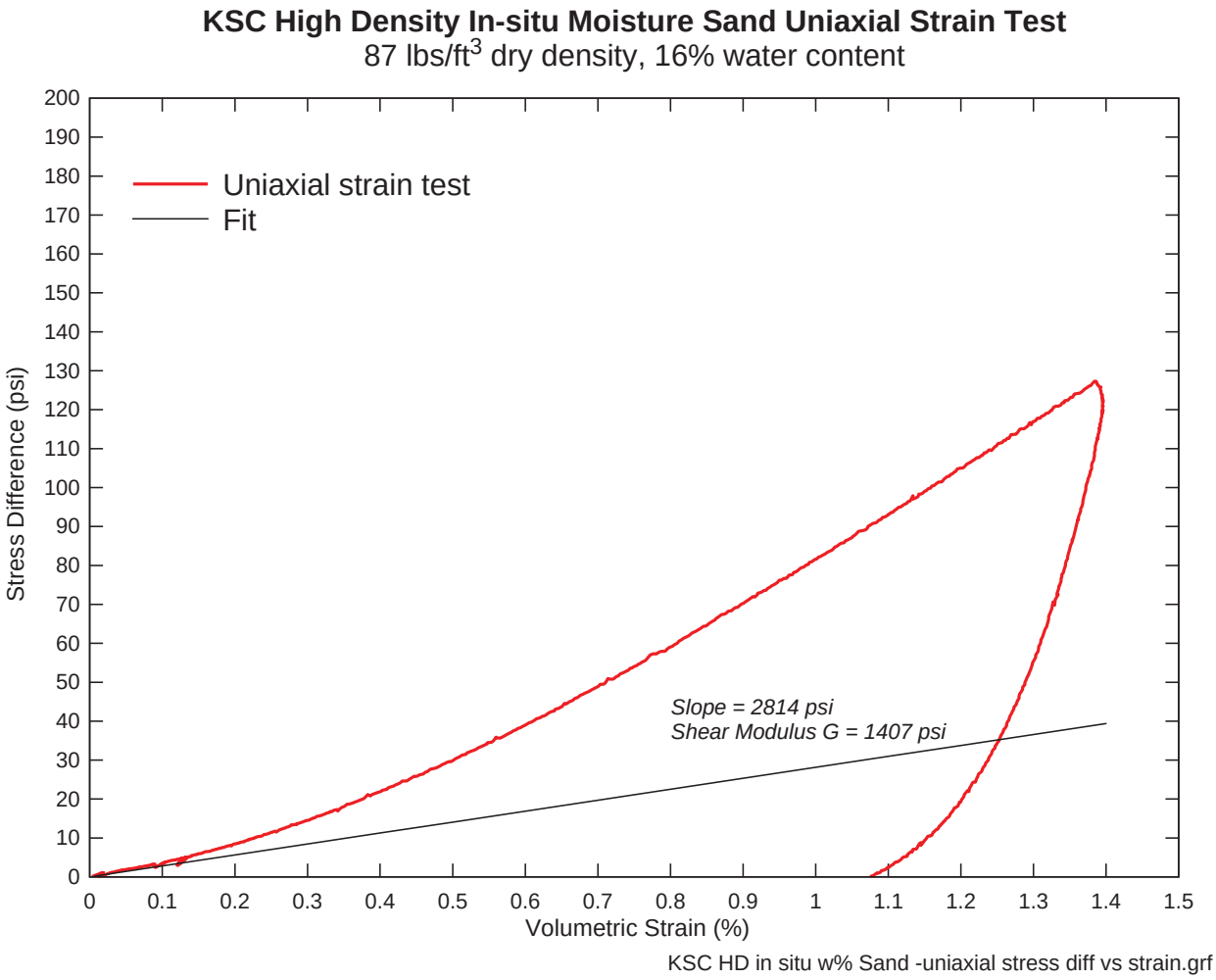

Figure 5-11: KSC HDI Sand model's uniaxial strain test. Stress difference vs. strain difference plotted to obtain shear modulus G.

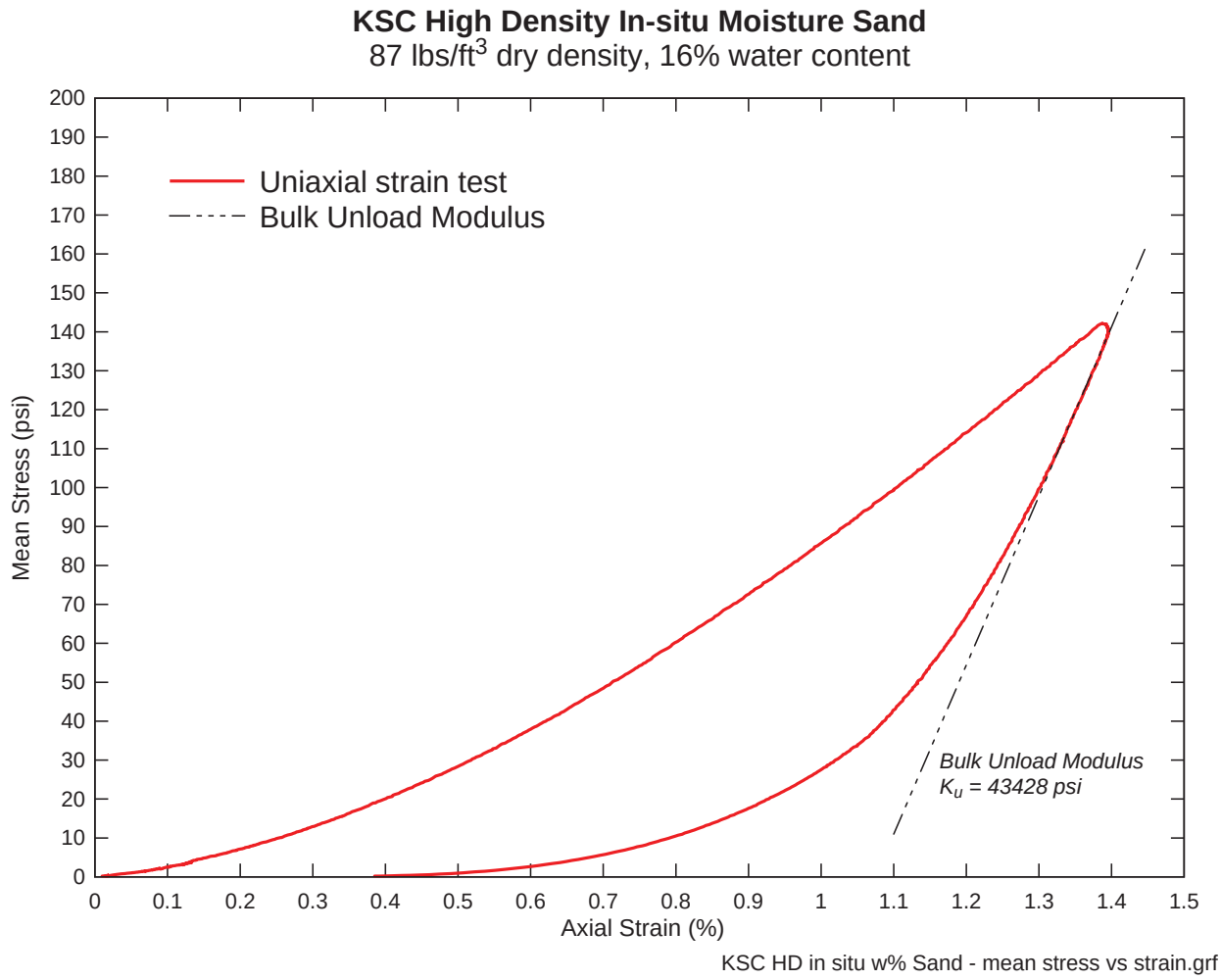

Figure 5-12: KSC HDI Sand model's uniaxial strain test. Mean stress vs. volumetric strain plotted to obtain bulk unloading modulus K_u (BULK). Fit drawn to initial unloading.

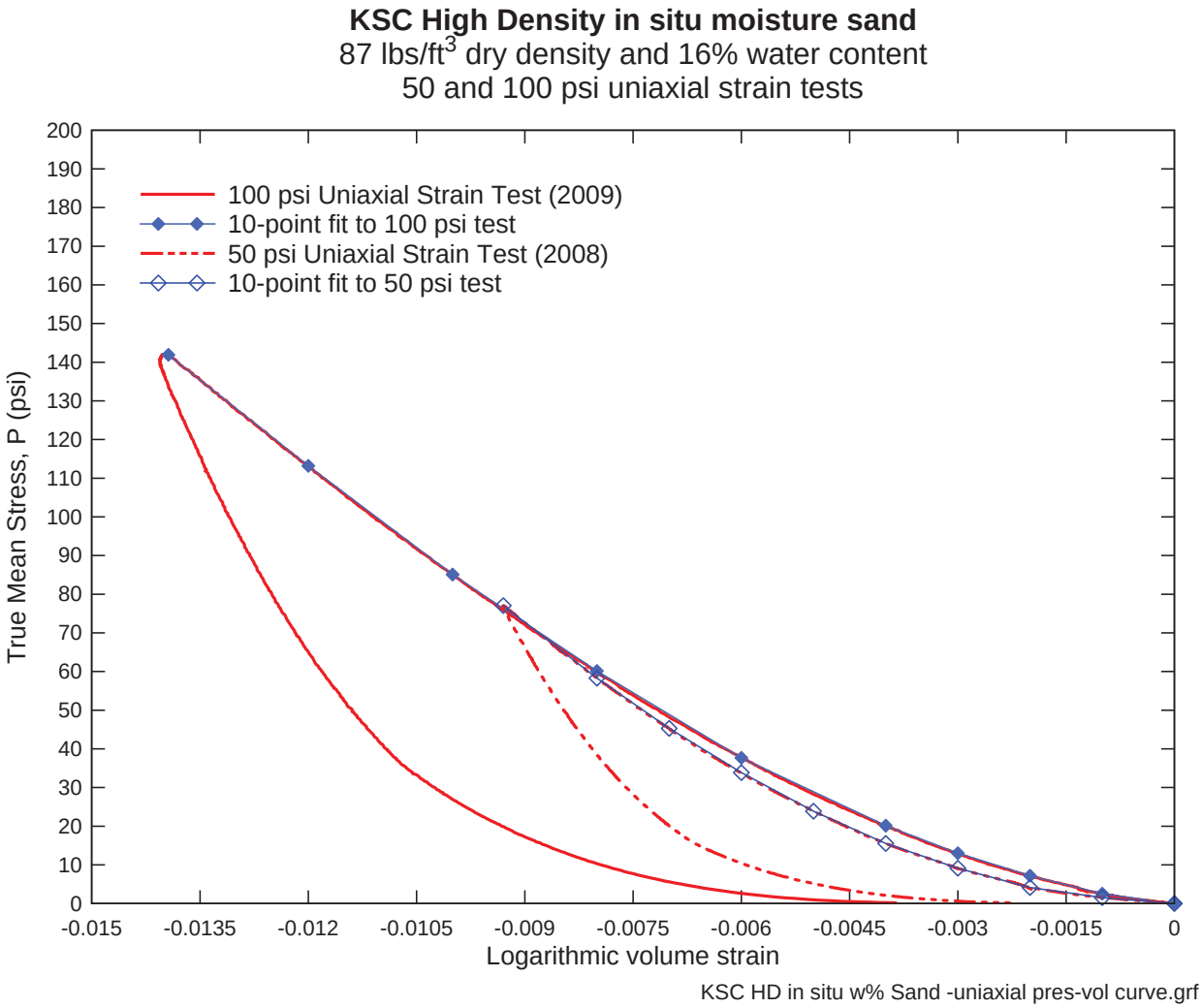

Figure 5-13: KSC HDI Sand model's uniaxial strain tests. Mean stress vs. logarithmic volume strain plotted to obtain 10 pressure-volume points for Material Model 5 compressibility curve.

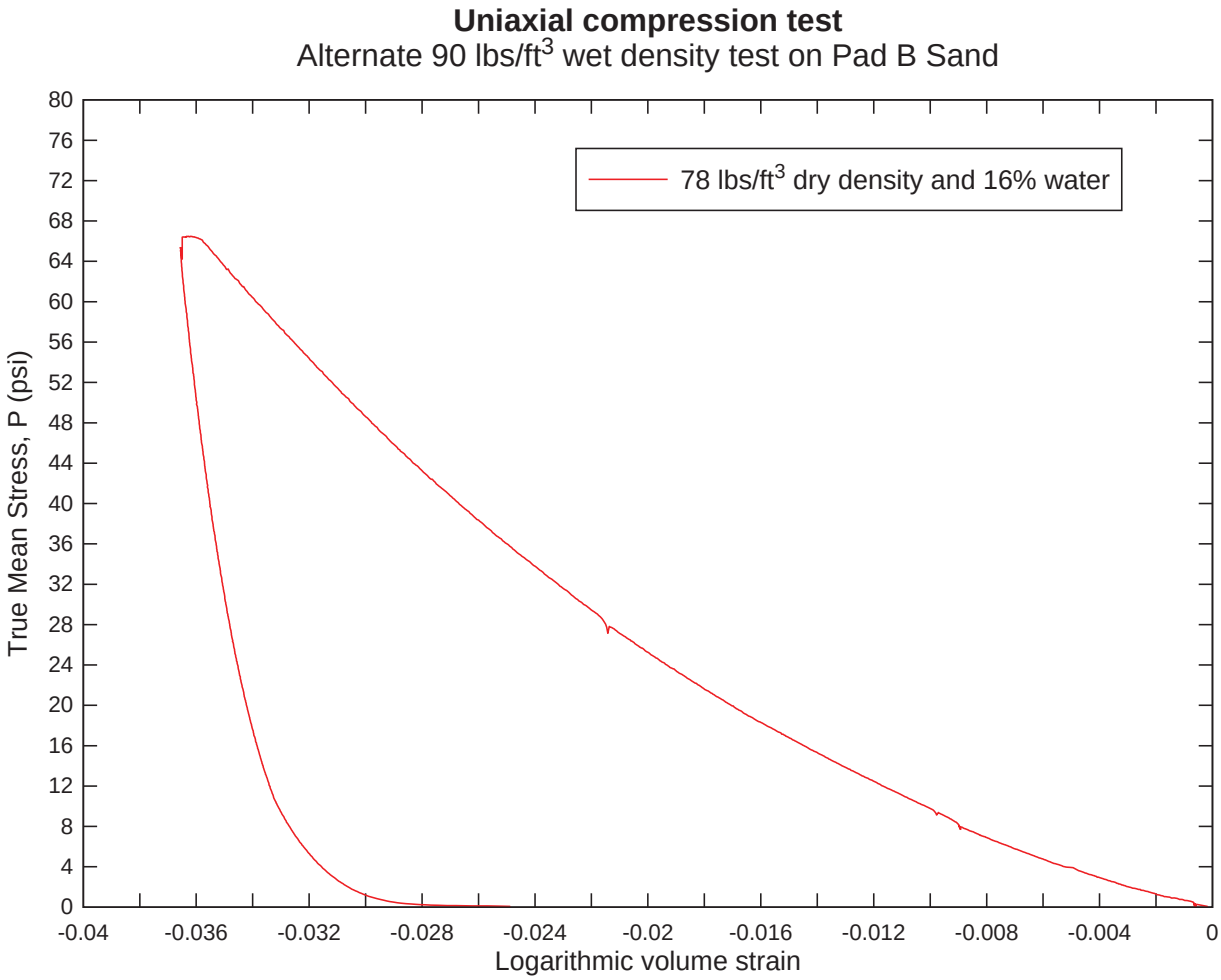

Figure 5-14: Alternate test run on Pad B sample material at 90 lbs/ft^3 wet density (see Table 5-3). This condition was not used to construct the KSC HDI Sand model.

5.4 LS-DYNA Material Model 5 inputs

The recommended set of inputs for modeling KSC HDI Sand at 87 lbs/ft^3 dry density and 16% water content in LS-DYNA Material Model 5: Soil and Foam is shown in the table below. The pressure-volume points are based on the 100 psi uniaxial test.

Table 5-4: Material Model 5 inputs for KSC HDI Sand

	Input	Value	Units
Mass density	**RO**	0.000150	lb s^2/in^4
Shear modulus	**G**	1407	psi
Bulk unloading modulus	**K**	43428	psi
Yield surface coefficient	**A0**	1.421	psi^2
Yield surface coefficient	**A1**	1.734	psi
Yield surface coefficient	**A2**	0.529	-
Pressure cutoff	**PC**	-1.0	psi

	Input	Value	Input	Value	Units
Pressure-volume point	**EPS1**	0	**P1**	0	psi
Pressure-volume point	**EPS2**	-0.001	**P2**	2.537	psi
Pressure-volume point	**EPS3**	-0.002	**P3**	7.191	psi
Pressure-volume point	**EPS4**	-0.003	**P4**	13.00	psi
Pressure-volume point	**EPS5**	-0.004	**P5**	20.12	psi
Pressure-volume point	**EPS6**	-0.006	**P6**	37.68	psi
Pressure-volume point	**EPS7**	-0.008	**P7**	60.14	psi
Pressure-volume point	**EPS8**	-0.010	**P8**	85.07	psi
Pressure-volume point	**EPS9**	-0.012	**P9**	113.2	psi
Pressure-volume point	**EPS10**	-0.01394	**P10**	141.9	psi

Table 5-5: Summary of elastic constants

Young's Modulus E	3594	psi
Poisson's Ratio ν	0.277	
Shear Modulus G	1407	psi
Initial Bulk Modulus K	2537	psi
Constrained Modulus M	4562	psi

6 Mason Sand at 97/4%

Mason Sand is the surrogate KSC sand used at the Orion boilerplate drop test site at LaRC. ARA produced four Mason Sand models at four distinct conditions. This chapter describes the Mason Sand model at 97 lbs/ft^3 dry density and 4% water content.

6.1 Laboratory test data

LaRC identified three locally available sands for purchase and requested ARA perform grain size analysis to identify the closest one to KSC sands. The results are shown in Figure 6-2. The Yorktown Mason Sand was the closest match to KSC Pad A sand. The coefficient of uniformity was the closest, and both were sub-angular to sub-rounded particle shape. After the Mason Sand was selected for use in the Orion boilerplate drop tests, ARA performed minimum and maximum density analysis. ARA dried the Mason Sand and carefully placed it into a 4 inch diameter by 8 inch tall cylinder to achieve the lowest density in that volume. ARA also compacted the dried sand in one inch lifts to achieve the maximum density. The results are shown in Table 6-1. Although similar in grain size distribution, Mason Sand's density values vary considerably from KSC LDD sand because the shell fragments in KSC LDD reduce the density. These fragments are much larger than the sand grains and are lower than the grain density (see Figure 6-1).

Table 6-1: Minimum and maximum density of Mason Sand

Based on 4"x8" cylinder mold	**Minimum**	**Maximum**
Dry Density (lbs/ft^3)	92.5	107.8

Figure 6-1: KSC LDD (left) and Mason Sand (right) visual comparison. Note the shell fragments in the KSC LDD sand.

ARA conducted five triaxial tests and two uniaxial tests for this Mason Sand model. The triaxial confining pressures were 10, 20, 50, 75, and 100 psi. The second uniaxial test was run at 96 lbs/ft^3, which was an early exploratory test to investigate the effects of lower density. There was

also a 100 psi hydrostatic compression test which unloaded and reloaded at 50 and 100 psi. The test log for Mason Sand at 97 lbs/ft^3 dry density and 4% water content is shown in Table 6-2.

Table 6-2: Test log for Mason Sand at 97/4%

Test ID	Sample ID	Type	Confining Pressure (psi)	Moisture content	Wet Density (lbs/ft^3)	Dry Density (lbs/ft^3)
L28B09	Mason Sand	Triax	10	4.16%	100.88	96.85
L29B09	Mason Sand	Triax	20	4.08%	100.88	96.92
L31E09	Mason Sand	Triax	50	4.04%	100.88	96.96
G3B09	Mason Sand	Triax	75	3.97%	100.88	97.02
G4G09	Mason Sand	Triax	100	4.01%	100.88	96.99
G25A09	Mason Sand	Uniax	100	4.05%	100.88	96.95
L14C09	*Mason Sand*	*Uniax*	*100*	*4.07%*	***99.84***	*95.94*

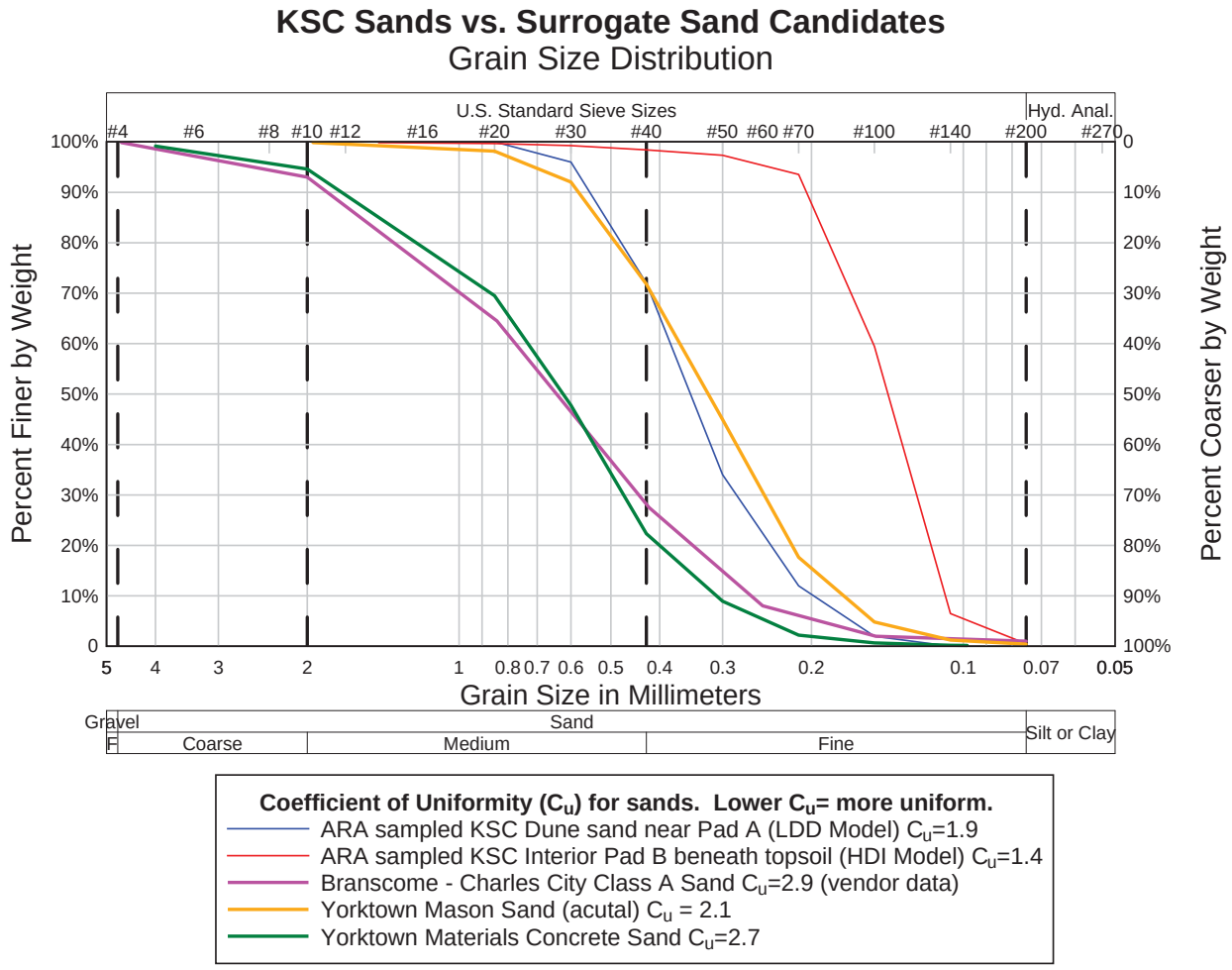

Figure 6-2: Grain size distribution for KSC surrogate sand candidates

6.1.1 Correlating Mason Sand to "Clean Sand" from 2008

LaRC also asked ARA to compare some sand that was already on-site at the gantry facility to the Mason Sand. This sand was tested and referred to as "clean sand" in the 2008 report. LaRC wished to ascertain the source of this sand by comparing the grain size distributions. The sand's vendor source was unknown. A new 2009 sample was taken and compared to the actual Mason Sand sample, as well as the older 2008 clean sand sample. The results of the analysis are shown in Figure 6-3. The clean sand is most likely the same as Mason Sand because it displays remarkably similar distributions.

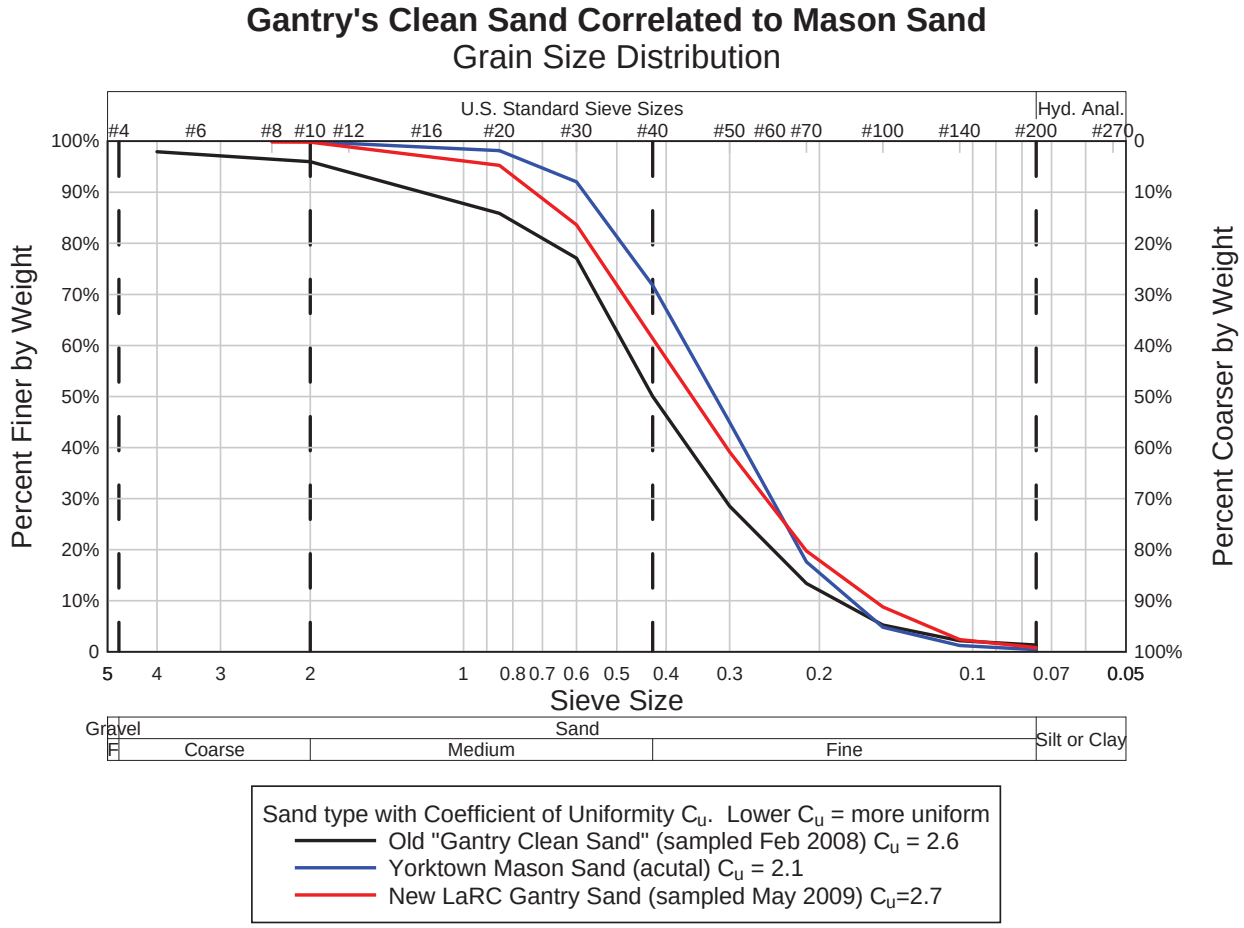

Figure 6-3: Correlation of Mason Sand and Gantry "Clean Sand".

6.1.2 Triaxial compression

ARA performed five triaxial tests for each condition of Mason Sand. Results are shown in Figure 6-3 through Figure 6-14. In Figure 6-14, the slightly denser 97 lbs/ft^3 was less stiff at mean stresses above ~30 psi than the 96 lbs/ft^3 sand. We believe this is due to natural variations of the material and experimental accuracies.

Figure 6-4 illustrates the physical deformation of the Mason Sand specimen after the triaxial test is complete. The zoom boxes show the radial strain gage before and after the test.

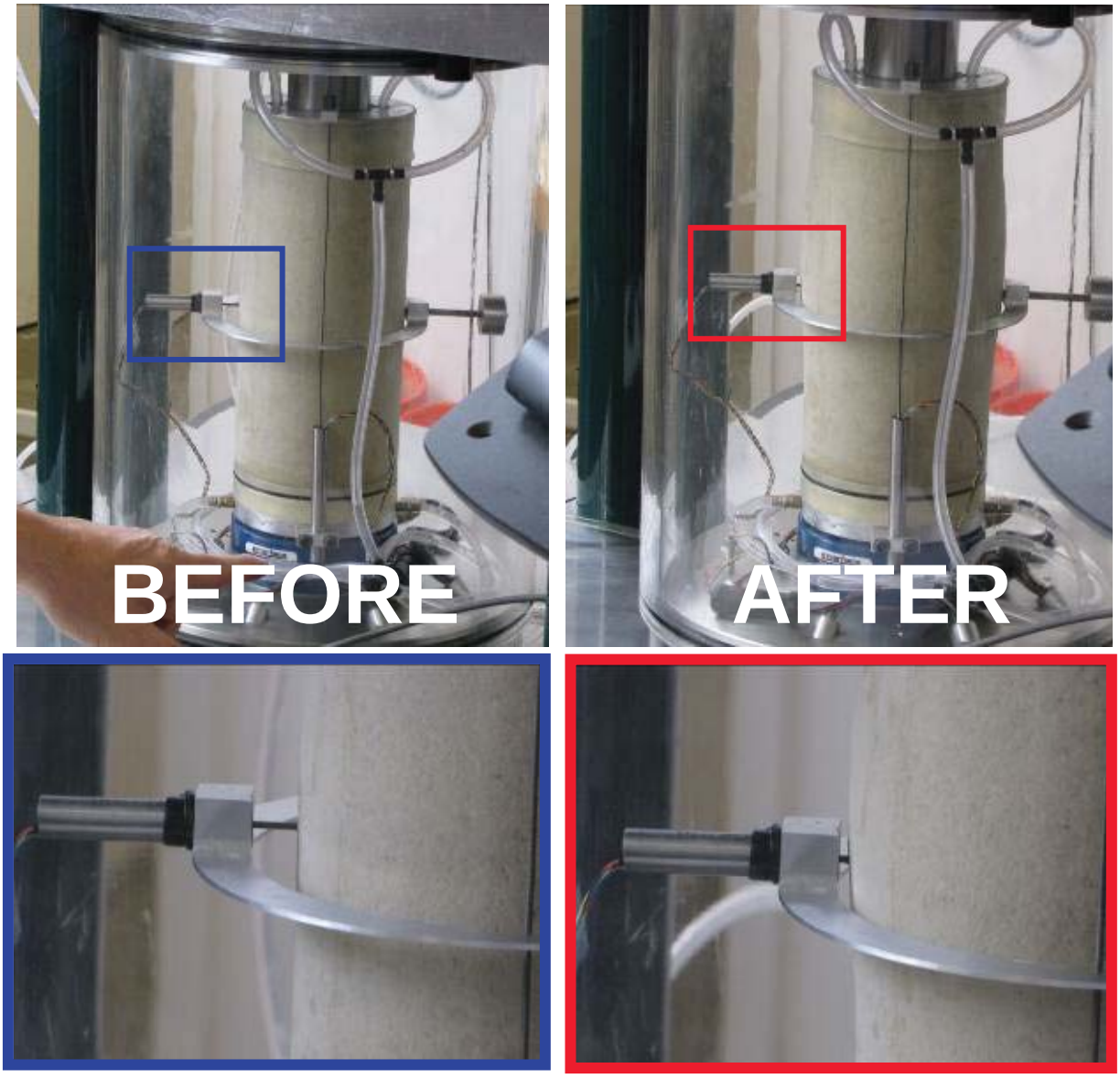

Figure 6-4: Photographs of Mason Sand triaxial test

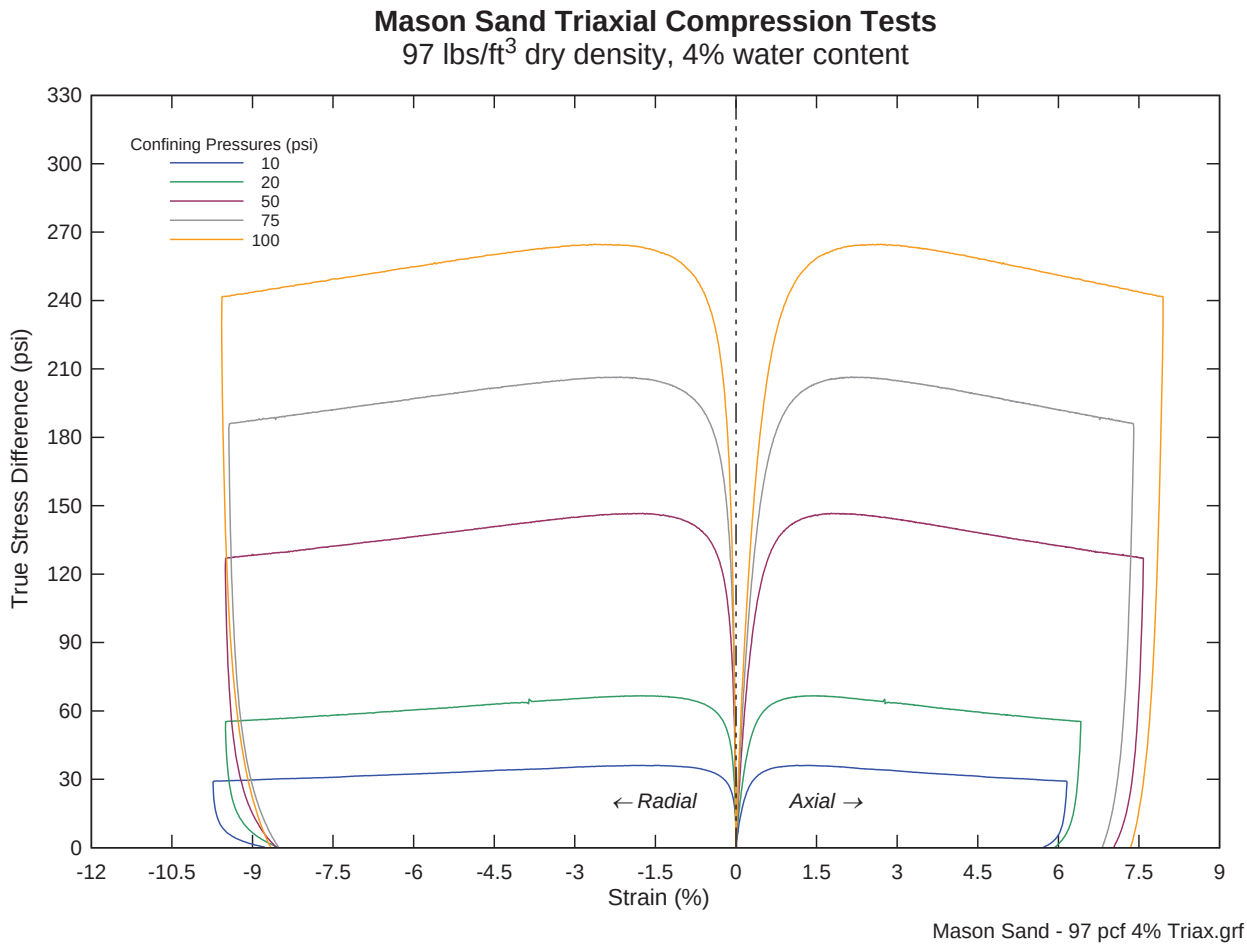

Figure 6-5: Mason Sand triaxial test results for 10, 20, 50, 75, and 100 psi confining pressures.

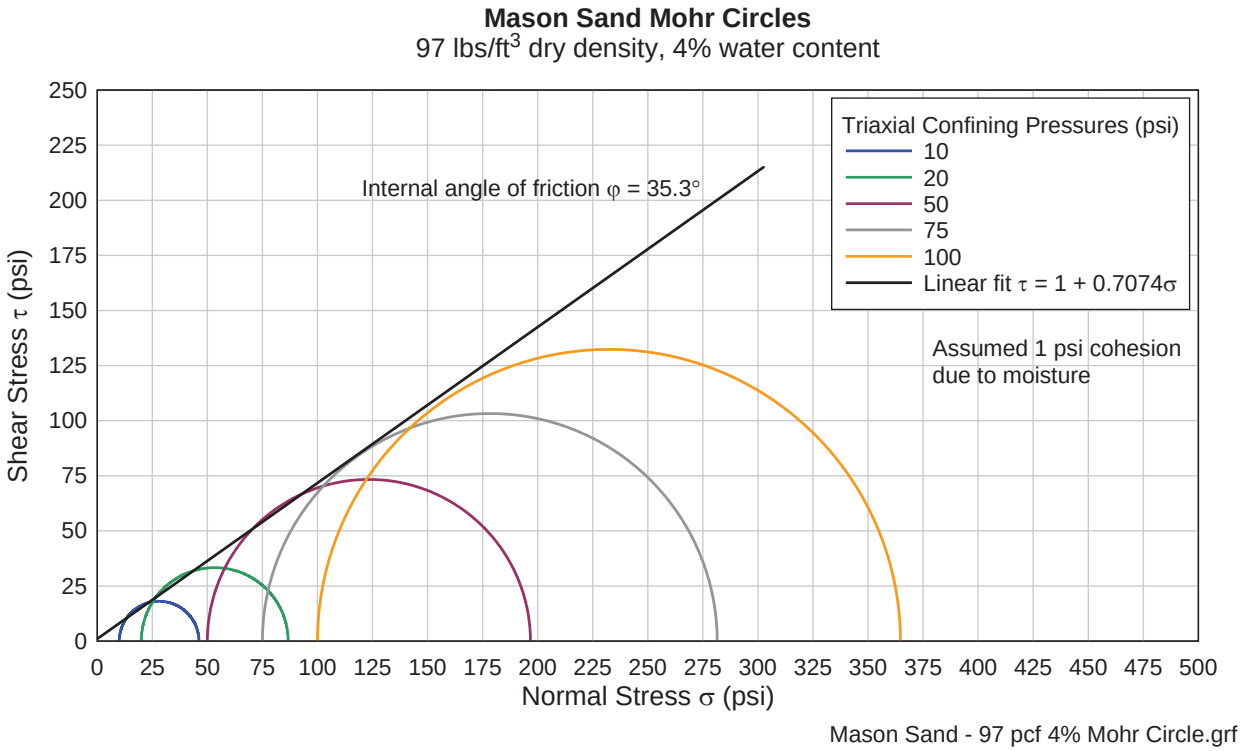

Figure 6-6: Mohr circles based on Mason Sand's triaxial tests

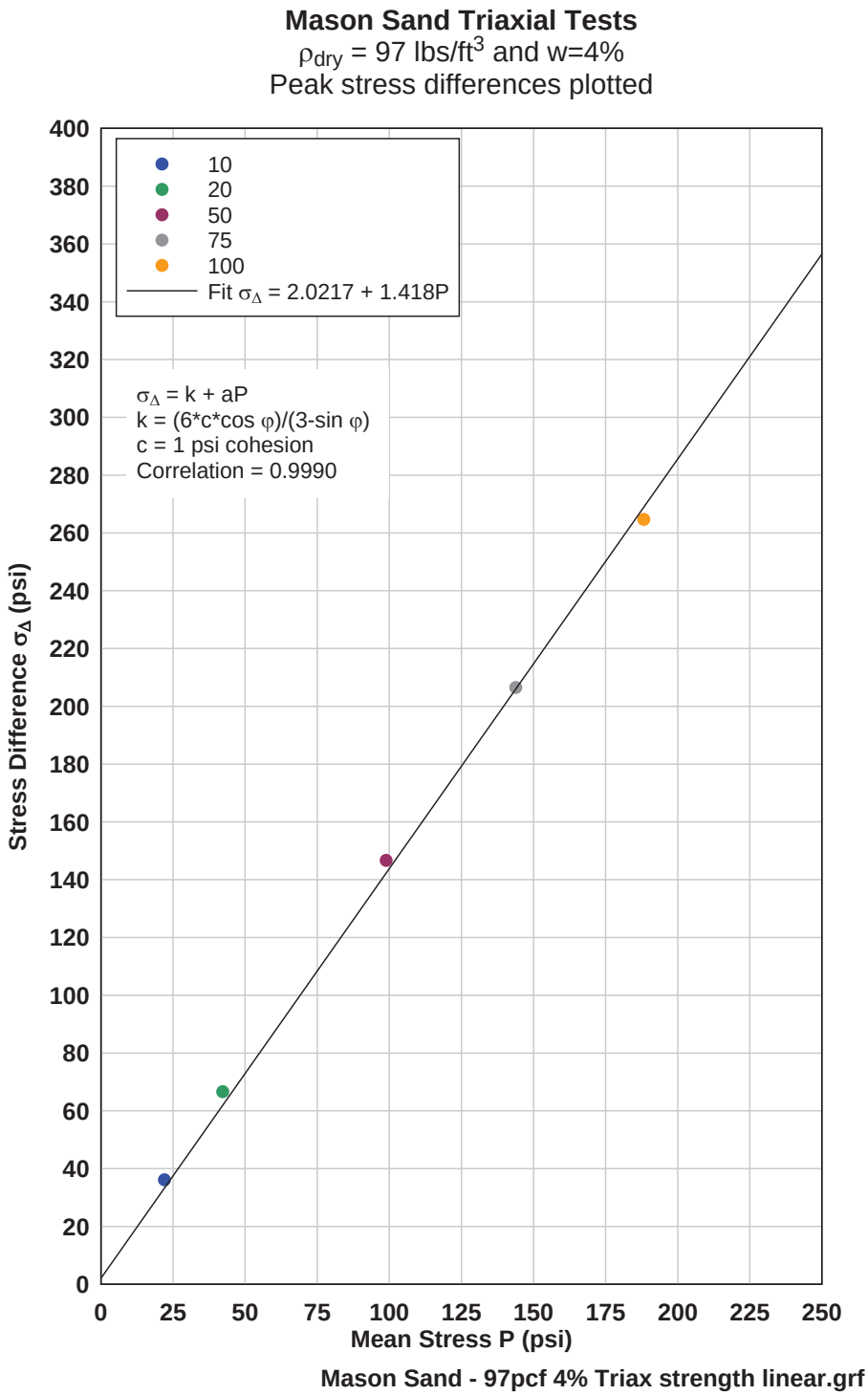

Figure 6-7: Mason Sand strength envelope results.

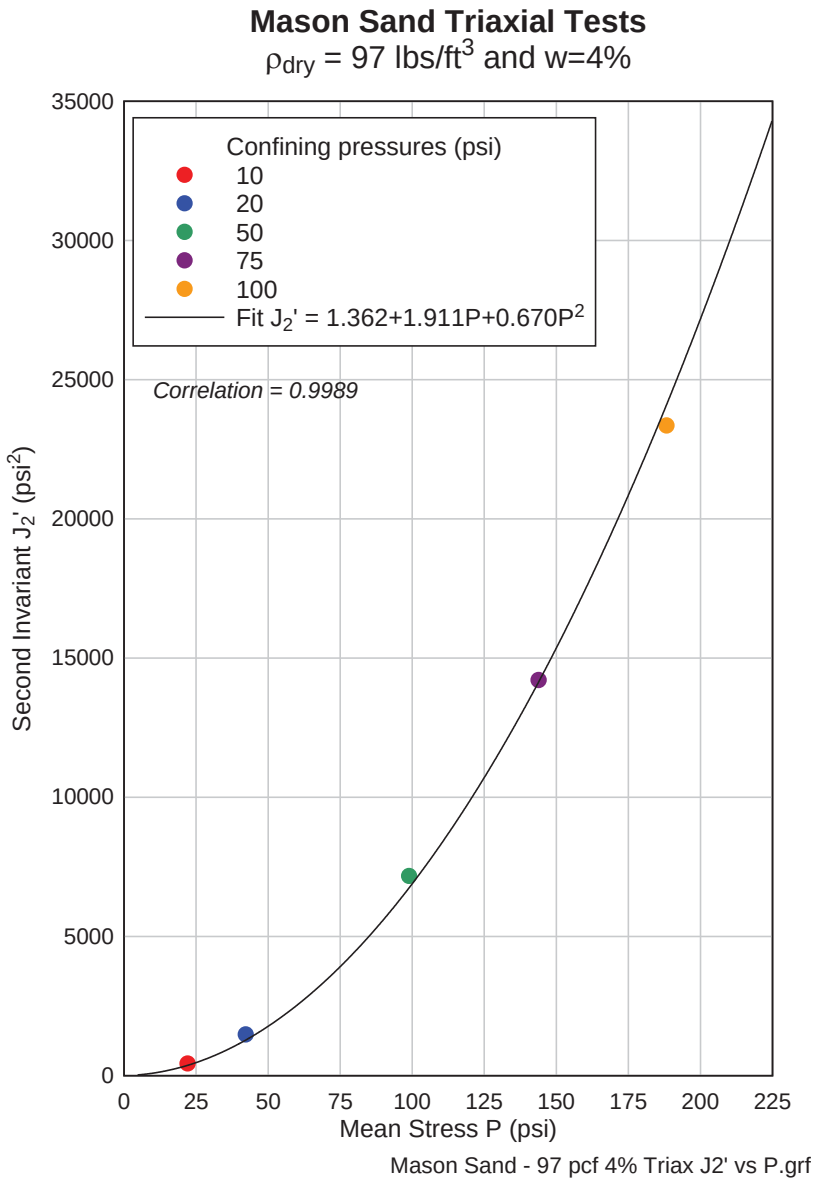

Figure 6-8: Mason Sand Material Model 5 yield surface fit from triaxial test data.

6.1.3 Hydrostatic compression

Following the loading prescription for KSC sands, the Mason Sands were hydrostatically compressed to 50 psi and unloaded to zero pressure. Then, they were loaded to 100 psi and unloaded again. Finally, they were returned to 100 psi for a second time. The hydrostatic loading preceded each of the triaxial tests. Figure 6-9 is the hydrostatic compression test preceding the 100 psi triaxial strength test.

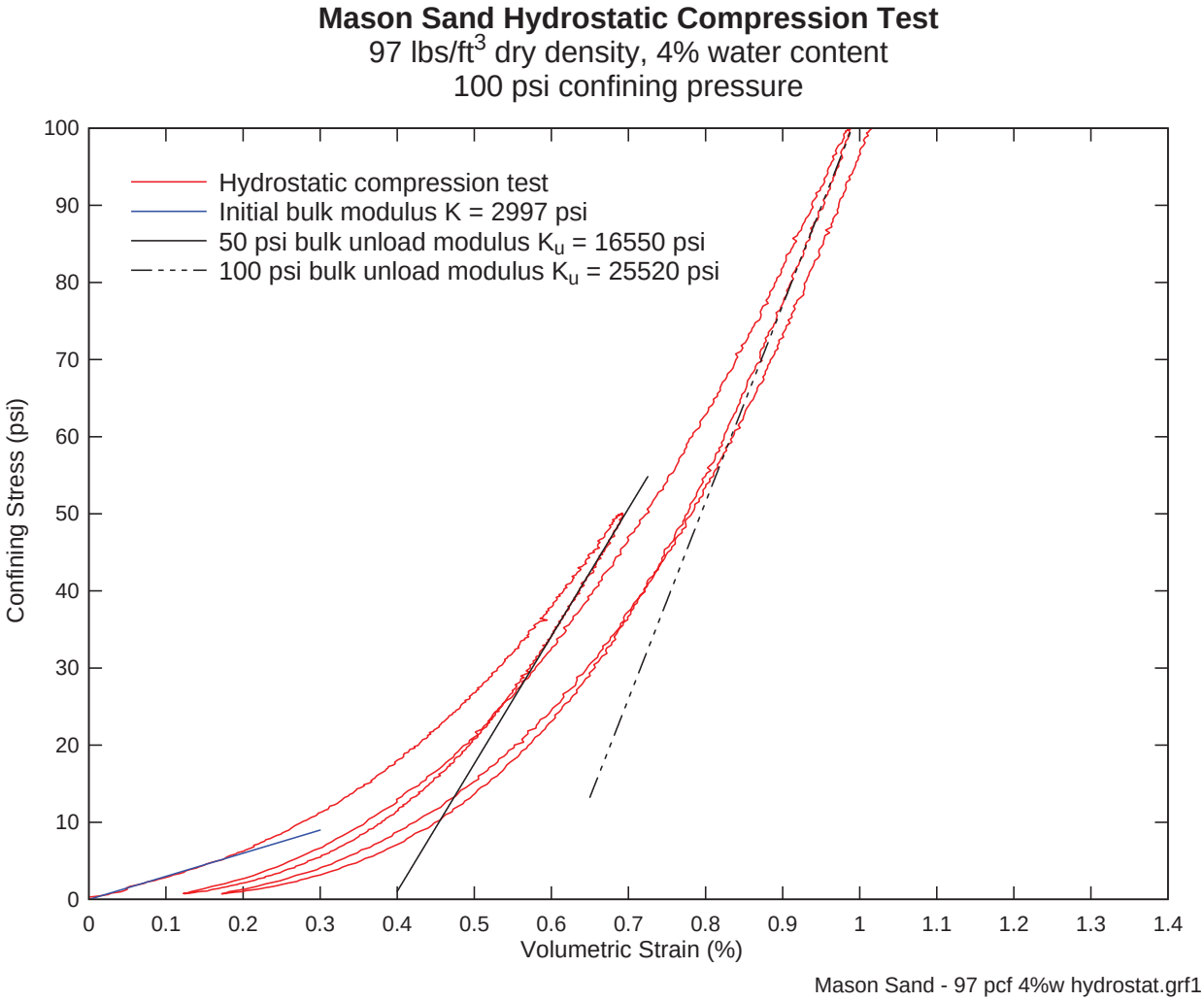

Figure 6-9: 100 psi hydrostatic compression test of Mason Sand at 97/4% condition. Hydrostatic fits drawn.

6.1.4 Uniaxial strain

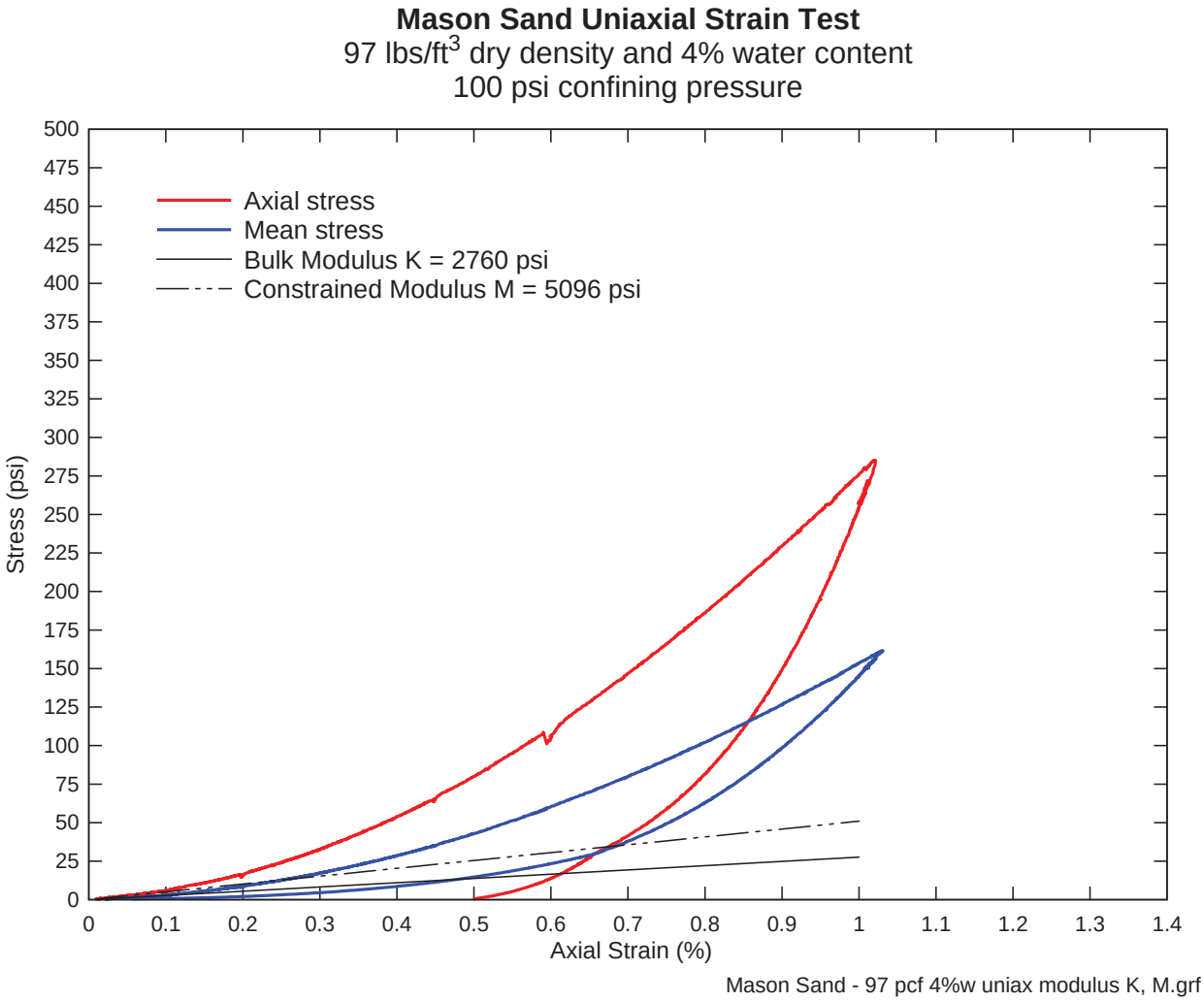

Figure 6-10: Mason Sand uniaxial strain test results. Constrained and bulk moduli fits shown.

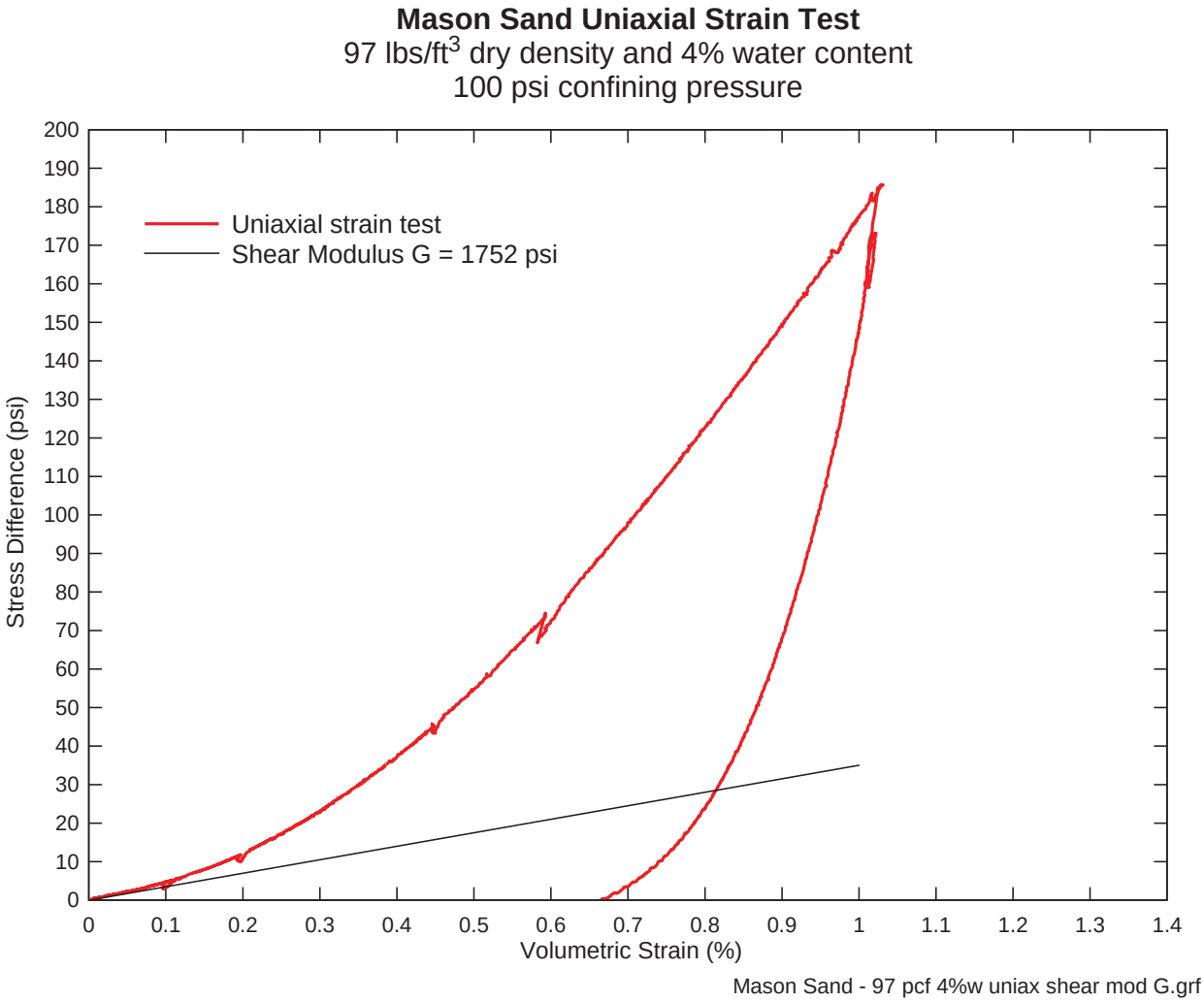

Figure 6-11: Mason Sand uniaxial strain test results plotted as stress difference vs. strain. Shear modulus G fit shown. Shear stress is half of stress difference. Uniaxial strain is equal to shear strain.

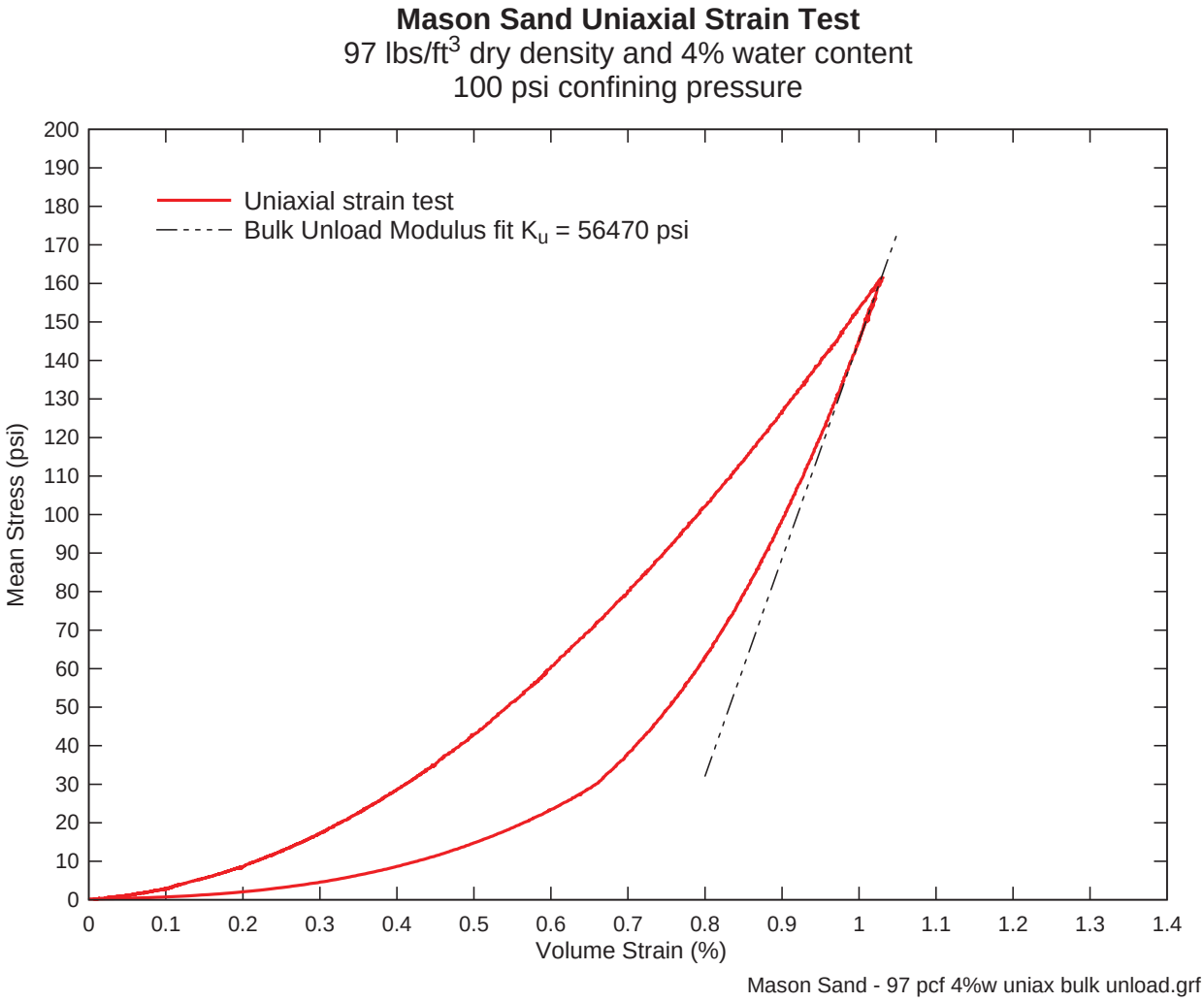

Figure 6-12: Mason Sand uniaxial strain unloading portion. Determination of bulk unloading modulus K_u (BULK) by linear fit.

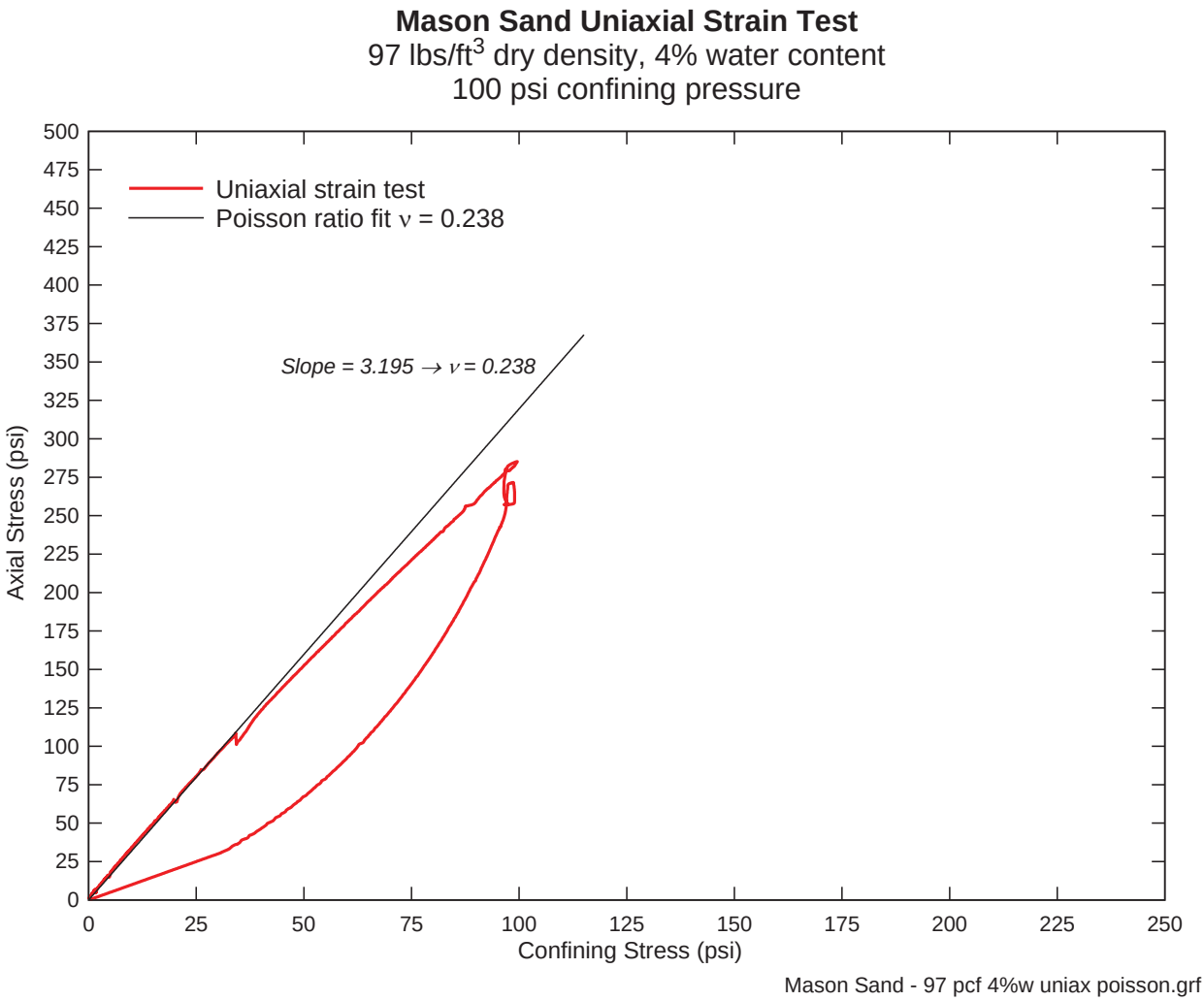

Figure 6-13: Determination of Poisson's ratio via uniaxial strain test.

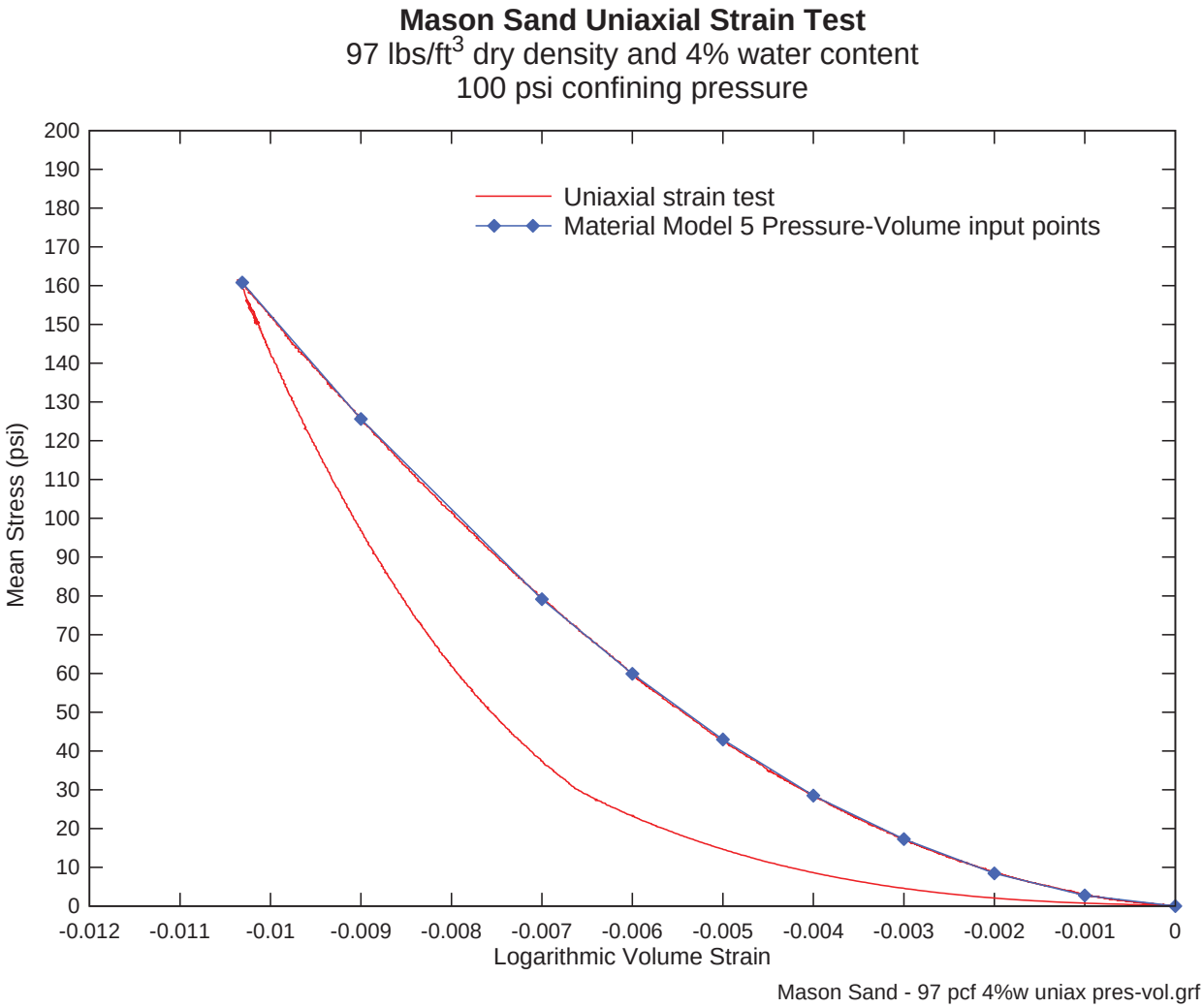

Figure 6-14: Mason Sand Material Model 5 pressure-logarithmic volume curve with 10 input points. Obtained from uniaxial strain test.

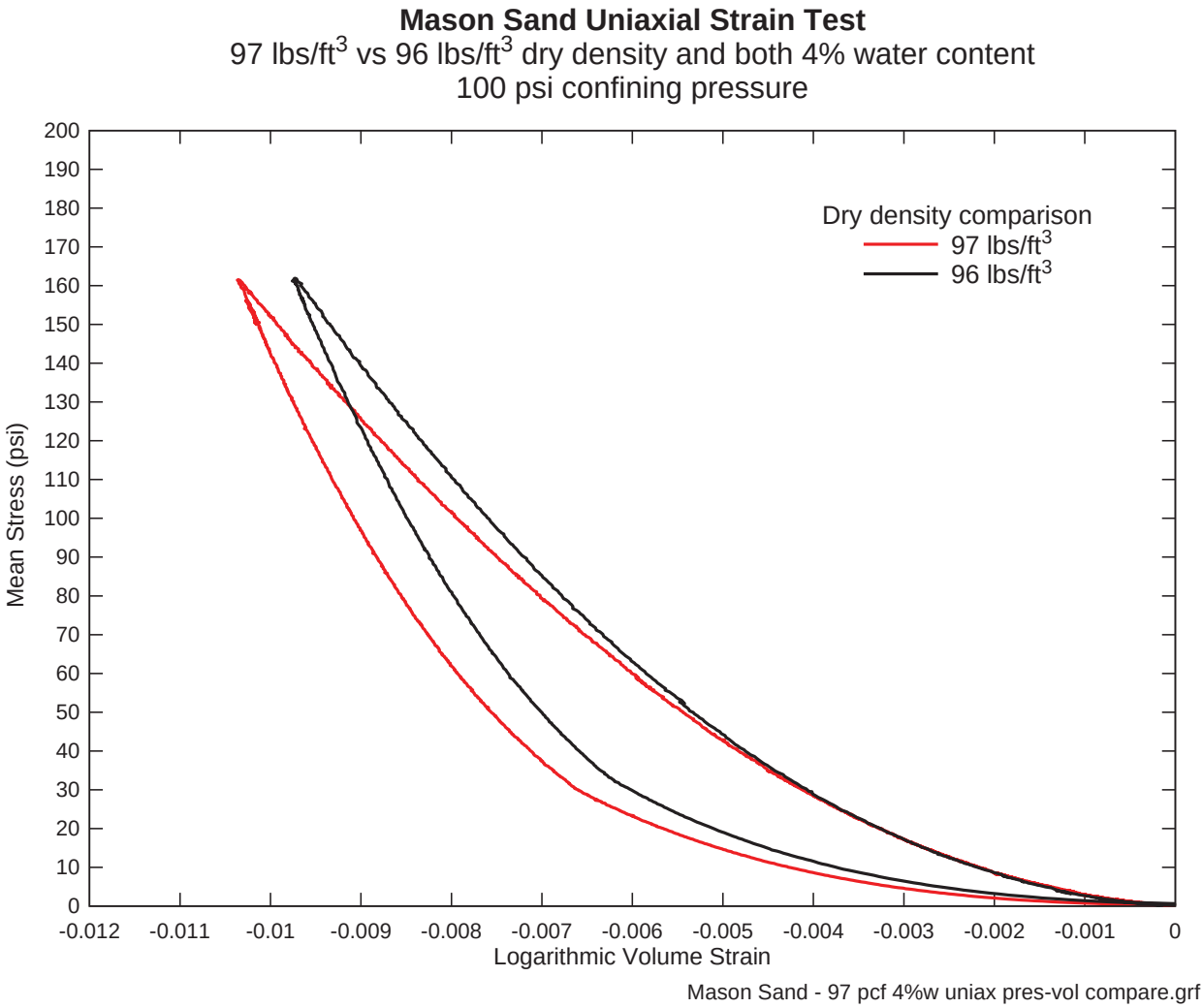

Figure 6-15: Comparison of 96 vs. 97 lbs/ft^3 dry densities at the same 4% water content.

6.2 LS-DYNA Material Model 5 inputs

The recommended set of inputs for modeling Mason Sand at 97 lbs/ft^3 dry density and 4% water content in LS-DYNA Material Model 5: Soil and Foam is shown in the table below.

Table 6-3: Material Model 5 inputs for Mason Sand

	Input	Value	Units
Mass density	**RO**	0.000151	lb s^2/in^4
Shear modulus	**G**	1752	psi
Bulk unloading modulus	**K**	56470	psi
Yield surface coefficient	**A0**	1.362	psi^2
Yield surface coefficient	**A1**	1.911	psi
Yield surface coefficient	**A2**	0.670	-
Pressure cutoff	**PC**	-0.5	psi

	Input	Value	Input	Value	Units
Pressure-volume point	**EPS1**	0	**P1**	0.00	psi
Pressure-volume point	**EPS2**	-0.001	**P2**	2.76	psi
Pressure-volume point	**EPS3**	-0.002	**P3**	8.43	psi
Pressure-volume point	**EPS4**	-0.003	**P4**	17.26	psi
Pressure-volume point	**EPS5**	-0.004	**P5**	28.49	psi
Pressure-volume point	**EPS6**	-0.005	**P6**	42.96	psi
Pressure-volume point	**EPS7**	-0.006	**P7**	59.90	psi
Pressure-volume point	**EPS8**	-0.007	**P8**	79.15	psi
Pressure-volume point	**EPS9**	-0.009	**P9**	125.63	psi
Pressure-volume point	**EPS10**	-0.01031	**P10**	160.80	psi

Table 6-4: Summary of elastic constants

Young's Modulus E	4339	psi
Poisson's Ratio ν	0.238	
Shear Modulus G	1752	psi
Initial Bulk Modulus K	2760	psi
Constrained Modulus M	5096	psi

7 Mason Sand at 96/8%

This chapter describes properties for the Mason Sand model at 96 lbs/ft^3 dry density and 8% water content. The test log is shown in Table 7-1.

Table 7-1: Test log for Mason Sand at 96/8%

Test ID	Sample ID	Type	Confining Pressure (psi)	Moisture content	Wet Density (lbs/ft^3)	Dry Density (lbs/ft^3)
G18B09	Mason Sand	Triax	10	8.04%	103.68	95.97
G19C09	Mason Sand	Triax	20	8.08%	103.68	95.93
G19E09	Mason Sand	Triax	50	7.86%	103.68	96.13
G19G09	Mason Sand	Triax	75	7.83%	103.68	96.16
G20A09	Mason Sand	Hydro	100	8.08%	103.68	95.93
G20B09	Mason Sand	Triax	100	8.08%	103.68	95.93
G21A09	Mason Sand	Uniax	100	8.09%	103.68	95.92

7.1 Triaxial compression

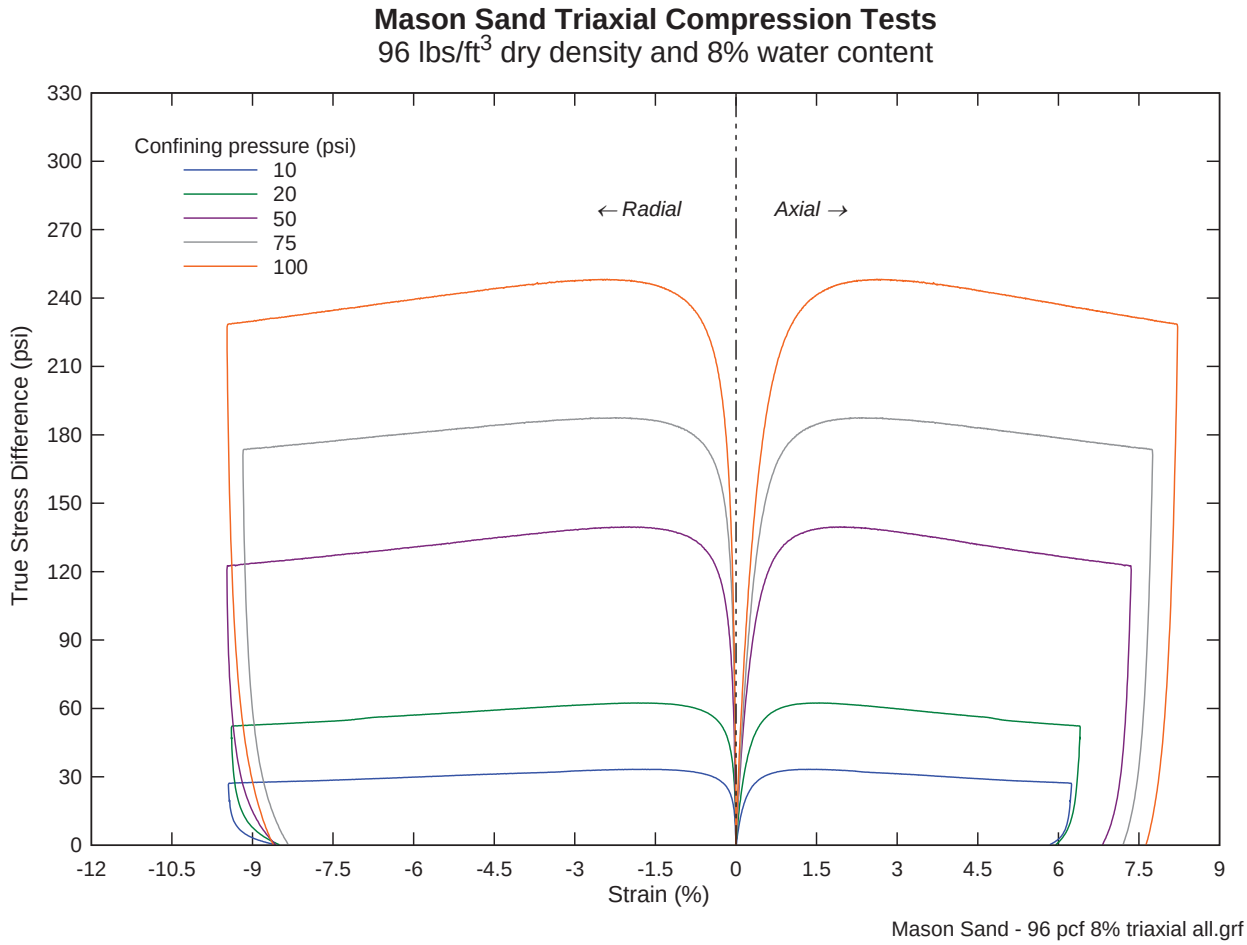

Figure 7-1: Mason Sand triaxial test results for 10, 20, 50, 75, and 100 psi confining pressures.

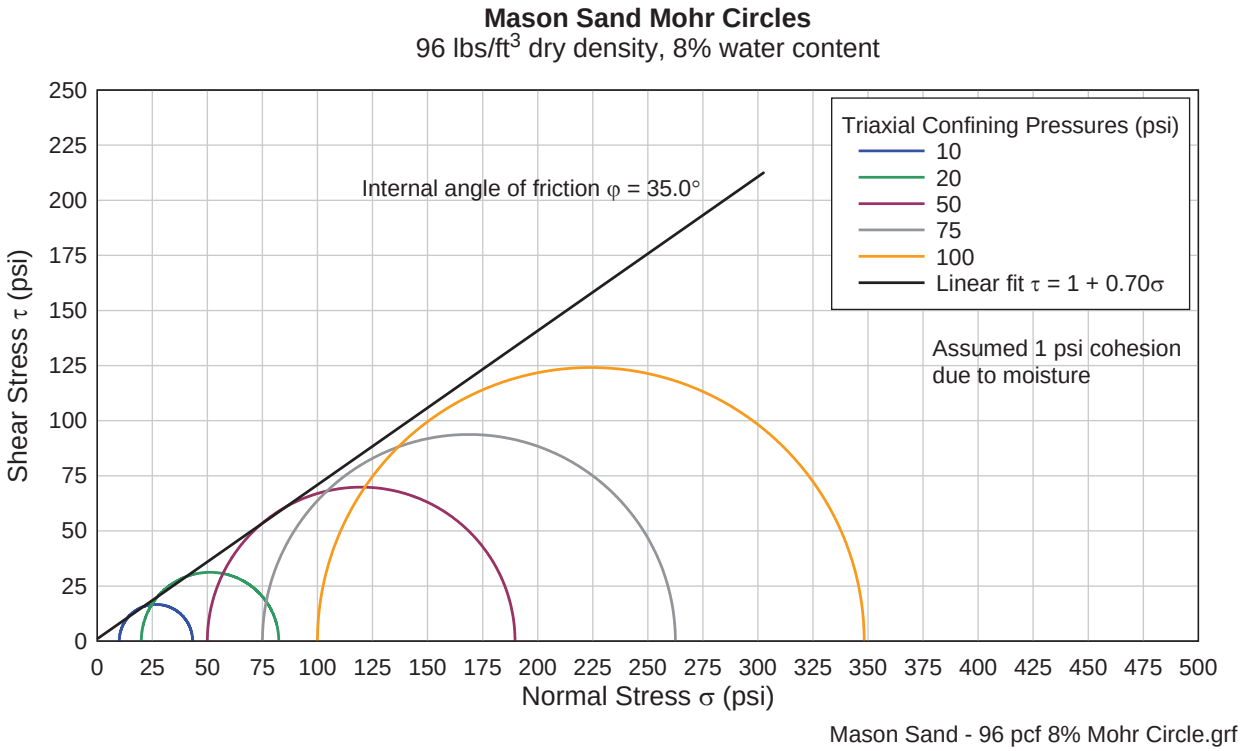

Figure 7-2: Mohr circles based on Mason Sand's triaxial tests

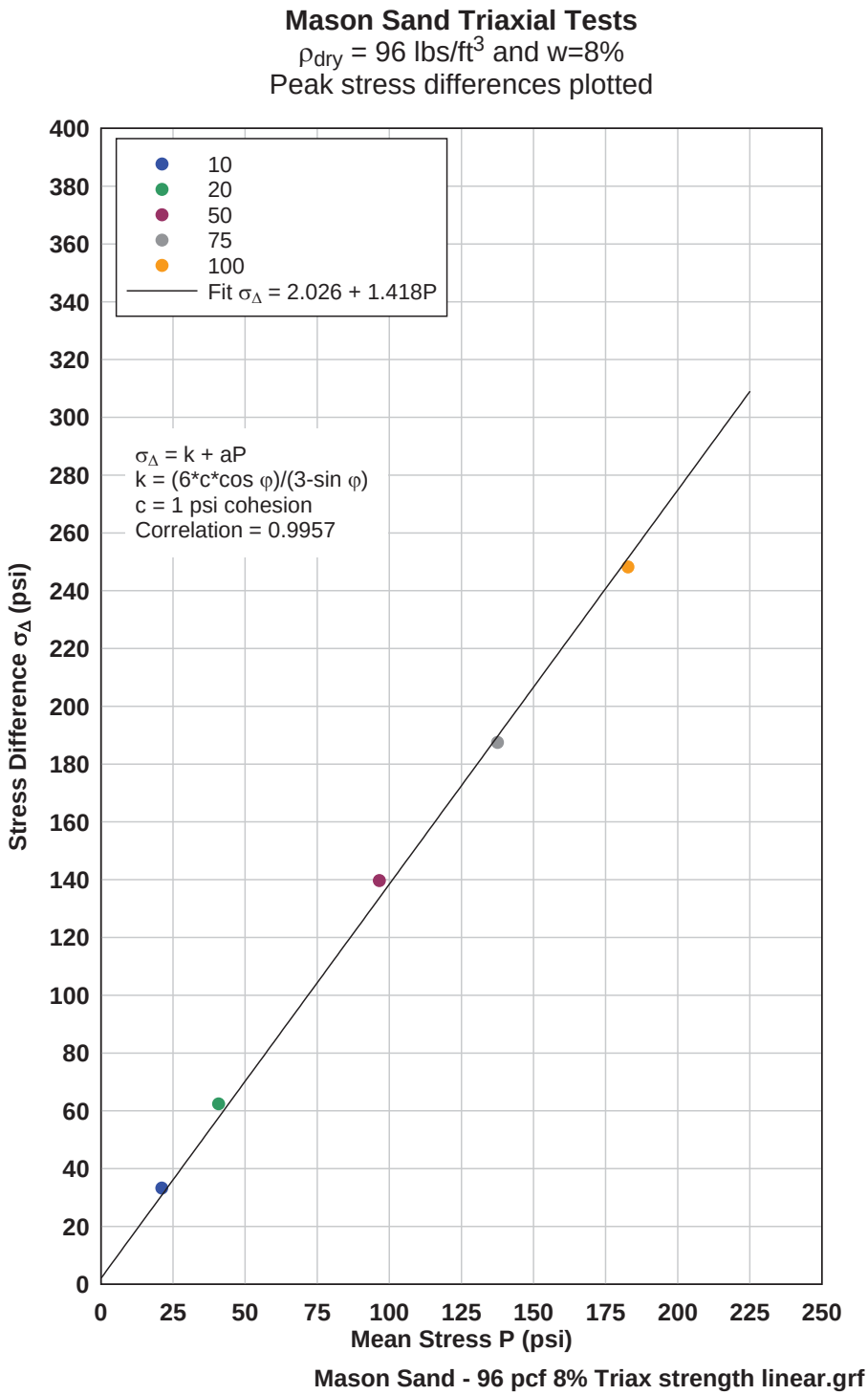

Figure 7-3: Mason Sand strength envelope results.

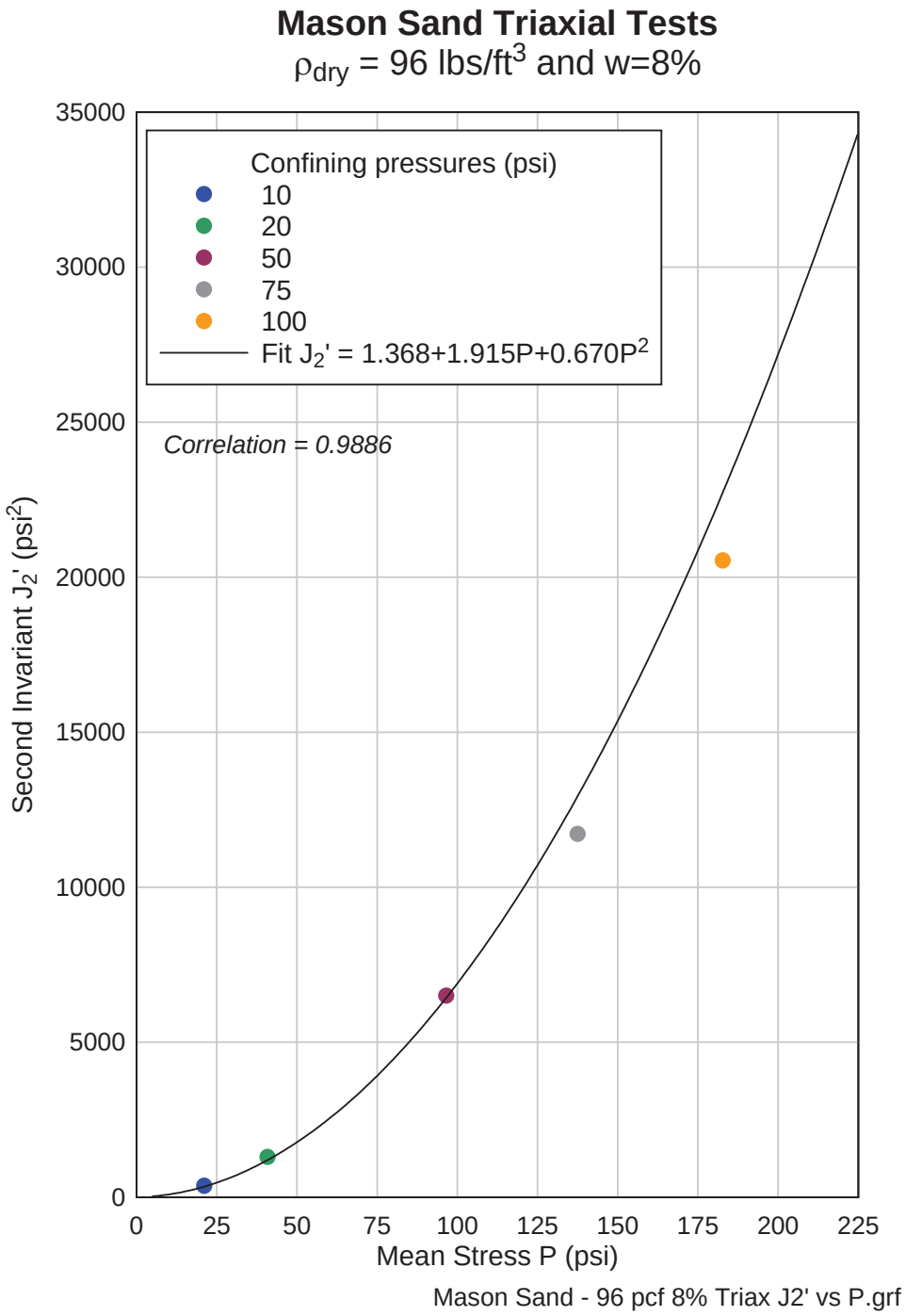

Figure 7-4: Mason Sand Material Model 5 yield surface fit from triaxial test data.

7.2 Hydrostatic compression

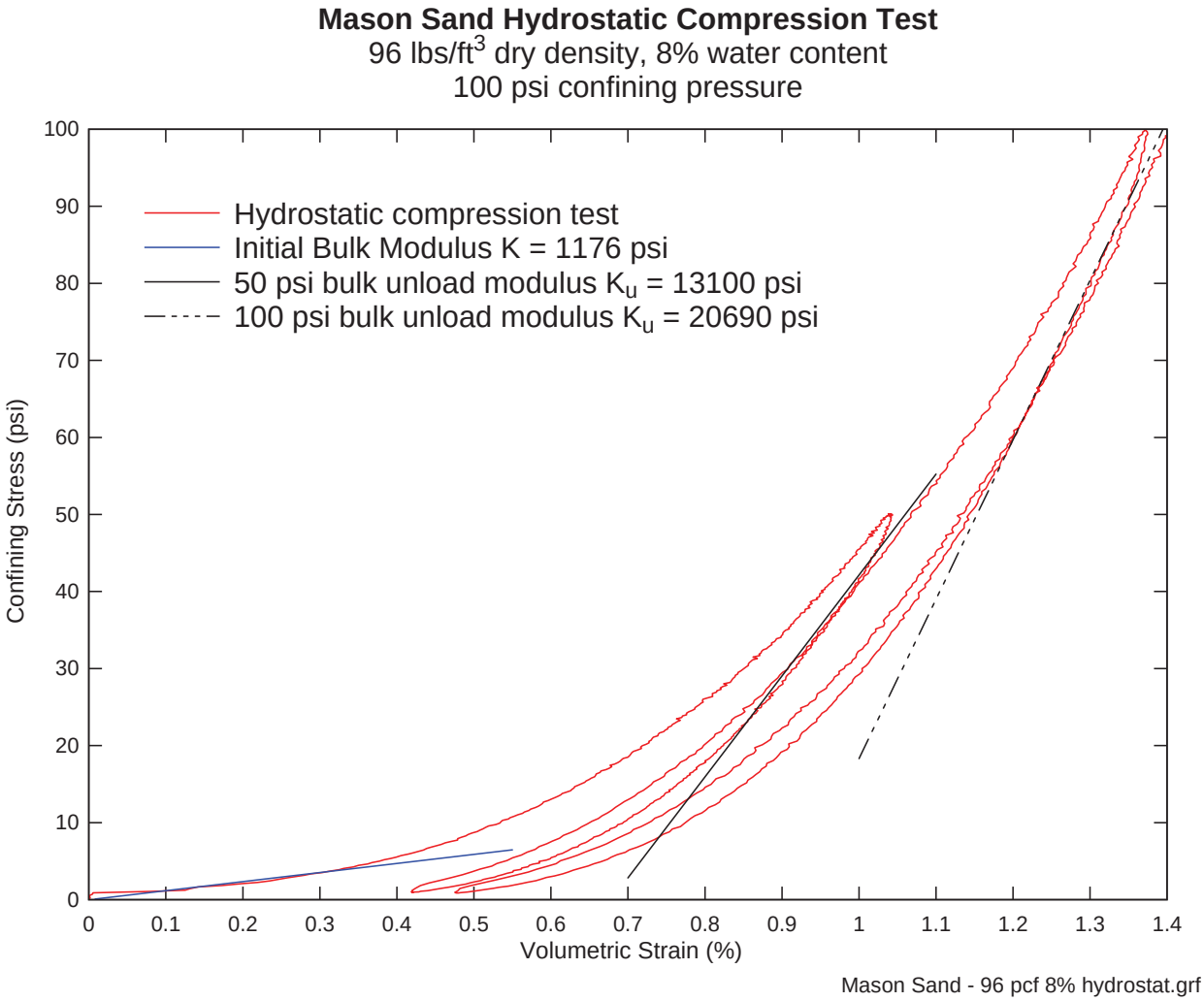

Figure 7-5: 100 psi hydrostatic compression test for Mason Sand at 96/8% condition.

7.3 Uniaxial strain

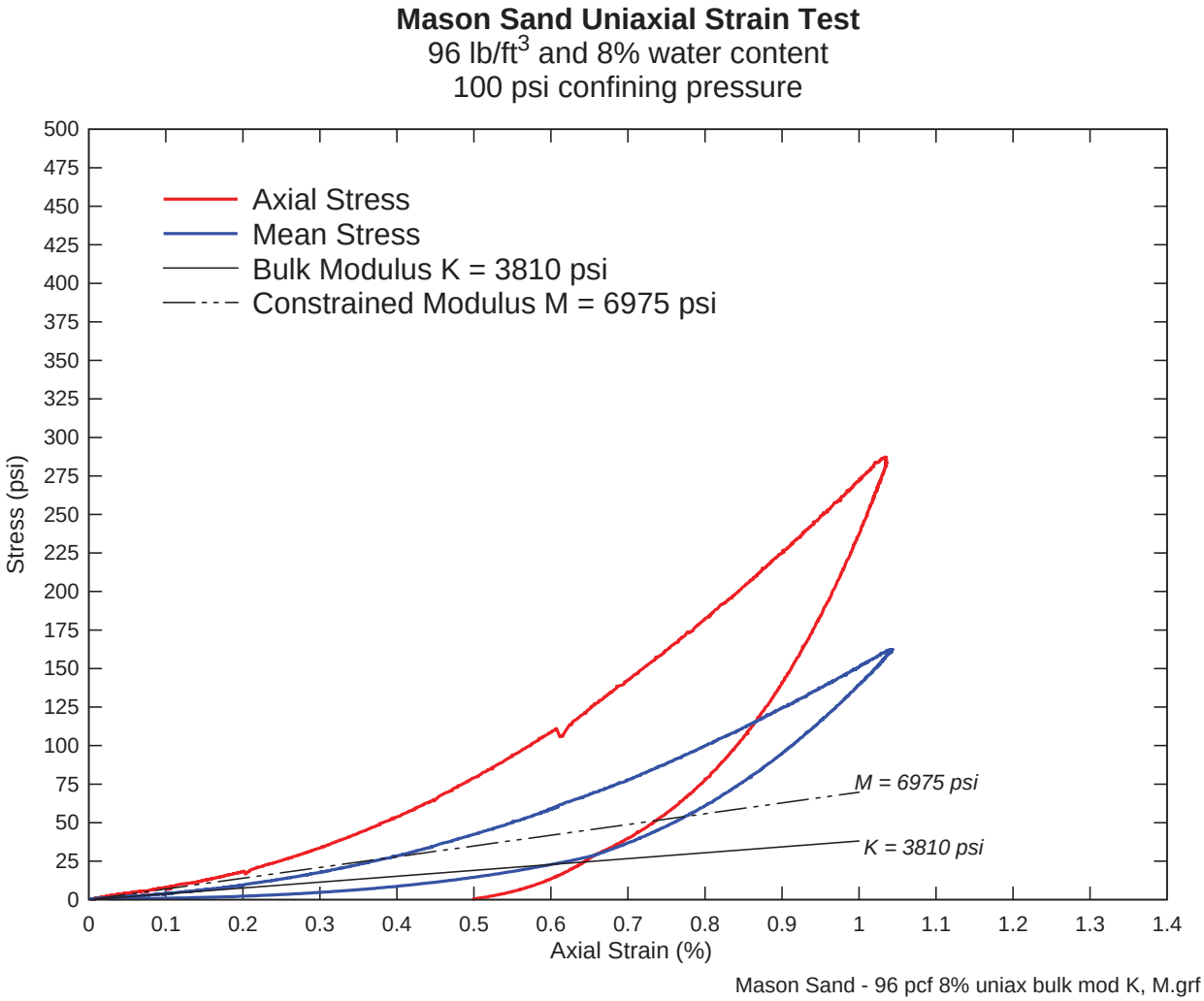

Figure 7-6: Mason Sand uniaxial strain test results. Constrained and bulk moduli fits shown.

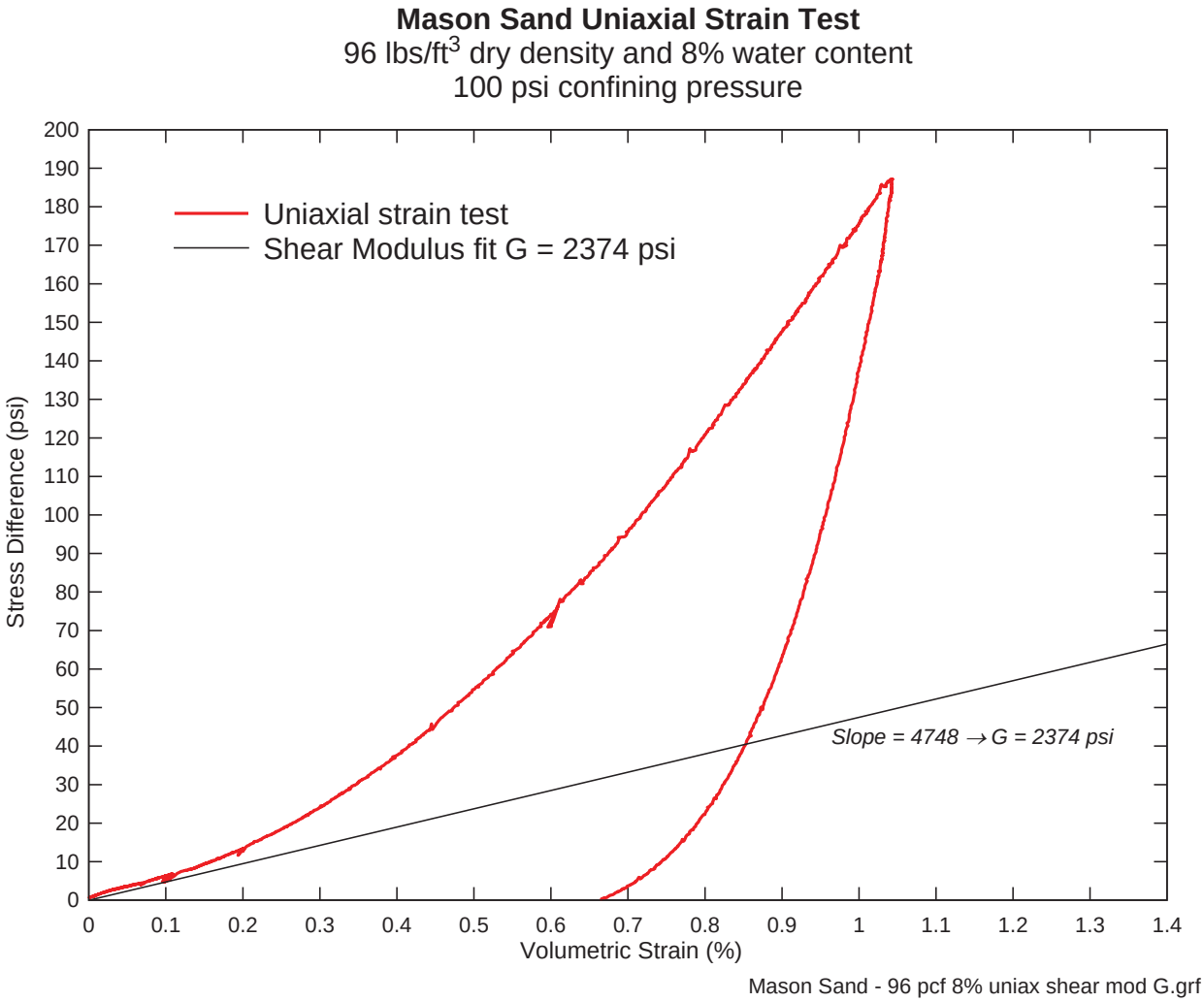

Figure 7-7: Mason Sand uniaxial strain test results plotted as stress difference vs. strain. Shear modulus G fit shown. Shear stress is half of stress difference. Uniaxial strain is equal to shear strain.

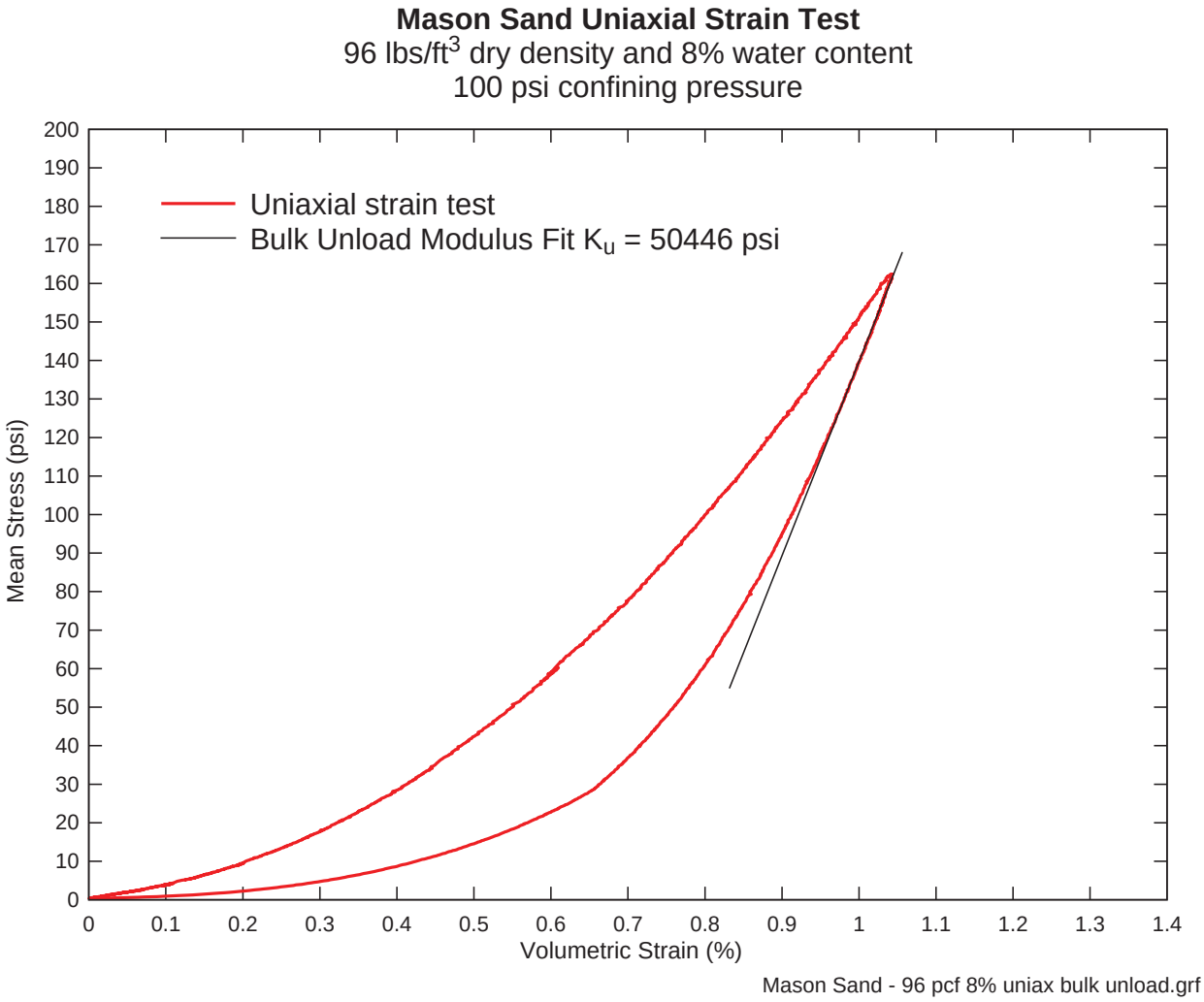

Figure 7-8: Mason Sand uniaxial strain unloading portion. Determination of bulk unloading modulus K_u (BULK) by linear fit to initial unloading portion.

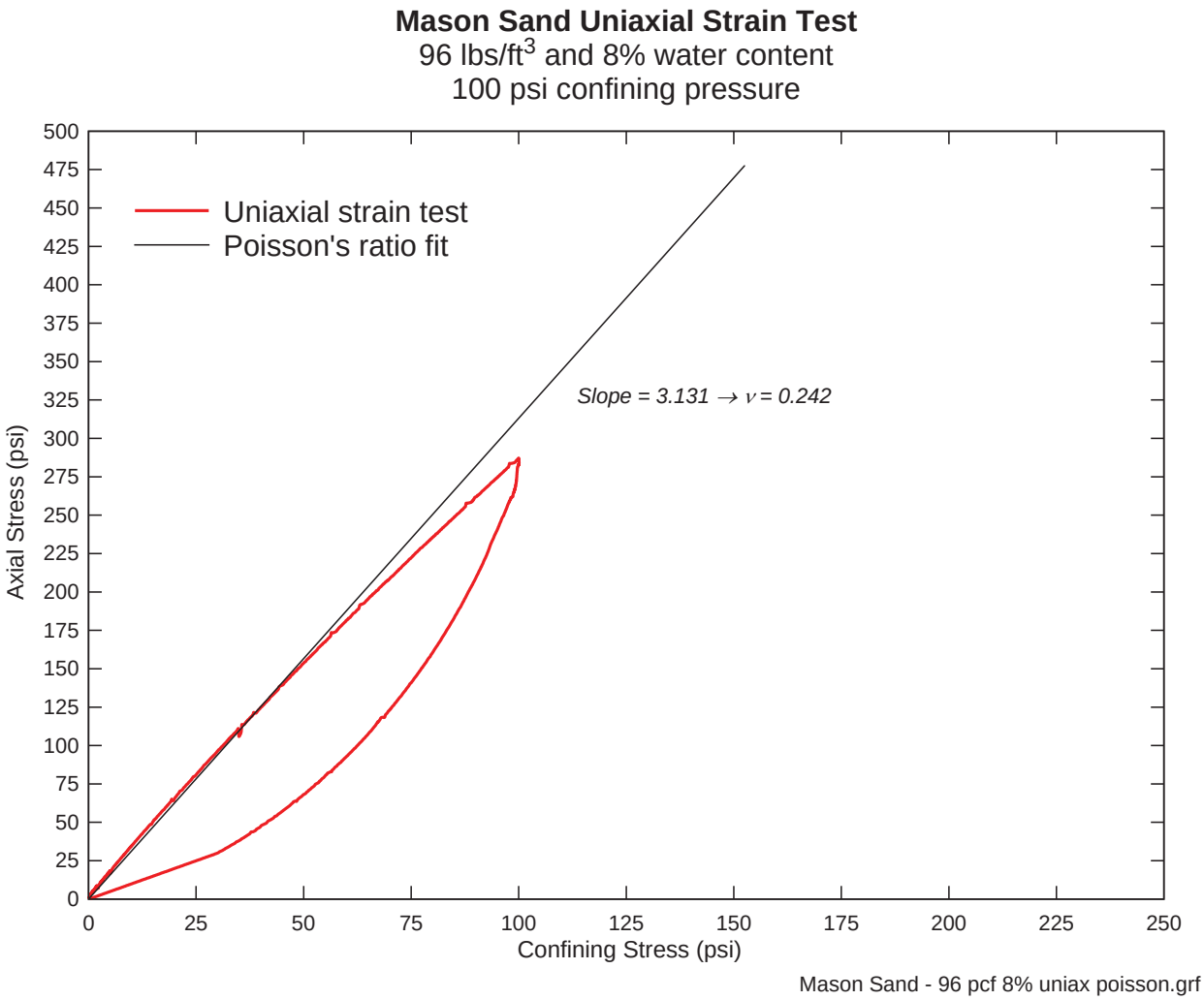

Figure 7-9: Determination of Poisson's ratio via uniaxial strain test.

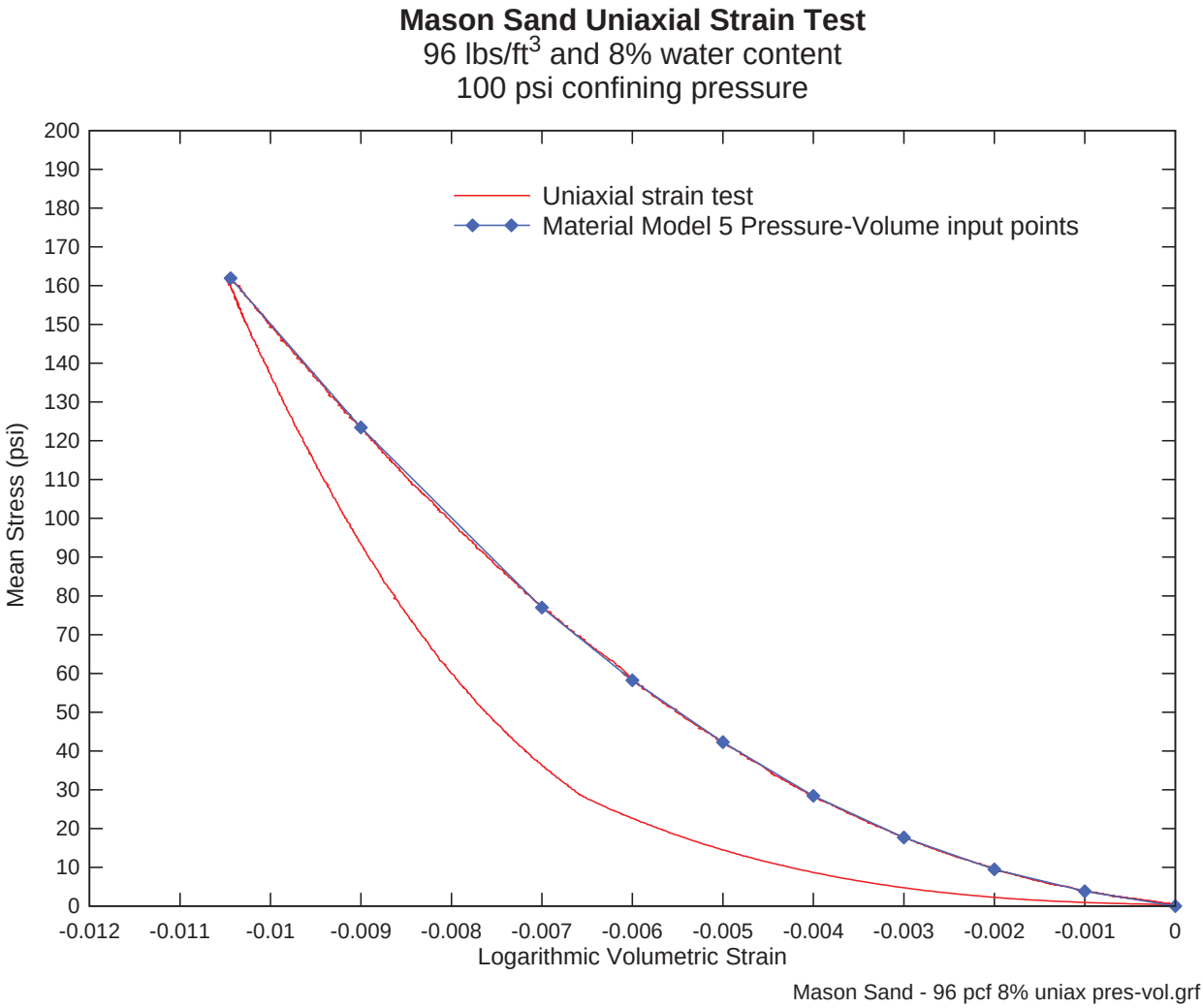

Figure 7-10: Mason Sand Material Model 5 pressure-logarithmic volume curve with 10 input points. Obtained from uniaxial strain test.

7.4 LS-DYNA Material Model 5 inputs

The recommended set of inputs for modeling Mason Sand at 96 lbs/ft^3 dry density and 8% water content in LS-DYNA Material Model 5: Soil and Foam is shown in the table below.

Table 7-2: Material Model 5 inputs for Mason Sand

	Input	Value	Units
Mass density	**RO**	0.000155	lb s^2/in^4
Shear modulus	**G**	2374	psi
Bulk unloading modulus	**K**	50446	psi
Yield surface coefficient	**A0**	1.368	psi^2
Yield surface coefficient	**A1**	1.915	psi
Yield surface coefficient	**A2**	0.670	-
Pressure cutoff	**PC**	-0.5	psi

	Input	Value	Input	Value	Units
Pressure-volume point	**EPS1**	0	**P1**	0	psi
Pressure-volume point	**EPS2**	-0.001	**P2**	3.81	psi
Pressure-volume point	**EPS3**	-0.002	**P3**	9.47	psi
Pressure-volume point	**EPS4**	-0.003	**P4**	17.68	psi
Pressure-volume point	**EPS5**	-0.004	**P5**	28.43	psi
Pressure-volume point	**EPS6**	-0.005	**P6**	42.28	psi
Pressure-volume point	**EPS7**	-0.006	**P7**	58.24	psi
Pressure-volume point	**EPS8**	-0.007	**P8**	76.99	psi
Pressure-volume point	**EPS9**	-0.009	**P9**	123.43	psi
Pressure-volume point	**EPS10**	-0.01044	**P10**	161.93	psi

Table 7-3: Summary of elastic constants

Young's Modulus E	5898	psi
Poisson's Ratio ν	0.242	
Shear Modulus G	2374	psi
Initial Bulk Modulus K	3810	psi
Constrained Modulus M	6975	psi

8 Properties for Mason Sand at 100 lbs/ft^3 dry density and 5% water content

This chapter describes properties for Mason Sand at 100 lbs/ft^3 dry density and 5% water content. The test log is shown in Table 8-1.

Table 8-1: Test log for Mason Sand at 100/5%

Test ID	Sample ID	Type	Confining Pressure (psi)	Moisture content	Wet Density (lbs/ft^3)	Dry Density (lbs/ft^3)
L1B09	Mason Sand	Triax	10	5.03%	105	99.97
L2B09	Mason Sand	Triax	20	4.56%	105	100.43
L6B09	Mason Sand	Triax	50	3.74%	105	101.22
L6D09	Mason Sand	Triax	75	4.71%	105	100.28
L7A09	Mason Sand	Hydro	100	5.02%	105	99.99
L7B09	Mason Sand	Triax	100	5.02%	105	99.99
L8A09	Mason Sand	Uniax	100	5.34%	105	99.68

8.1 Triaxial compression

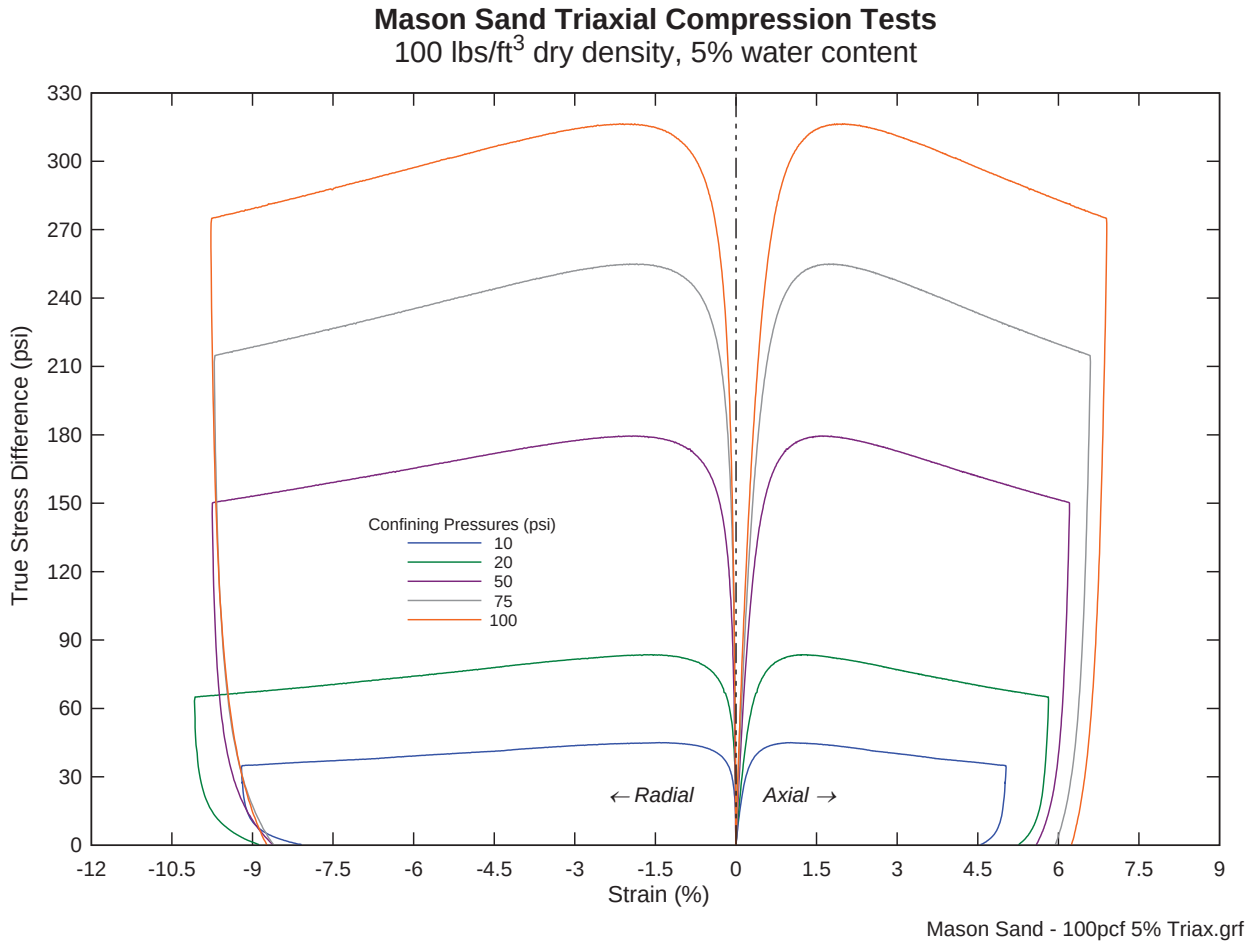

Figure 8-1: Mason Sand triaxial test results for 10, 20, 50, 75, and 100 psi confining pressures.

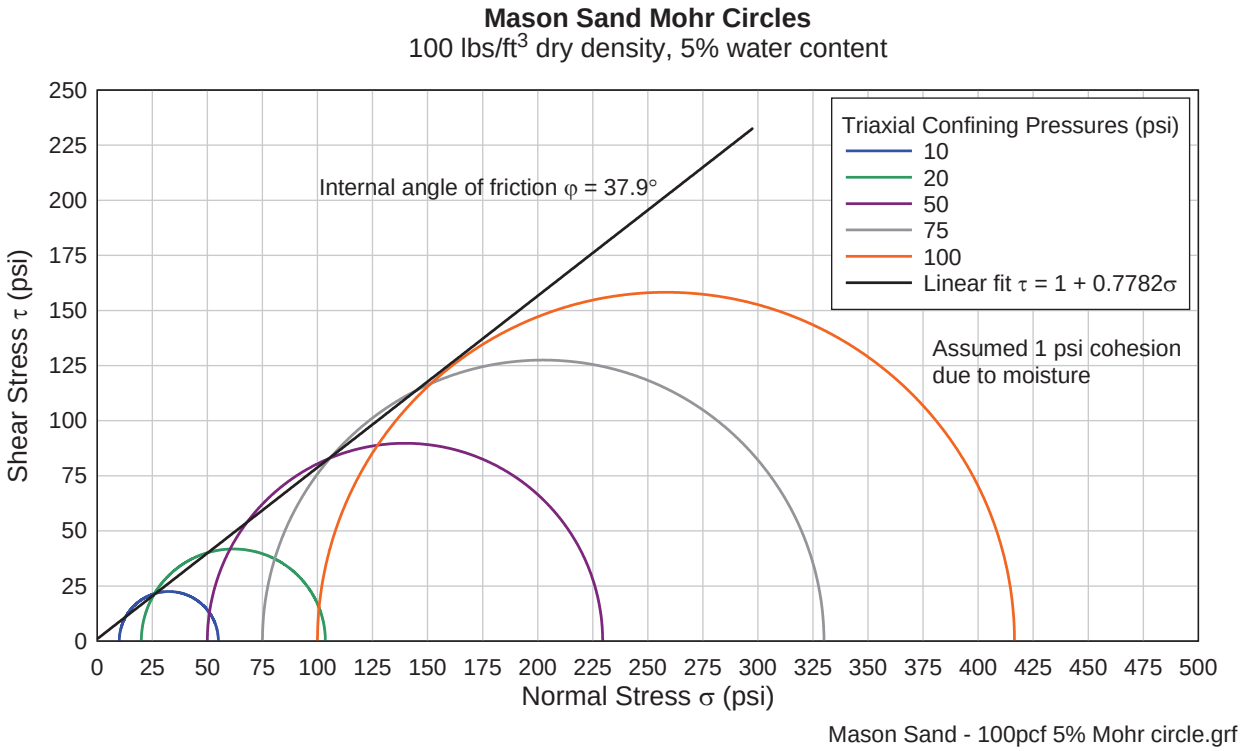

Figure 8-2: Mohr circles based on Mason Sand's triaxial tests

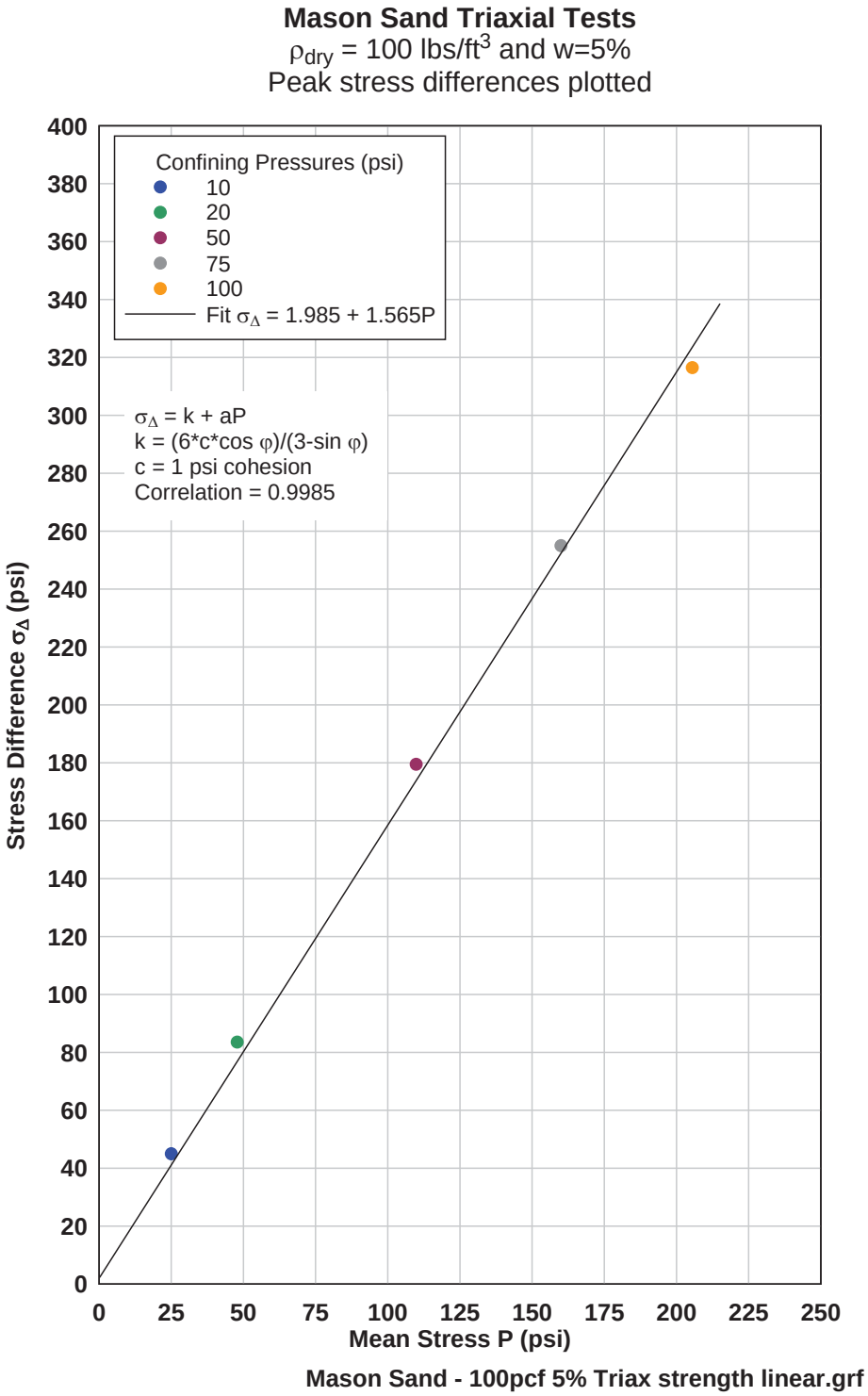

Figure 8-3: Mason Sand strength envelope results.

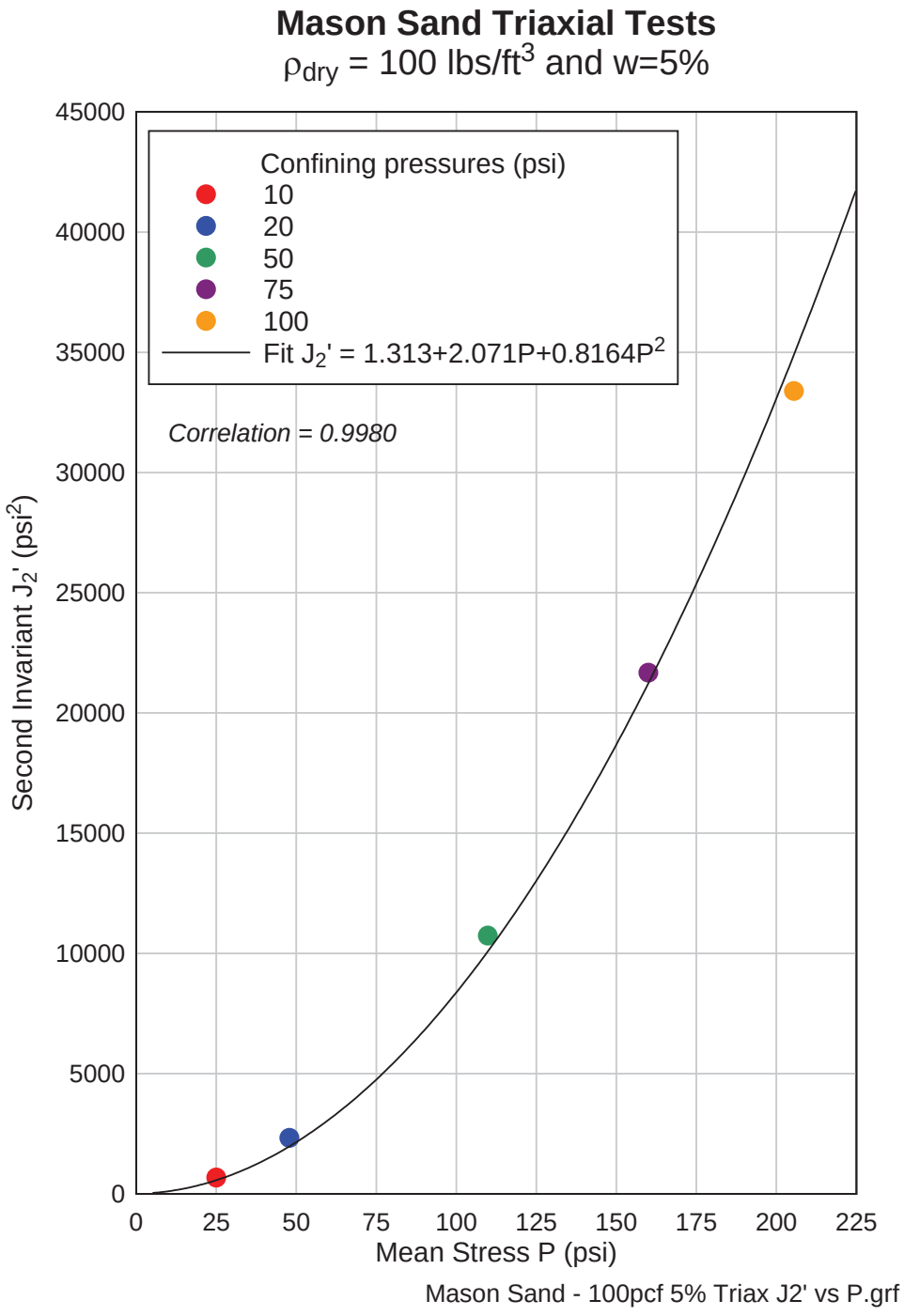

Figure 8-4: Mason Sand Material Model 5 yield surface fit from triaxial test data.

8.2 Hydrostatic compression

The hydrostatic test on the 100/5% Mason Sand was more extensive than the previous Mason Sand models. The 100/5% Mason Sand was loaded and unloaded a total of five times; one for each triaxial test pressure. In Figure 8-5, the Mason Sand is loaded and unloaded from 10, 20, 50, 75, and 100 psi pressures. Again, the Mason Sand is returned to 100 psi for the triaxial strength test.

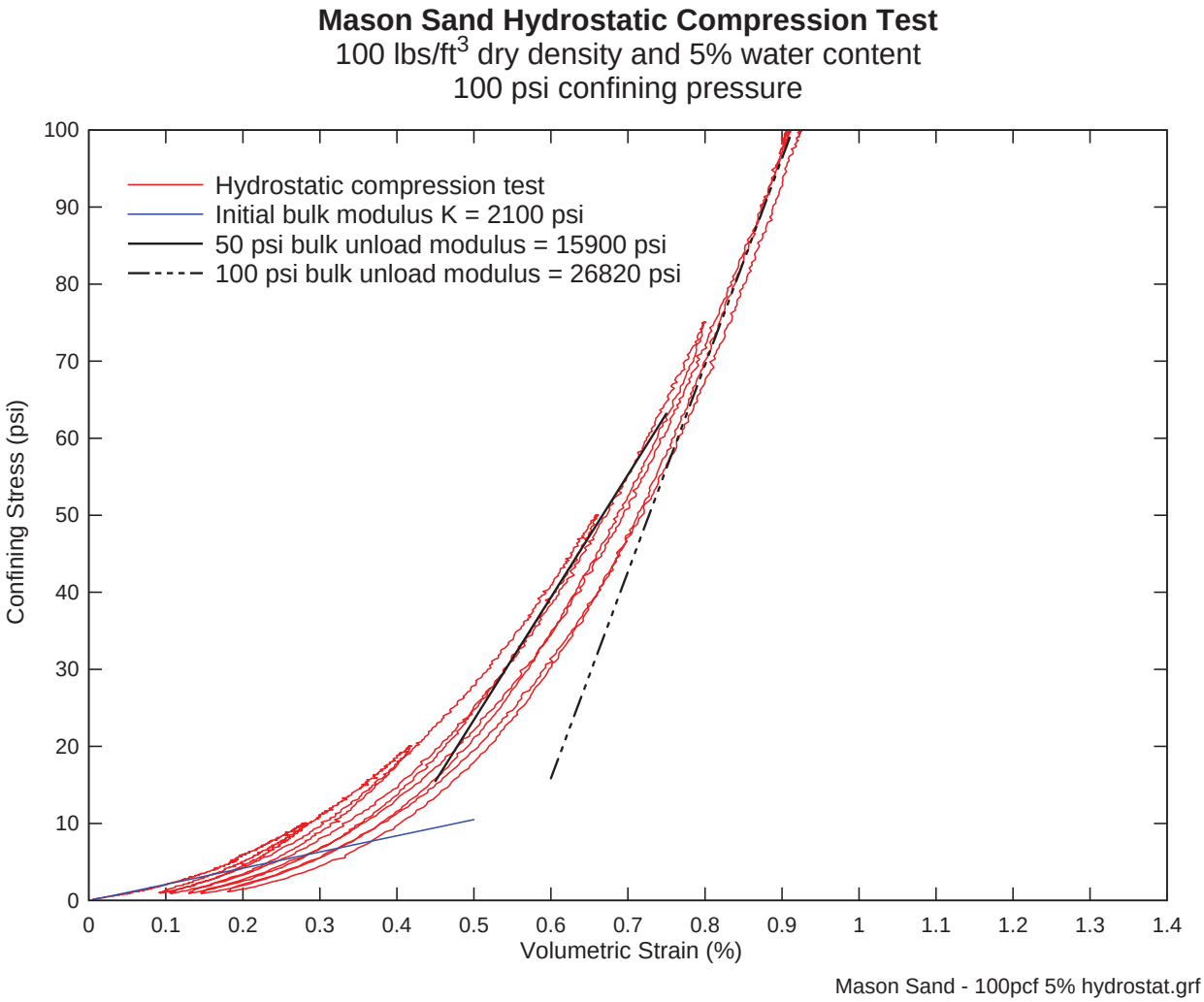

Figure 8-5: 100 psi hydrostatic compression test on Mason Sand at 100/5% condition.

8.3 Uniaxial strain

The 100/5% Mason Sand uniaxial test is shown in Figure 8-6 through Figure 8-9. The loading portions of the uniaxial strain test are emphasized in bold on the data curves. These loading portions illustrate the corresponding fit.

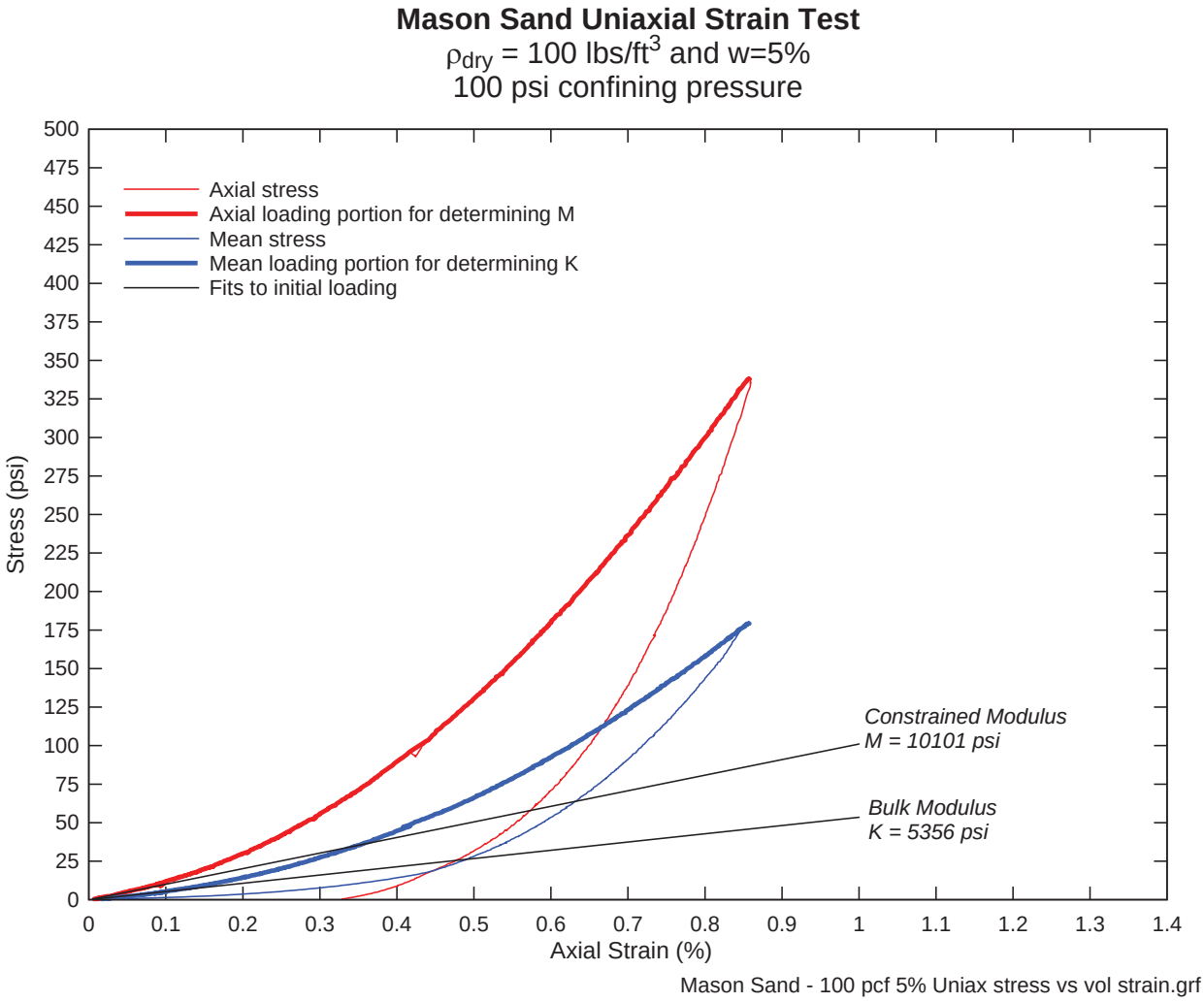

Figure 8-6: Mason Sand uniaxial strain test results. Constrained and bulk moduli fits shown.

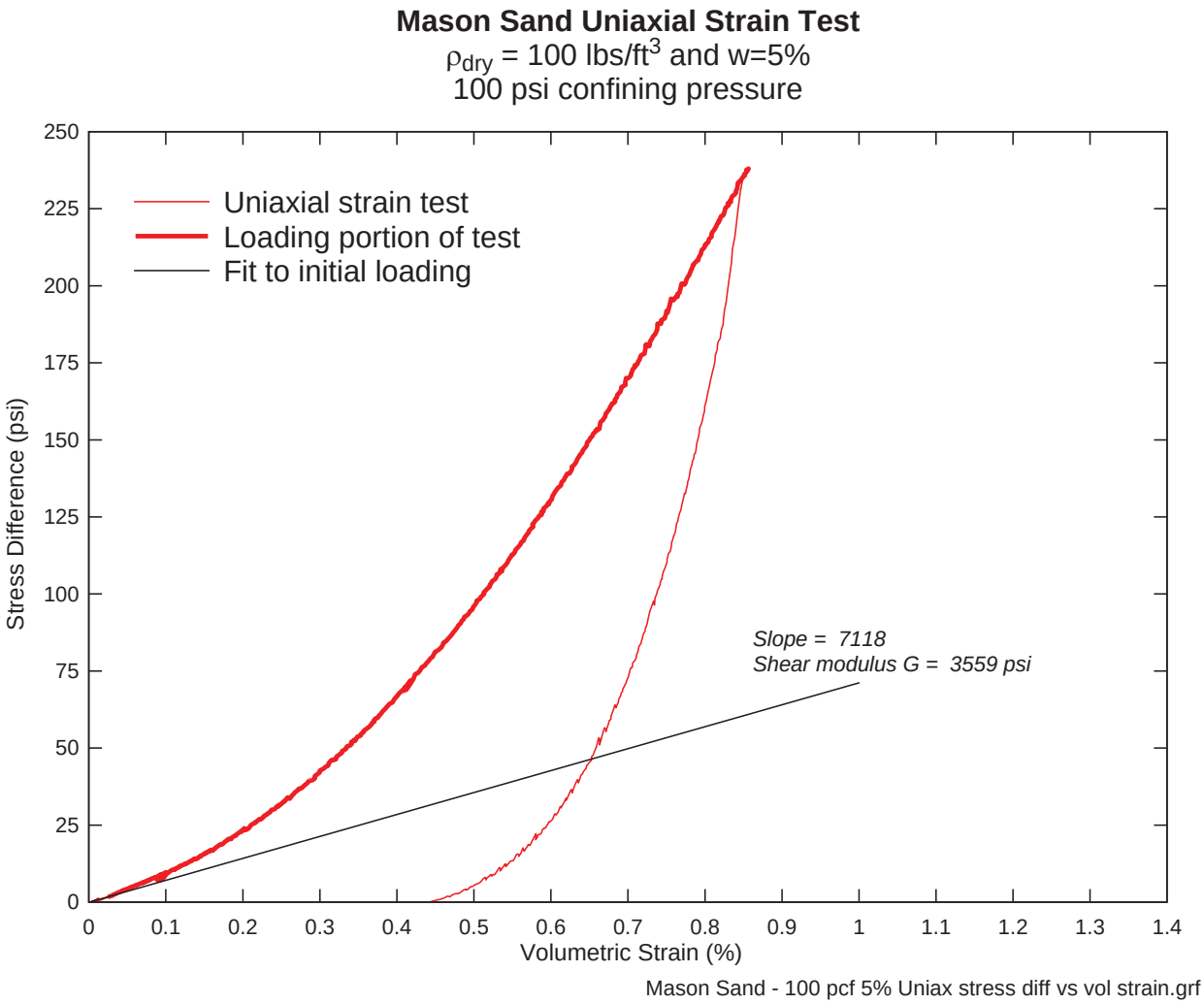

Figure 8-7: Mason Sand uniaxial strain test results plotted as stress difference vs. strain. Shear modulus G fit shown. Shear stress is half of stress difference. Uniaxial strain is equal to shear strain.

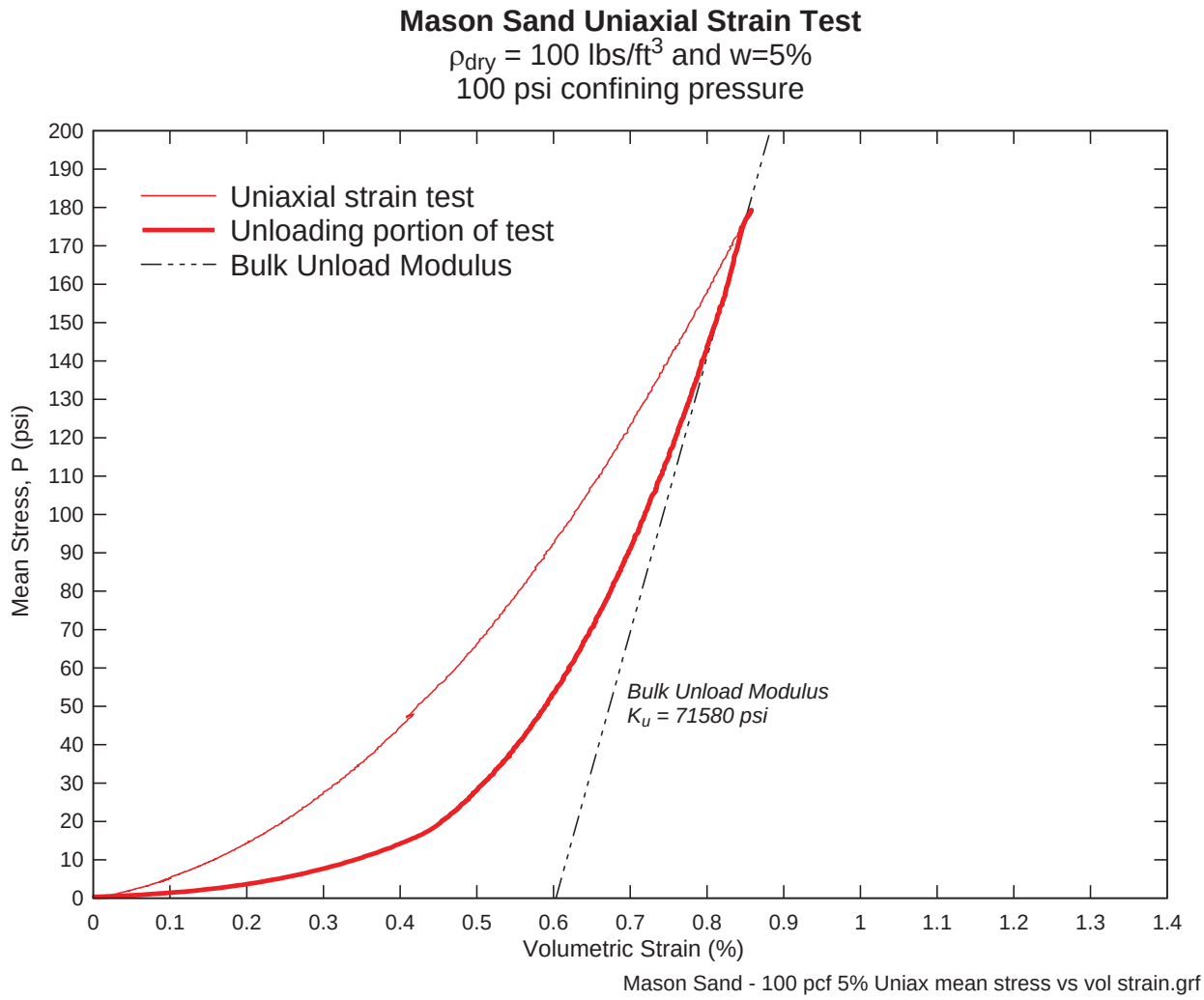

Figure 8-8: Mason Sand uniaxial strain unloading portion. Determination of bulk unloading modulus K_u (BULK) by linear fit.

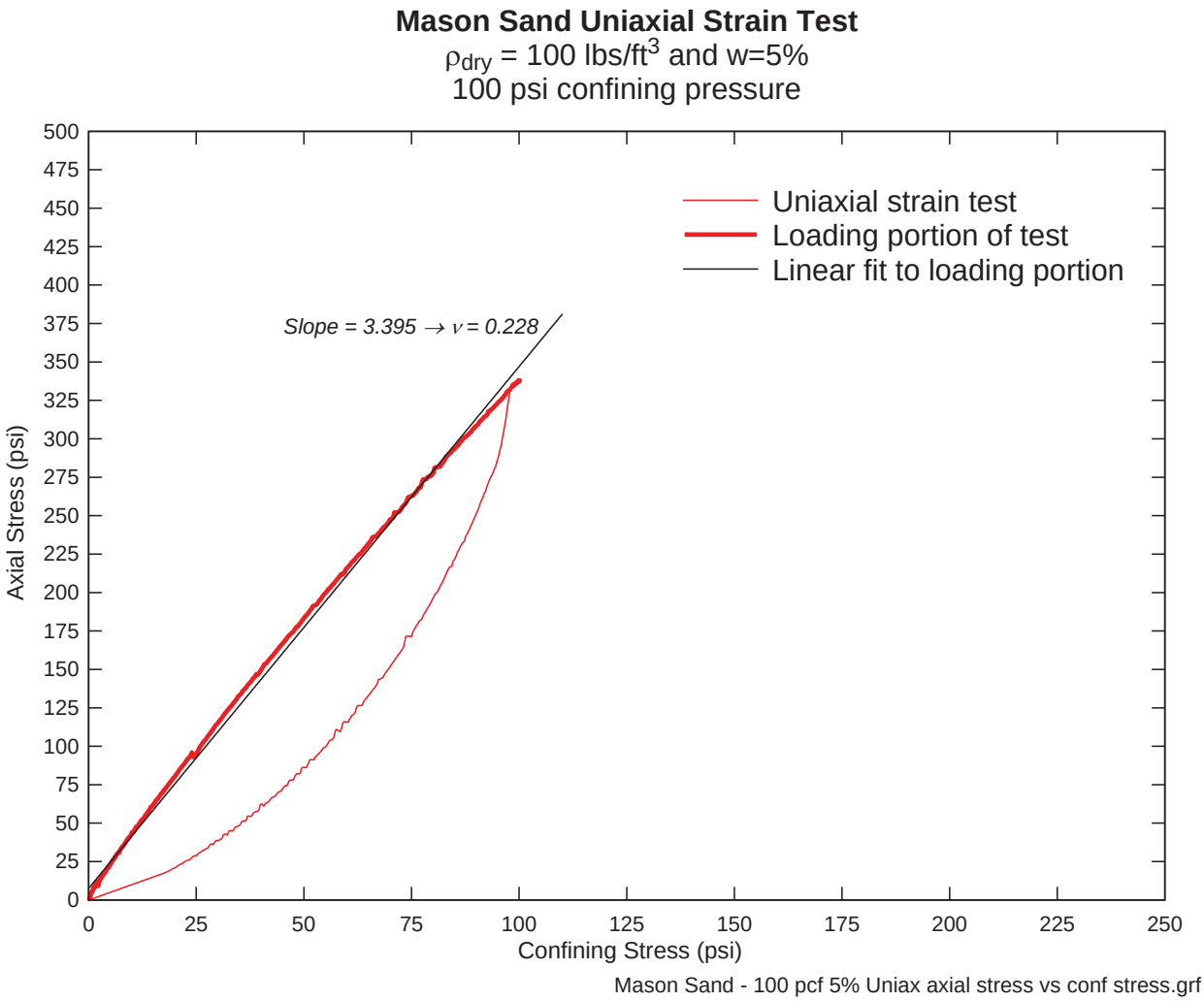

Figure 8-9: Determination of Poisson's ratio via uniaxial strain test.

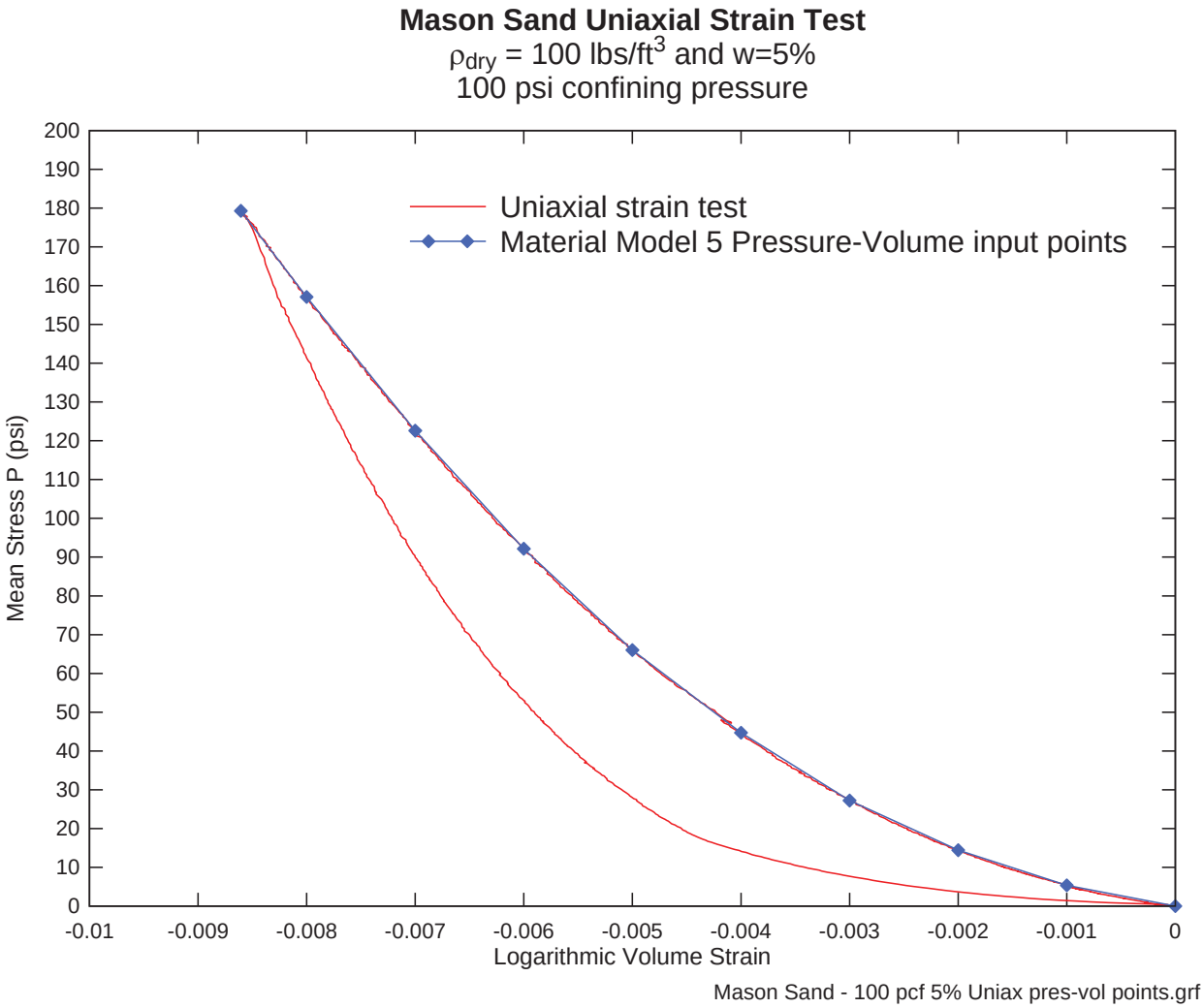

Figure 8-10: Mason Sand Material Model 5 pressure-logarithmic volume curve with 10 input points. Obtained from uniaxial strain test.

8.4 LS-DYNA Material Model 5 inputs

The recommended set of inputs for modeling Mason Sand at 100 lbs/ft^3 dry density and 5% water content in LS-DYNA Material Model 5: Soil and Foam is shown in the table below.

Table 8-2: Material Model 5 inputs for Mason Sand

	Input	Value	Units
Mass density	**RO**	0.000157	lb s^2/in^4
Shear modulus	**G**	3559	psi
Bulk unloading modulus	**K**	71580	psi
Yield surface coefficient	**A0**	1.313	psi^2
Yield surface coefficient	**A1**	2.071	psi
Yield surface coefficient	**A2**	0.8164	-
Pressure cutoff	**PC**	-0.5	psi

	Input	Value	Input	Value	Units
Pressure-volume point	**EPS1**	0.0000	**P1**	0	psi
Pressure-volume point	**EPS2**	-0.001	**P2**	5.356	psi
Pressure-volume point	**EPS3**	-0.002	**P3**	14.41	psi
Pressure-volume point	**EPS4**	-0.003	**P4**	27.22	psi
Pressure-volume point	**EPS5**	-0.004	**P5**	44.71	psi
Pressure-volume point	**EPS6**	-0.005	**P6**	66.03	psi
Pressure-volume point	**EPS7**	-0.006	**P7**	92.15	psi
Pressure-volume point	**EPS8**	-0.007	**P8**	122.6	psi
Pressure-volume point	**EPS9**	-0.008	**P9**	157.1	psi
Pressure-volume point	**EPS10**	-0.00861	**P10**	179.3	psi

Table 8-3: Summary of elastic constants

Young's Modulus E	8741	psi
Poisson's Ratio ν	0.228	
Shear Modulus G	3559	psi
Initial Bulk Modulus K	5356	psi
Constrained Modulus M	10101	psi

9 Mason Sand at 100/15%

This chapter describes properties for Mason Sand at 100 lbs/ft^3 dry density and 15% water content. The test log is shown in Table 9-1.

Table 9-1: Test log for Mason Sand at 100/15%. *Moisture content not available in test log.

Test ID	Sample ID	Type	Confining Pressure (psi)	Post-test Moisture content	Wet Density (lbs/ft^3)	Dry Density (lbs/ft^3)
L15C09	Mason Sand	Uniax	100	15%*	115	N/A
L17D09	Mason Sand	Triax	10	14.42%	115	100.50
L20B09	Mason Sand	Triax	20	14.37%	115	100.54
L21C09	Mason Sand	Triax	50	14.11%	115	100.78
L22C09	Mason Sand	Triax	75	14.53%	115	100.40
L22D09	Mason Sand	Hydro	100	13.63%	115	101.20
L22E09	Mason Sand	Triax	100	13.63%	115	101.20

9.1 Triaxial compression

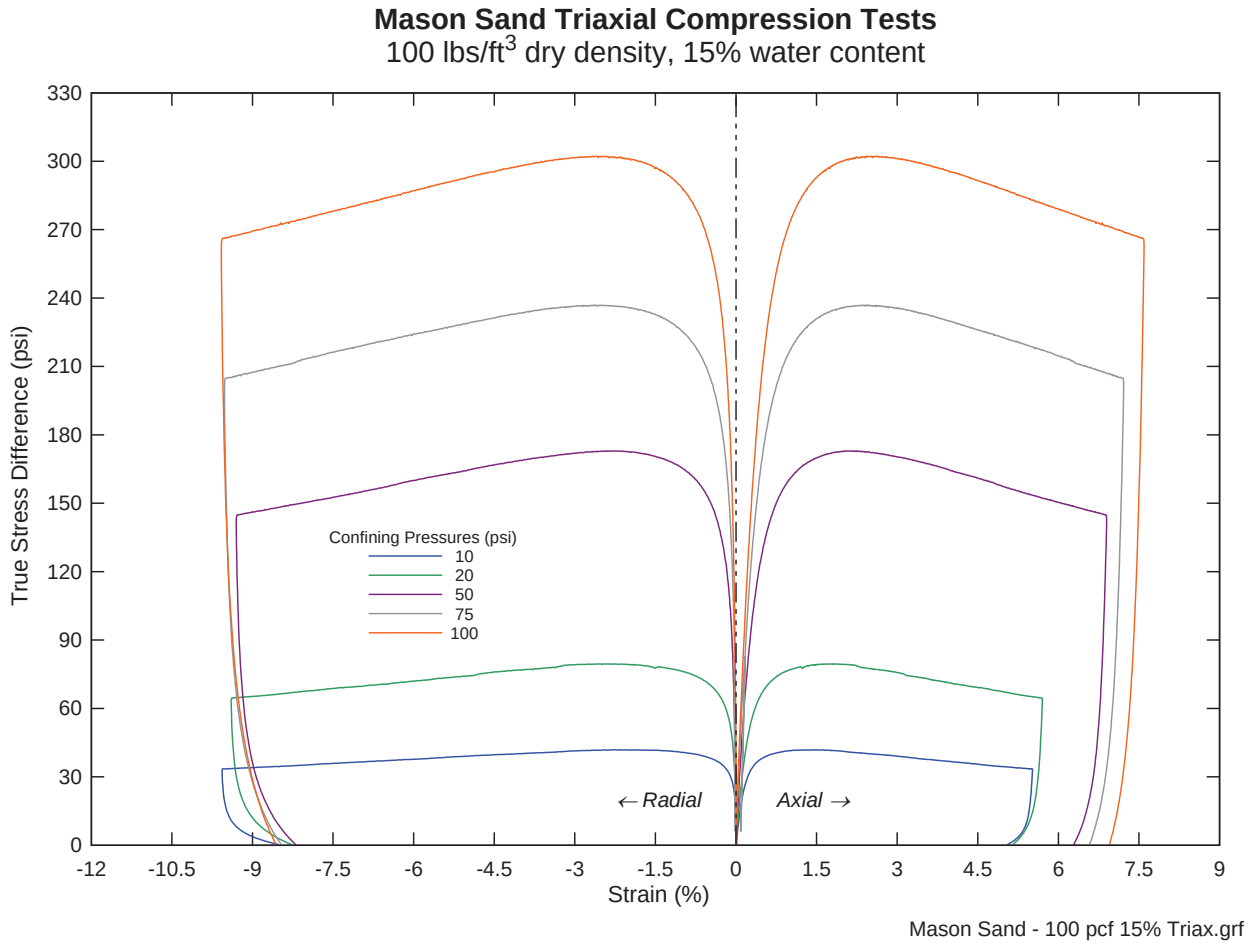

Figure 9-1: Mason Sand triaxial test results for 10, 20, 50, 75, and 100 psi confining pressures.

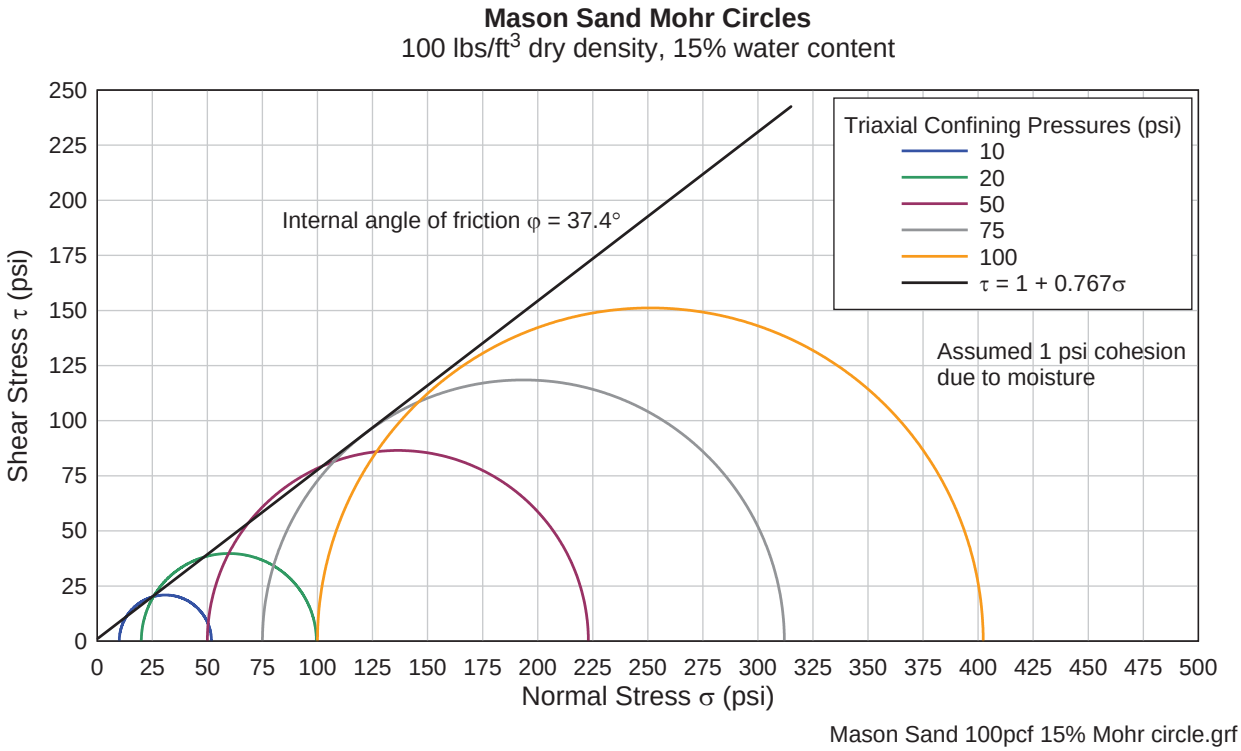

Figure 9-2: Mohr circles based on Mason Sand's triaxial tests

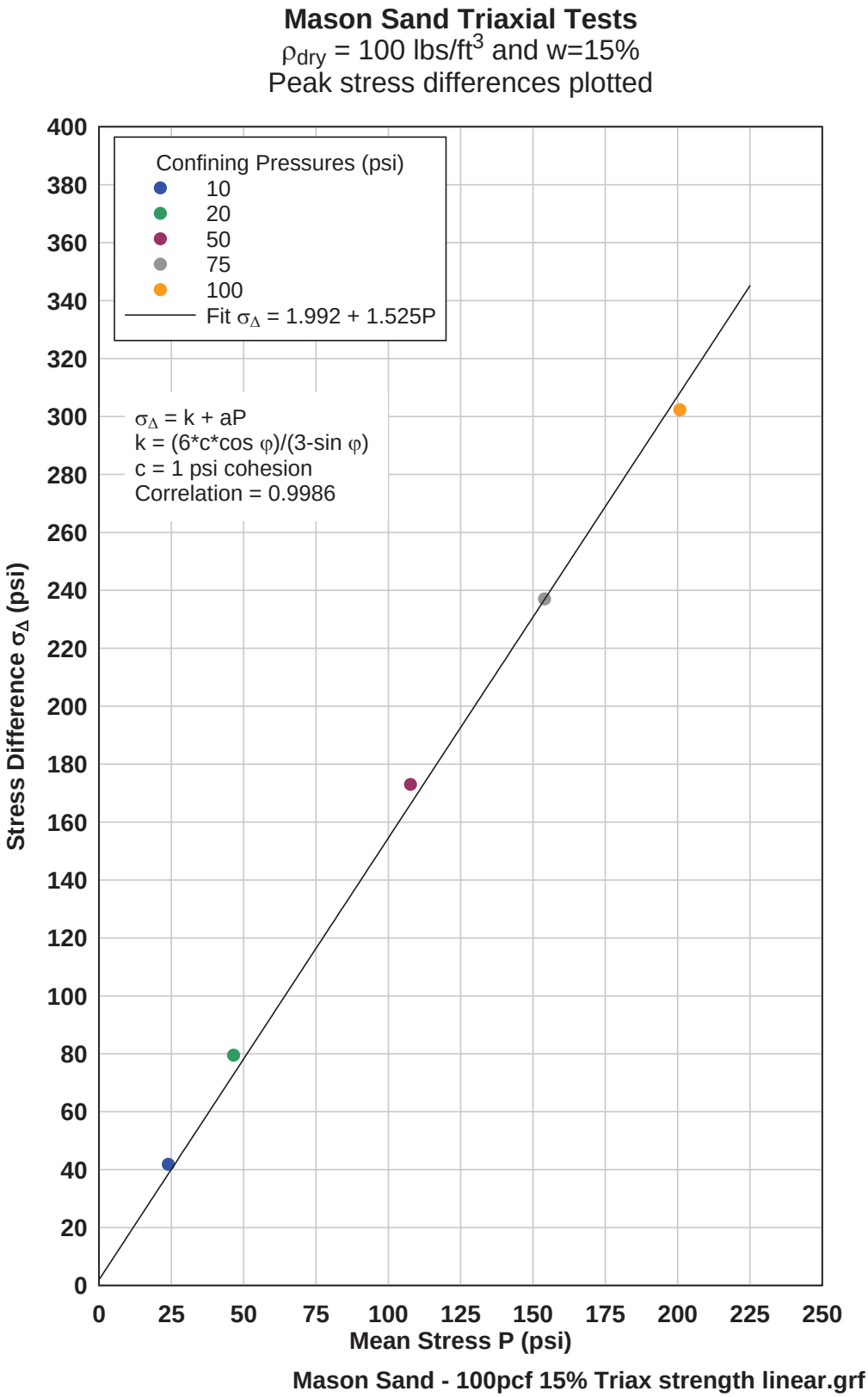

Figure 9-3: Mason Sand strength envelope results.

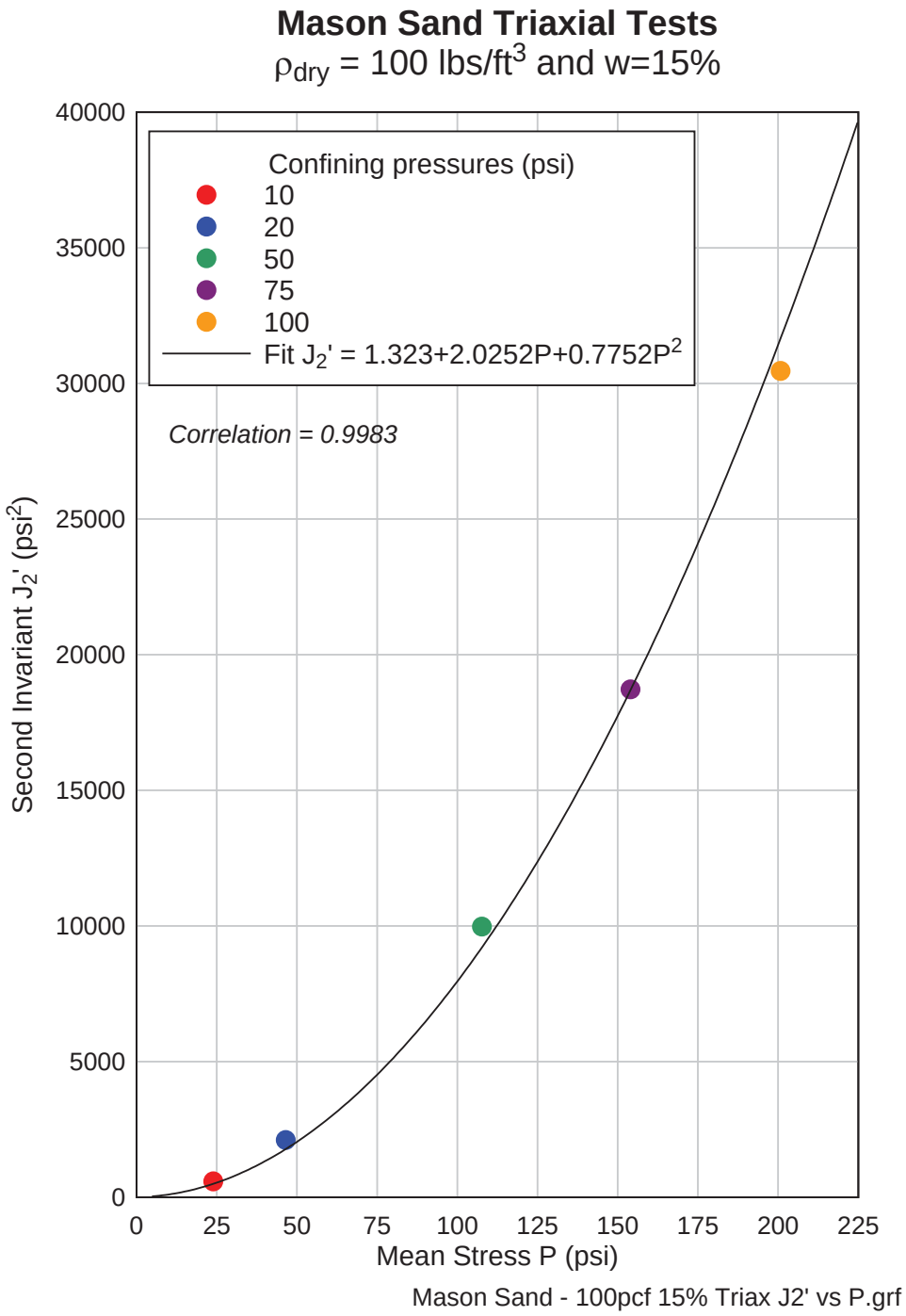

Figure 9-4: Mason Sand Material Model 5 yield surface fit from triaxial test data.

9.2 Hydrostatic compression

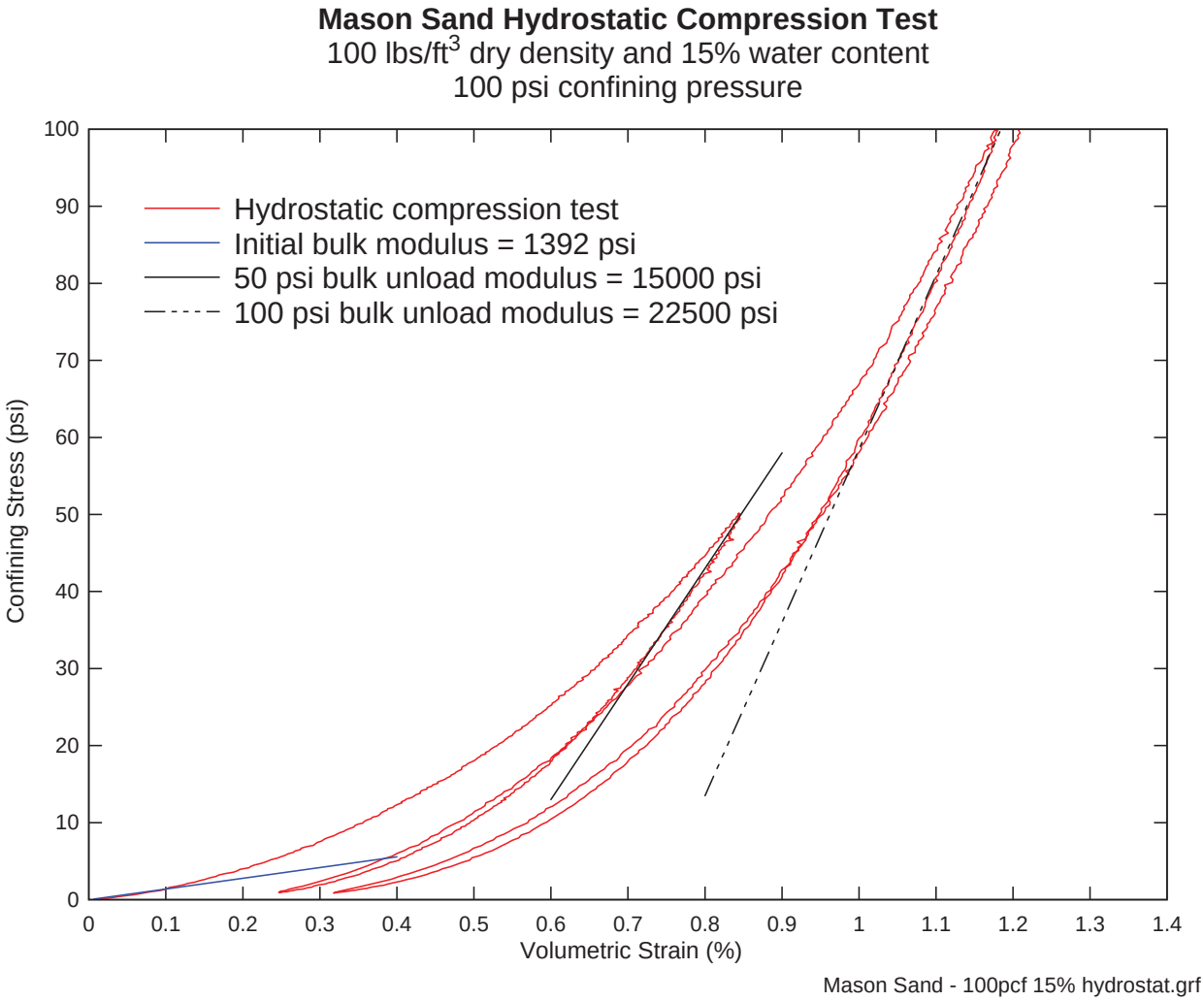

Figure 9-5: 100 psi hydrostatic compression test for Mason Sand at 100/15% condition.

9.3 Uniaxial strain

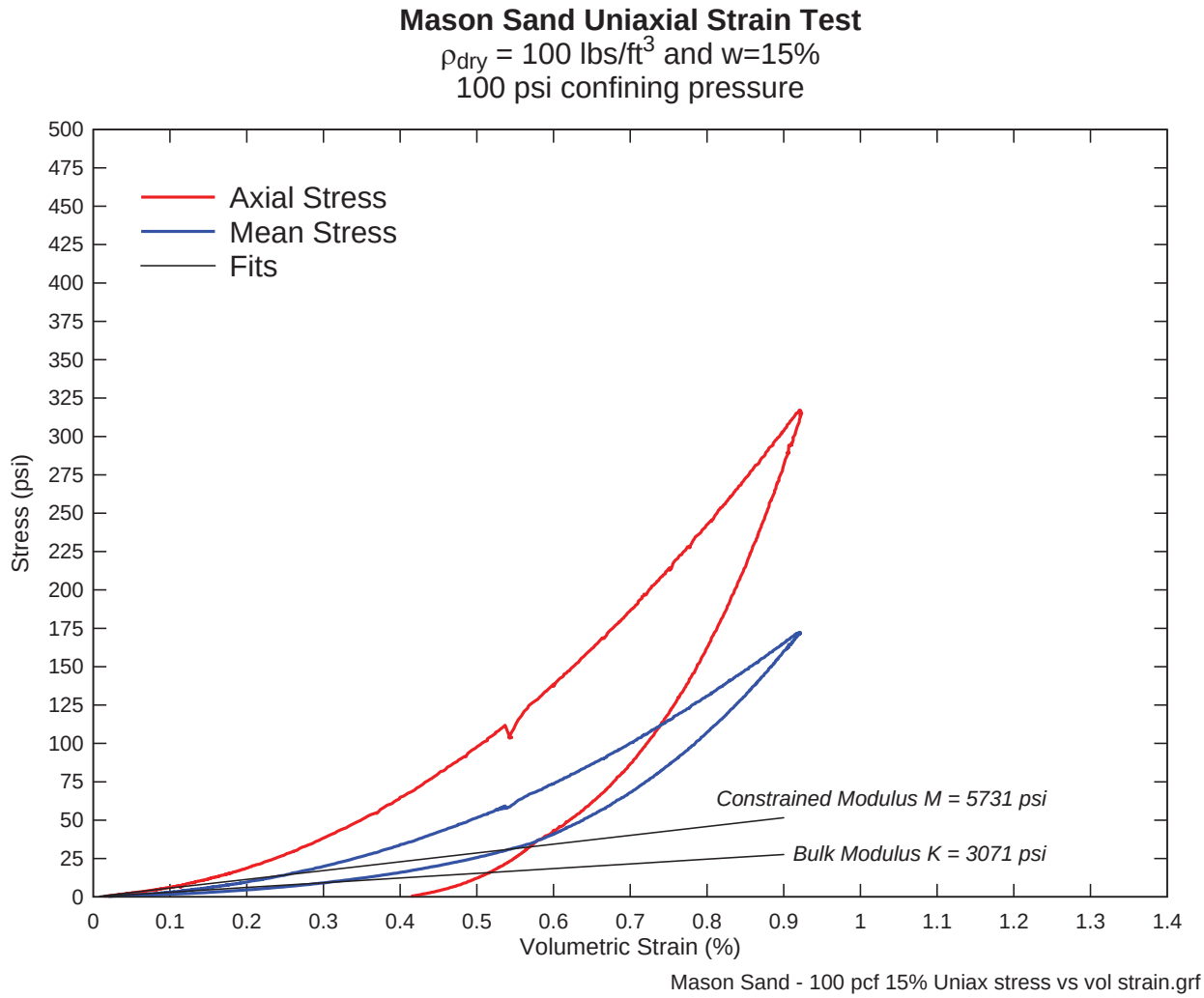

Figure 9-6: Mason Sand uniaxial strain test results. Constrained and bulk moduli fits shown.

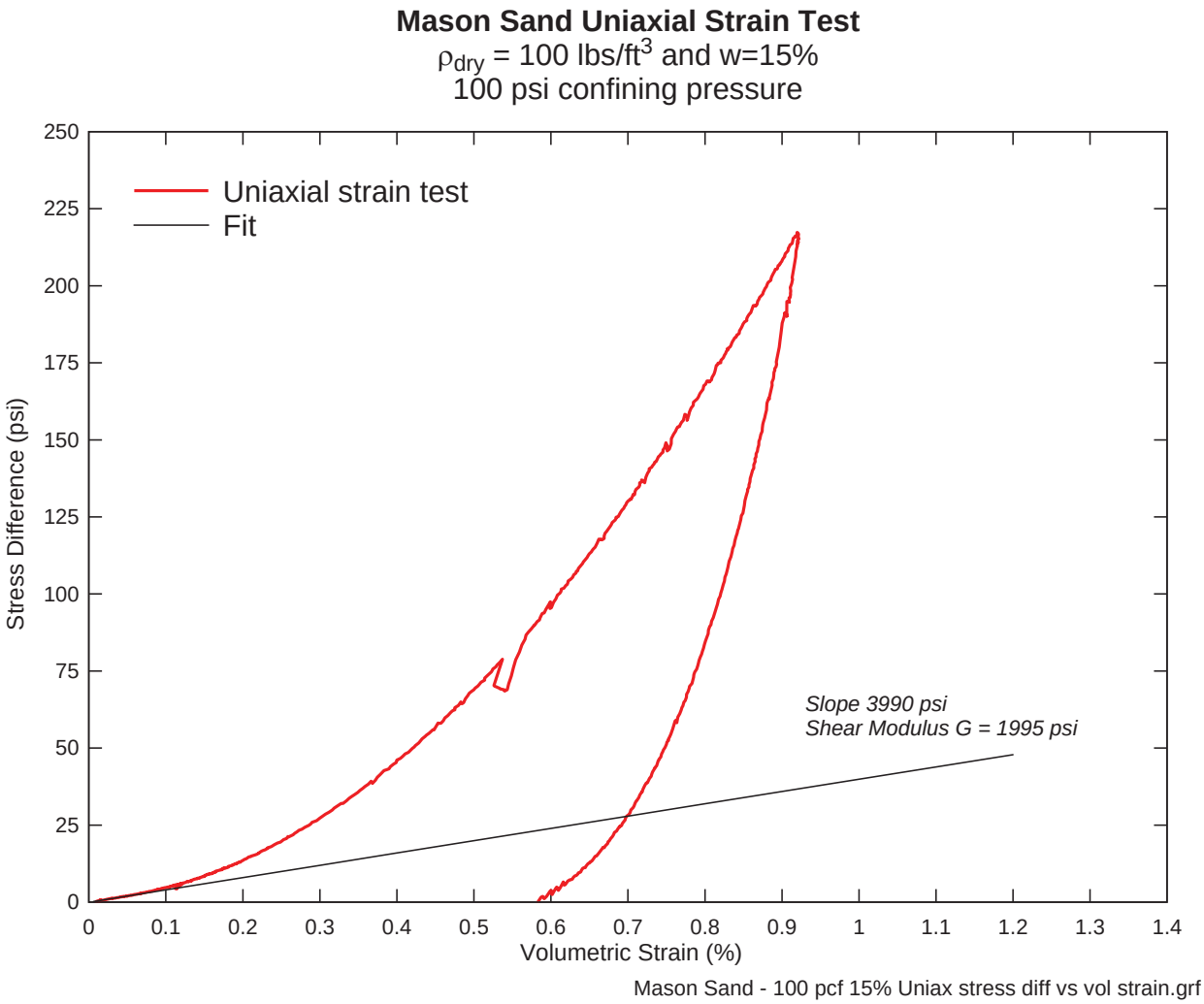

Figure 9-7: Mason Sand uniaxial strain test results plotted as stress difference vs. strain. Shear modulus G fit shown. Shear stress is half of stress difference. Uniaxial strain is equal to shear strain.

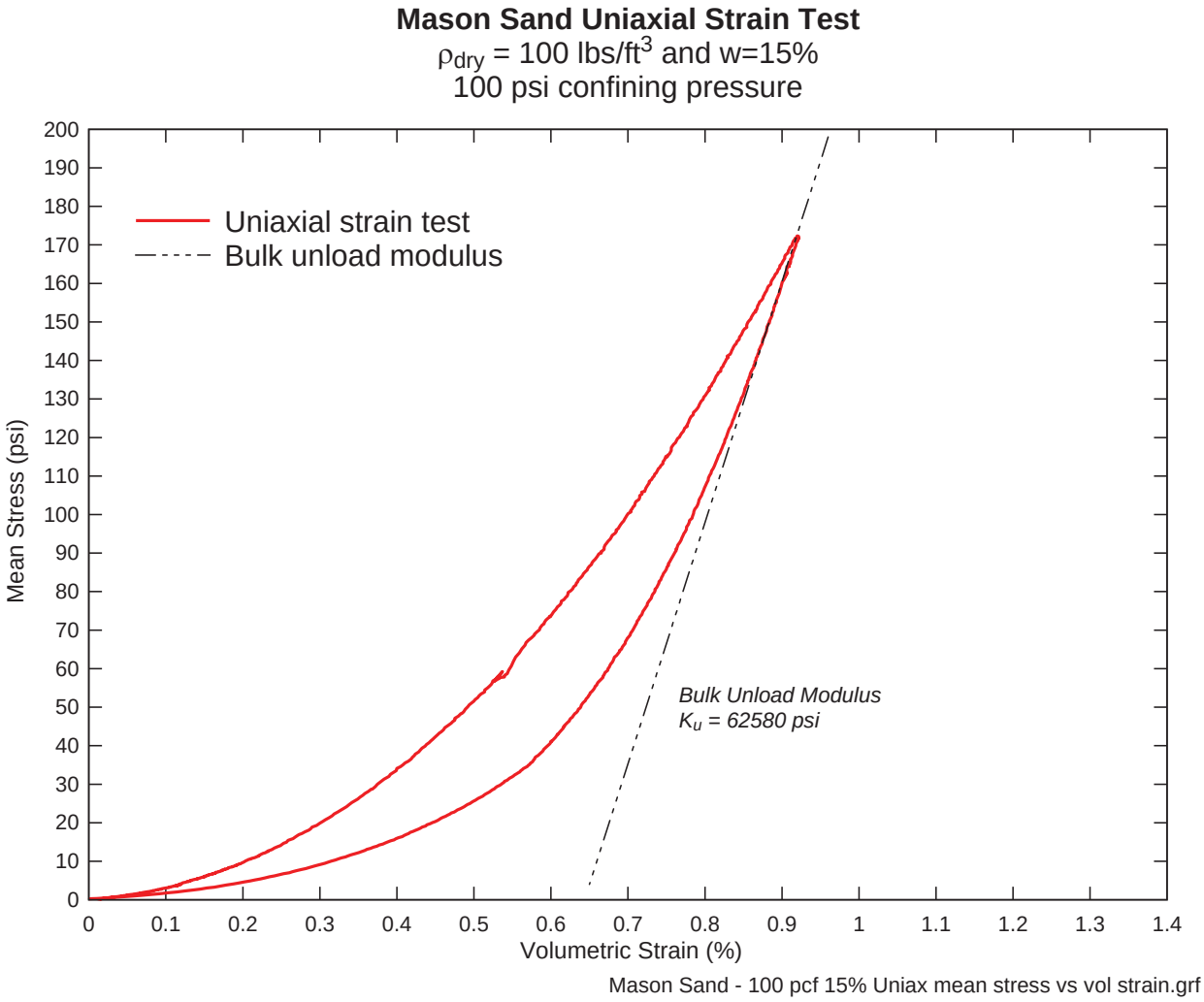

Figure 9-8: Mason Sand uniaxial strain unloading portion. Determination of bulk unloading modulus K_u (BULK) by linear fit.

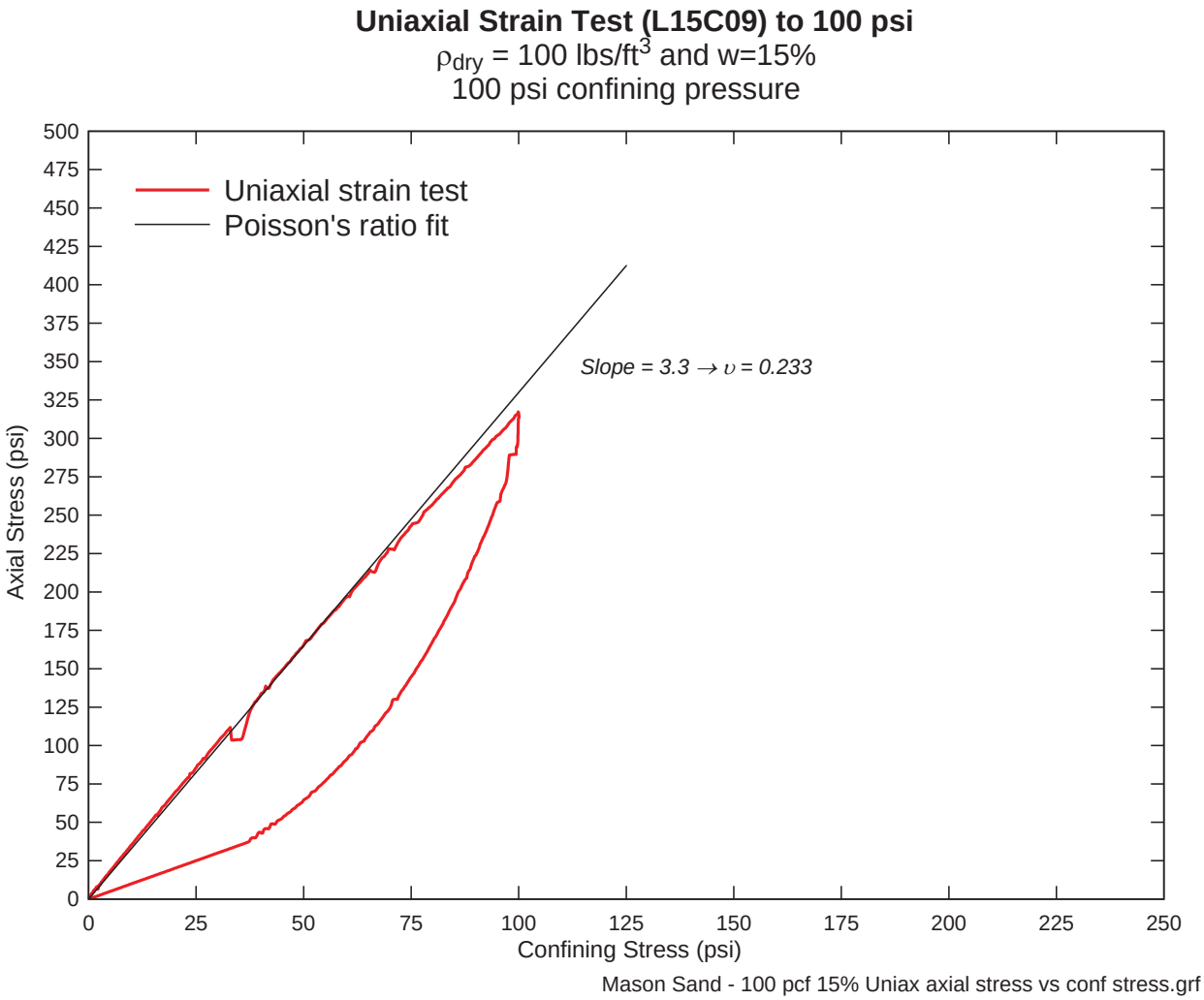

Figure 9-9: Determination of Poisson's ratio via uniaxial strain test.

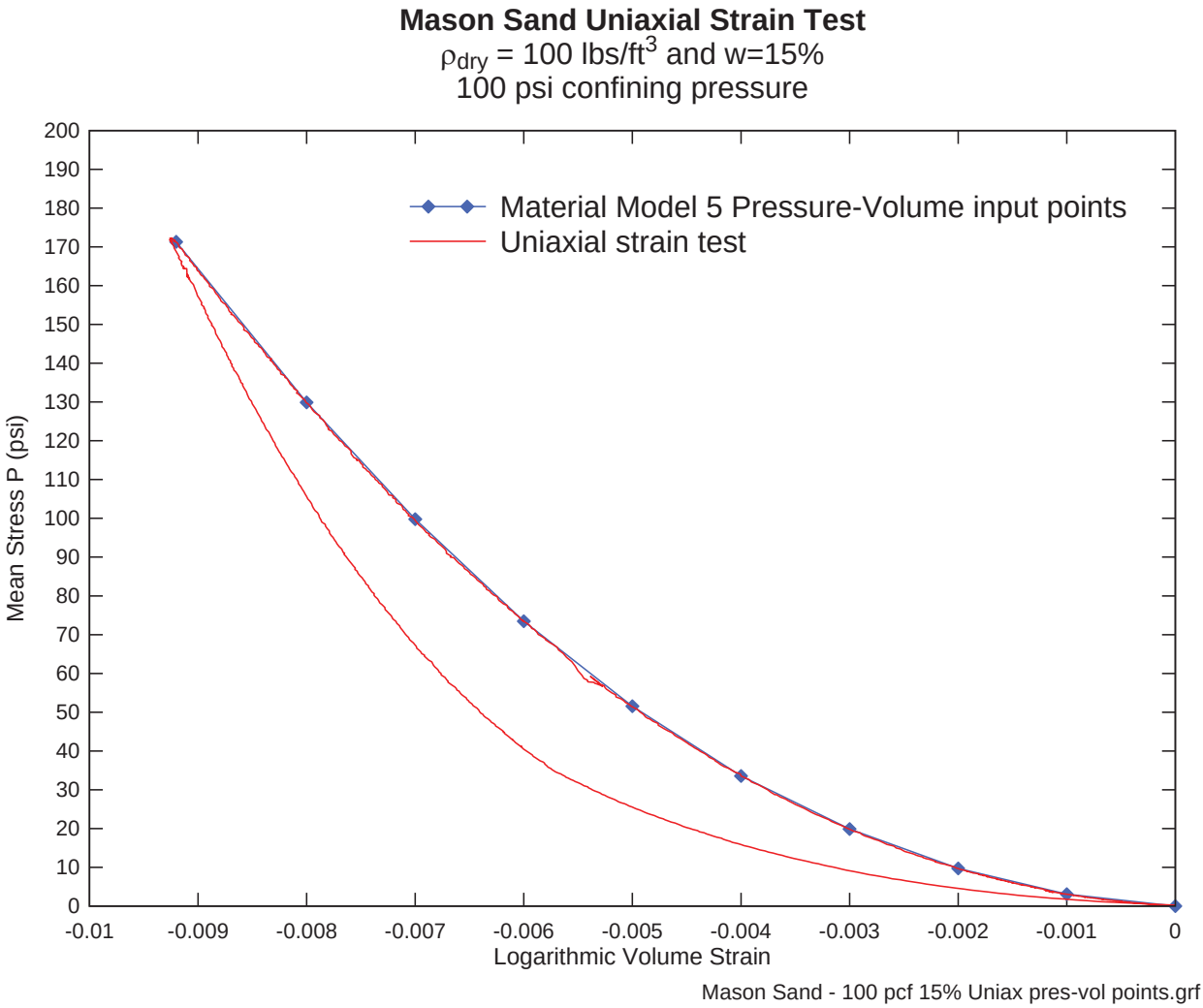

Figure 9-10: Mason Sand Material Model 5 pressure-logarithmic volume curve with 10 input points. Obtained from uniaxial strain test.

9.4 LS-DYNA Material Model 5 inputs

The recommended set of inputs for modeling Mason Sand at 100 lbs/ft^3 dry density and 15% water content in LS-DYNA Material Model 5: Soil and Foam is shown in the table below.

Table 9-2: Material Model 5 inputs for Mason Sand

	Input	Value	Units
Mass density	**RO**	0.000172	lb s^2/in^4
Shear modulus	**G**	1995	psi
Bulk unloading modulus	**K**	62580	psi
Yield surface coefficient	**A0**	1.323	psi^2
Yield surface coefficient	**A1**	2.025	psi
Yield surface coefficient	**A2**	0.7752	-
Pressure cutoff	**PC**	-1.0	psi

	Input	Value	Input	Value	Units
Pressure-volume point	**EPS1**	0.0000	**P1**	0	psi
Pressure-volume point	**EPS2**	-0.001	**P2**	3.071	psi
Pressure-volume point	**EPS3**	-0.002	**P3**	9.715	psi
Pressure-volume point	**EPS4**	-0.003	**P4**	19.86	psi
Pressure-volume point	**EPS5**	-0.004	**P5**	33.54	psi
Pressure-volume point	**EPS6**	-0.005	**P6**	51.55	psi
Pressure-volume point	**EPS7**	-0.006	**P7**	73.46	psi
Pressure-volume point	**EPS8**	-0.007	**P8**	99.78	psi
Pressure-volume point	**EPS9**	-0.008	**P9**	129.9	psi
Pressure-volume point	**EPS10**	-0.00920	**P10**	171.3	psi

Table 9-3: Summary of elastic constants

Young's Modulus E	4920	psi
Poisson's Ratio ν	0.233	
Shear Modulus G	1995	psi
Initial Bulk Modulus K	3071	psi
Constrained Modulus M	5731	psi

10 Model to Model Comparisons

Plots of model to model comparisons for all Mason Sand conditions and KSC sands are included as Figure 10-1 and Figure 10-2. These figures demonstrate the relative strength and compressibility of each soil model. The strengths are compared using the linear fits of stress difference versus mean stress. The compressibility is compared by the 10 point pressure-volume fit for each model. Ranked from strongest to weakest in terms of strength, the order is: Mason Sand 100 / 5%, Mason Sand 100 / 15%, Mason Sand 97 /4%, Mason Sand 96 / 8%, KSC HDI, KSC LDD.

Ranked in terms of stiffest to softest compressibility, the order is the same, with the exception that the Mason Sand 97 / 4% and 96 / 8% are almost tied. Figure 10-2 shows an anomaly for Mason Sand. The extra uniaxial test on Mason Sand at 96 / 4% produced an overall stiffer model than the 97 / 4%. Generally speaking, as density increases, the stiffness will also increase. In this case, the slightly less dense specimen produced less strain at the end of the test. However, when the curves are examined closely, the 97 / 4% model was stiffer until 0.03 strain. The two models crossed, and the 96 / 4% model experienced 0.0006 less strain at the same peak mean stress of 161 psi. This anomaly is probably due to variations in the material samples.

Comparisons to older constitutive models, such as Carson Sink and Cuddeback Lake, are shown in Figure 10-4 and Figure 10-5.

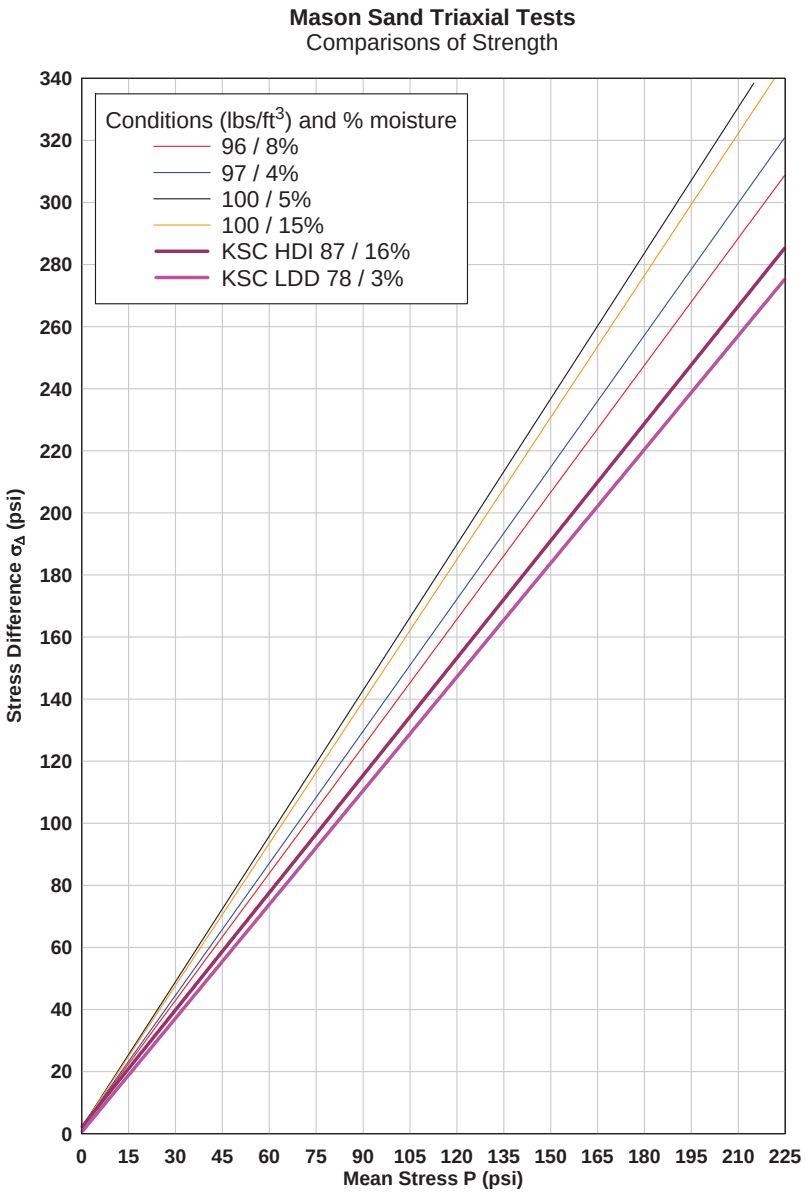

Figure 10-1: Comparison of sand strengths between models.

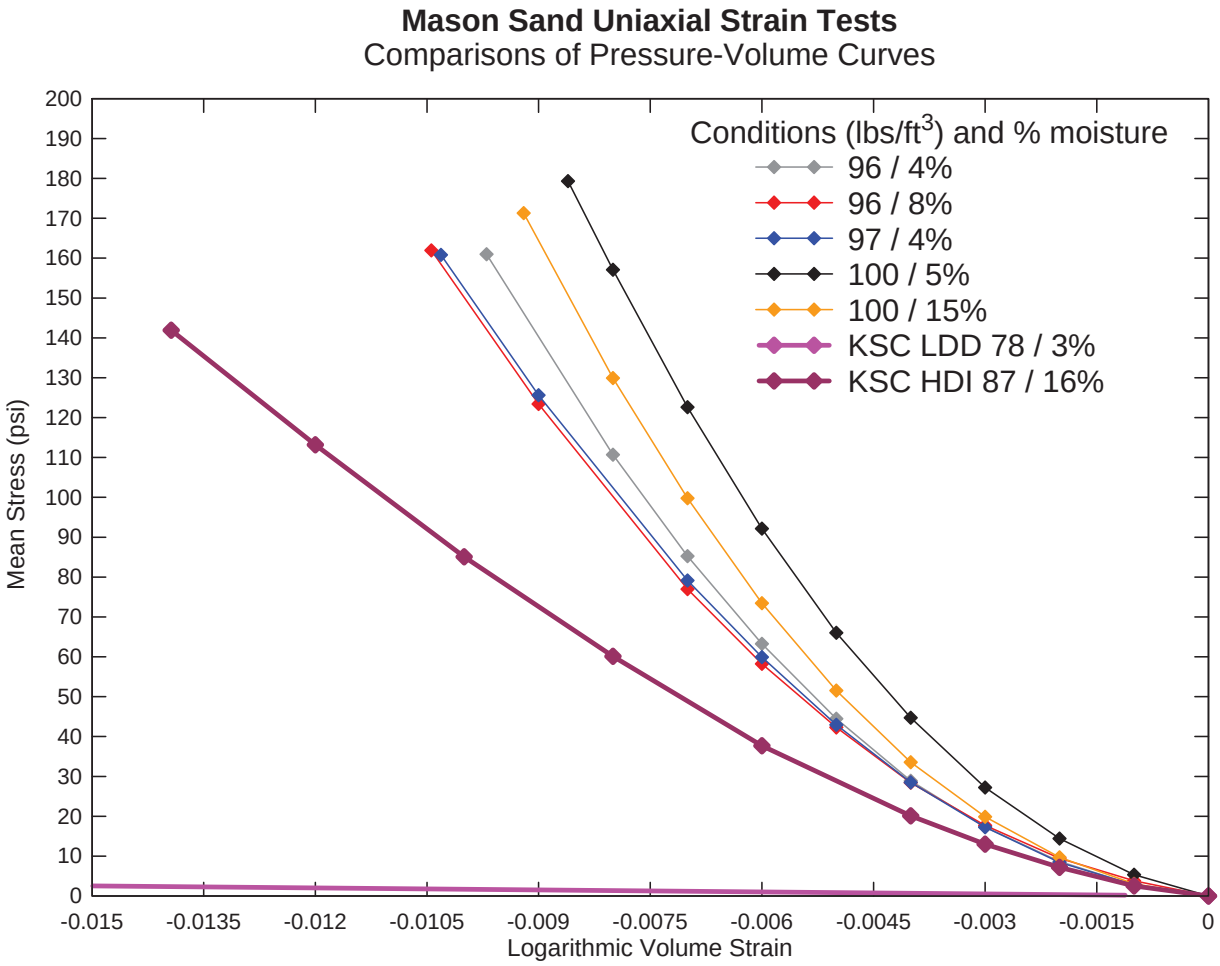

Figure 10-2: KSC and Mason Sand comparison of stiffness. Plot enlarged between 0 and -0.015 strain to display Mason Sands more clearly. KSC LDD Sand extends beyond the plot range.

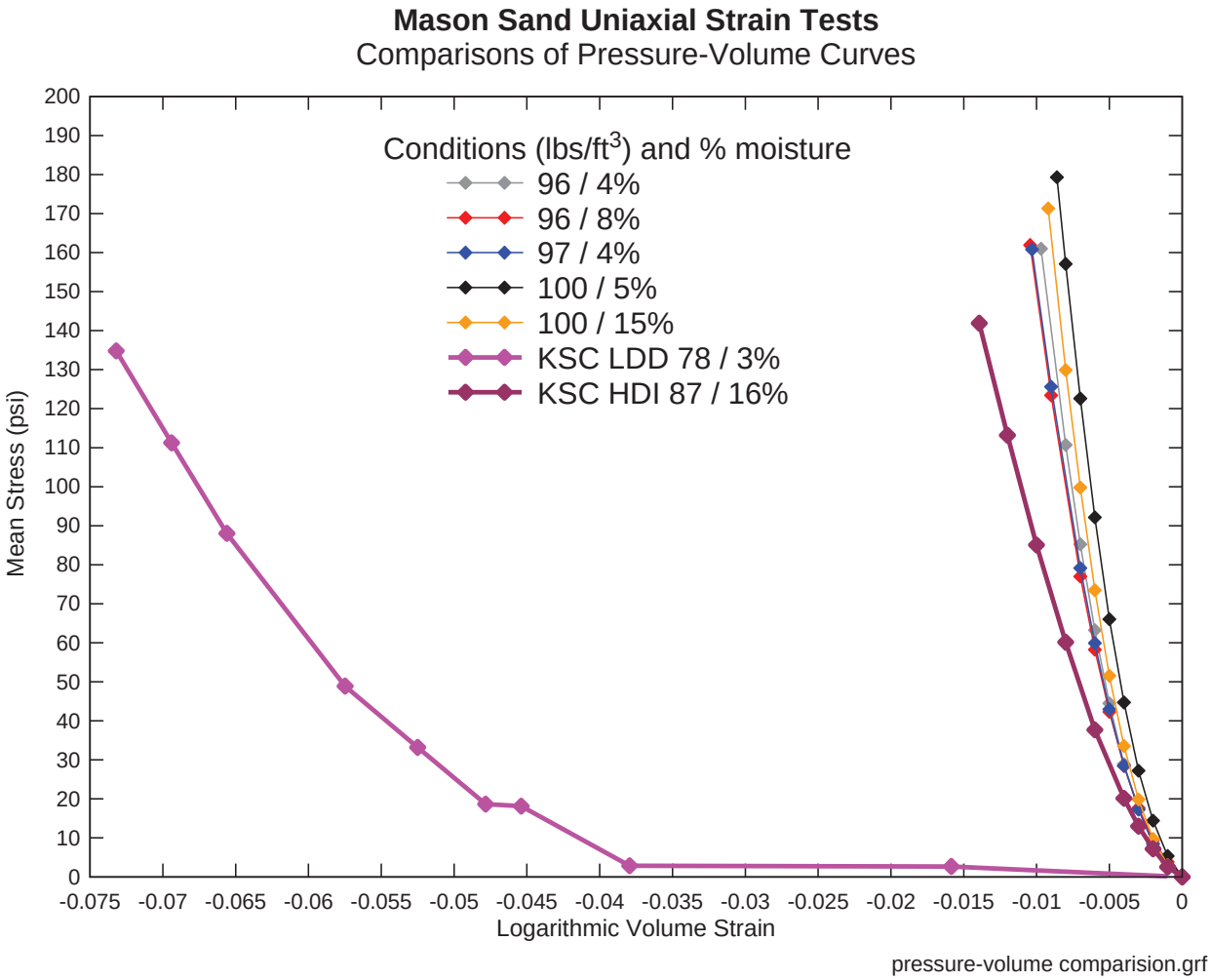

Figure 10-3: KSC and Mason Sand comparison over entire strain range. Note how significantly more compressible the KSC LDD Sand model is compared to the other sands.

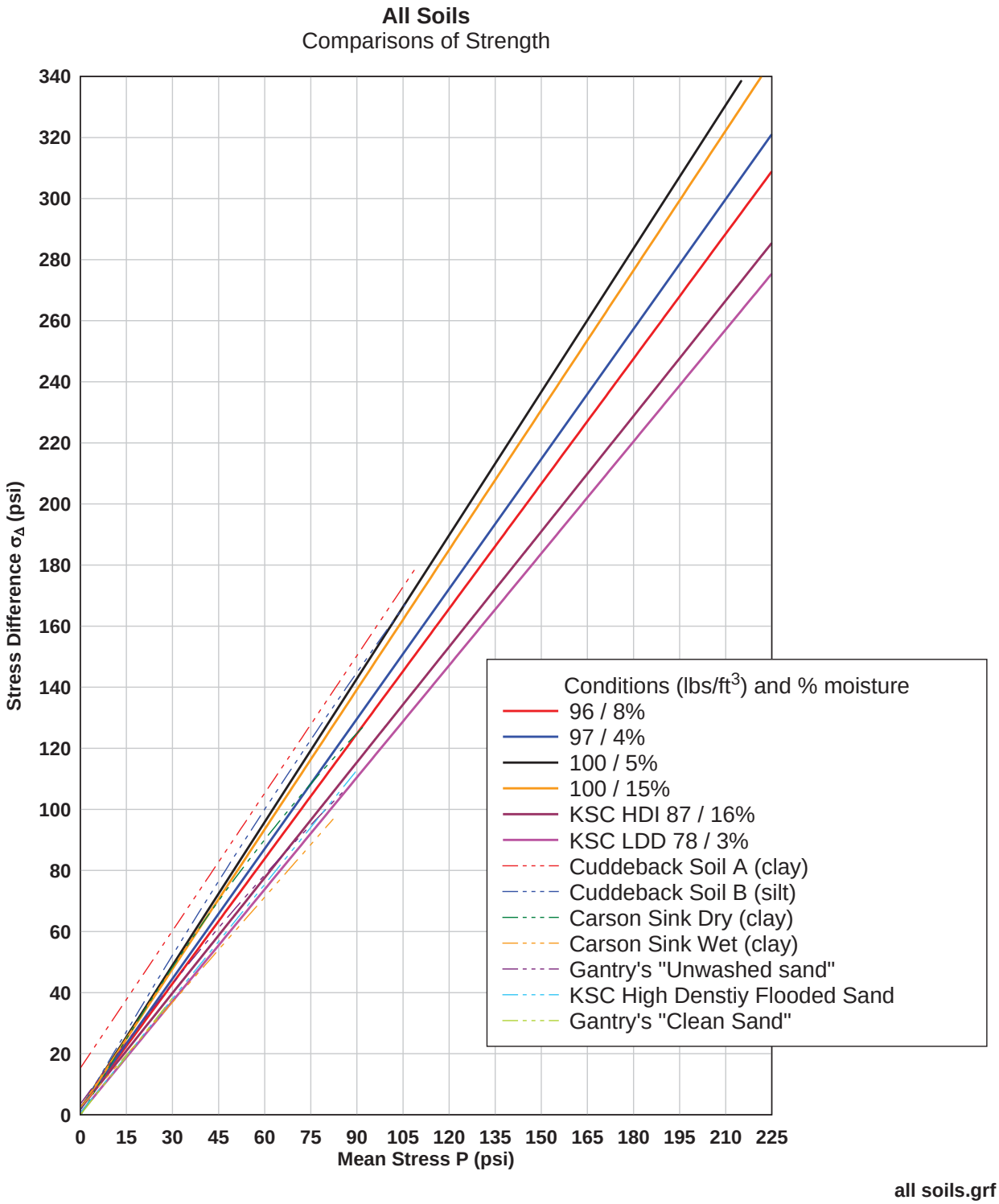

Figure 10-4: Strength comparison of all soils.

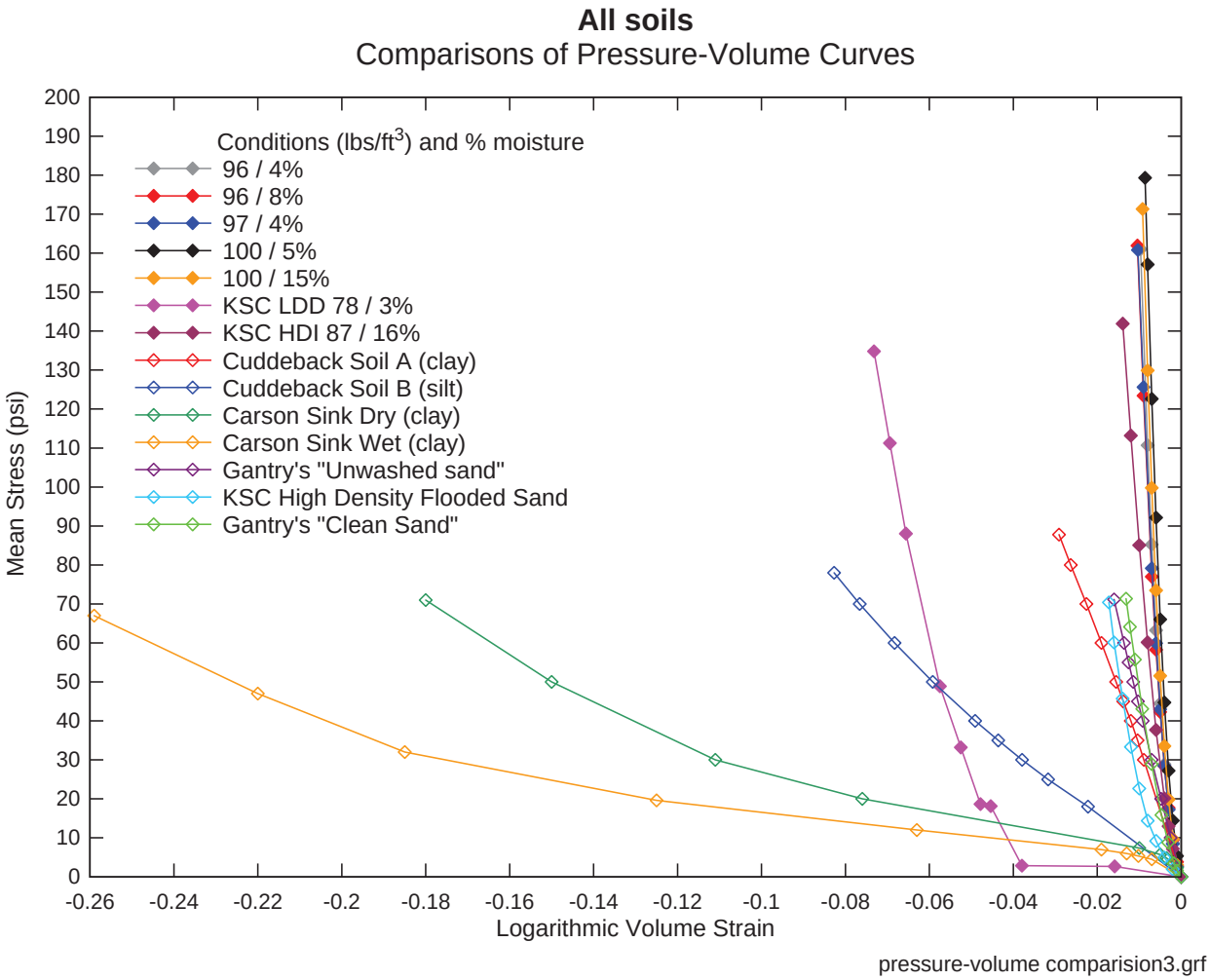

Figure 10-5: Compressibility comparison of all soils.

11 Closing Remarks

The tests on Mason Sand reveal a significantly stronger and stiffer material than the KSC sands. The differences in both strength and compressibility create a harsher impact material. From the new testing on KSC sands, there minimal changes to the KSC models. The varying amounts of strain in the KSC LDD model is sensitive to the low density testing. For Mason Sands, multiple uniaxial test excursions helped quantify compressibility sensitivity to density and moisture.

The soil models presented here are based on static strength and compressibility tests. No attempt was made at impact loading the soil, nor accounting for strain rate effects. All test specimens were reconstituted from field acquired samples. Mason Sand was purchased from a local construction vendor, Yorktown Materials, and shipped to ARA. ARA constructed the Mason Sand specimens to LaRC specifications.

LS-DYNA *Material Model 5: Soil and Foam* is a basic model well suited for preliminary design purposes. However, this is not the only soil model available. There have been many pressure-dependent material strength models developed for LS-DYNA, one of which is Material Model 25, the *Geological Cap* model. It is more complex than Material Model 5 because it uses kinematic hardening parameters. It uses two surfaces, an initial yield surface and a failure surface. The kinematic hardening parameters alter the behavior of the soil when moving from the initial yield to failure. This feature makes Material Model 25 a higher fidelity soil model because it accounts for more dynamic effects. The laboratory tests required to construct Material Model 25 are the same as Material Model 5. Using the test data presented here, it is possible to construct a *Geological Cap* model. It is also possible to construct other models with the hydrostatic compression unload/reload test data.

12 References

1. "LS-DYNA Theory Manual," 2006, Livermore Software Technology Corporation, Livermore, California.

2. ASTM D2850-03a(2007) Standard Test Method for Unconsolidated-Undrained Triaxial Compression Test on Cohesive Soils.

3. ASTM D6938-08 Standard Test Method for In-Place Density and Water Content of Soil and Soil-Aggregate by Nuclear Methods (Shallow Depth).

4. ASTM D6913-04e1 Standard Test Methods for Particle-Size Distribution (Gradation) of Soils Using Sieve Analysis.

5. ASTM D2216-05 Standard Test Methods for Laboratory Determination of Water (Moisture) Content of Soil and Rock by Mass.

6. ASTM D854-06 Standard Test Methods for Specific Gravity of Soil Solids by Water Pycnometer.

7. ASTM D6951-03 Standard Test Method for Use of the Dynamic Cone Penetrometer in Shallow Pavement Applications.

8. ASTM D4318-05 Standard Test Methods for Liquid Limit, Plastic Limit, and Plasticity Index of Soils (Atterberg Limits).

9. "Soil, Groundwater, Surface Water, and Sediments of Kennedy Space Center, Florida: Background Chemical and Physical Characteristics," 2000, Dynamac Corporation, NASA Environmental Program Office, KSC, FL.

10. "Constitutive Soil Properties for Cuddeback Lake, CA and Carson Sink, NV," 2008, Applied Research Associates, NASA Langley Research Center, Hampton, VA.

11. "Geology, Geohydrology And Soils Of Kennedy Space Center: A Review", 1990, Bionetics Corporation, Kennedy Space Center, FL.

12. Leonard Schwer, LS-DYNA Instructor at Livermore Software Technology Corporation. Class materials used in Figure 3-6.

Appendix A: LS-DYNA Theory Manual for Material Model 5

Appendix A is taken from the "LS-DYNA Theory Manual," 2006, Livermore Software Technology Corporation, Livermore, California. The excerpts shown below are from the Material Model 5 description starting on Page 19.21 of the LS-DYNA Theory Manual.

LS-DYNA is a registered trademark of the Livermore Software Technology Corporation.

The following boxed figures are copied from the LS-DYNA Theory Manual. The copied pages refer to the equations used in deriving constitutive parameters in Chapter 3.

Material Model 5: Soil and Crushable Foam

This model, due to Krieg [1972], provides a simple model for foam and soils whose material properties are not well characterized. We believe the other foam models in LS-DYNA are superior in their performance and are recommended over this model which simulates the crushing through the volumetric deformations. If the yield stress is too low, this foam model gives nearly fluid like behavior.

A pressure-dependent flow rule governs the deviatoric behavior:

$$\phi_s = \frac{1}{2} s_{ij} s_{ij} - \left(a_0 + a_1 p + a_2 p^2 \right) \qquad (19.5.1)$$

where a_0, a_1, and a_2 are user-defined constants. Volumetric yielding is determined by a tabulated curve of pressure versus volumetric strain. Elastic unloading from this curve is assumed to a tensile cutoff as illustrated in Figure 19.5.1.

Implementation of this model is straightforward. One history variable, the maximum volumetric strain in compression, is stored. If the new compressive volumetric strain exceeds the stored value, loading is indicated. When the yield condition is violated, the updated trial stresses, s_{ij}^*, are scaled back using a simple radial return algorithm:

$$s_{ij}^{n+1} = \left(\frac{a_0 + a_1 p + a_2 p^2}{\frac{1}{2} s_{ij} \, s_{ij}} \right)^{1/2} s_{ij}^* \qquad (19.5.2)$$

If the hydrostatic tension exceeds the cutoff value, the pressure is set to the cutoff value and the deviatoric stress tensor is zeroed.

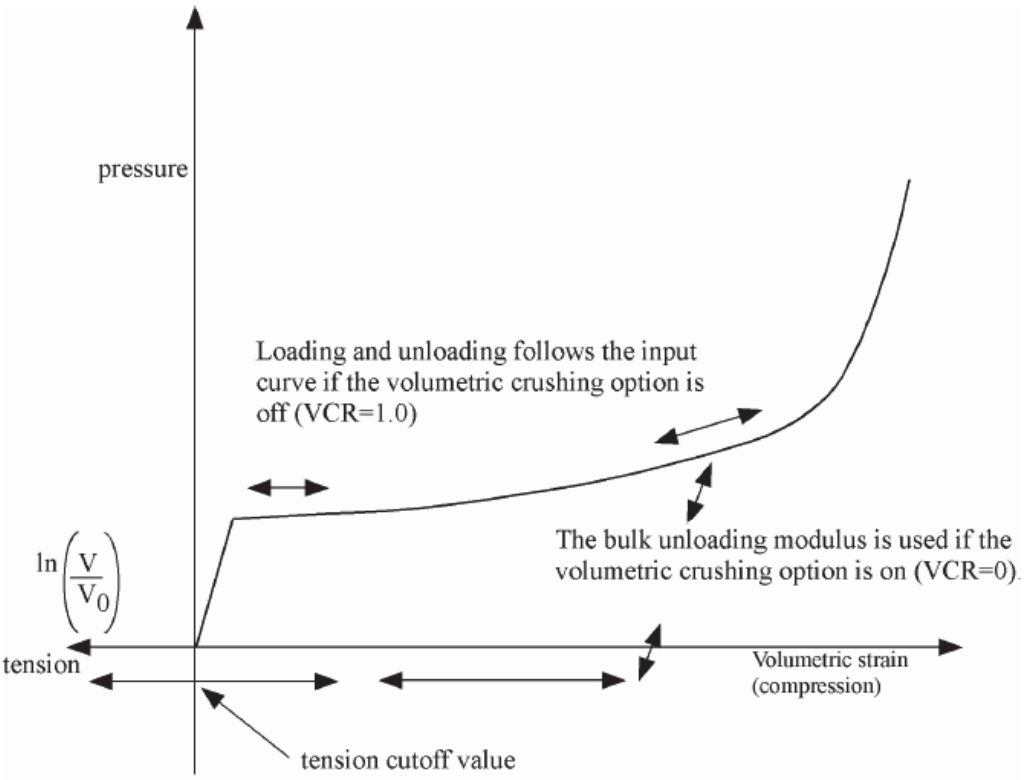

Figure 19.5.1. Volumetric strain versus pressure curve for soil and crushable foam model.

Krieg, R. D., "A Simple Constitutive Description for Cellular Concrete," Sandia National Laboratories, Albuquerque, NM, Rept. SC-DR-72-0883 (1972).

REPORT DOCUMENTATION PAGE

Form Approved
OMB No. 0704-0188

1. REPORT DATE *(DD-MM-YYYY)*	2. REPORT TYPE	3. DATES COVERED *(From - To)*
01- 12 - 2011	Contractor Report	

4. TITLE AND SUBTITLE

Constituitive Soil Properties for Mason Sand and Kennedy Space Center

5a. CONTRACT NUMBER

NNL07AA00B

5b. GRANT NUMBER

5c. PROGRAM ELEMENT NUMBER

6. AUTHOR(S)

Thomas, Michael A., Chitty, Daniel E.

5d. PROJECT NUMBER

5e. TASK NUMBER

5f. WORK UNIT NUMBER

747797.06.13.06.31.04.40

7. PERFORMING ORGANIZATION NAME(S) AND ADDRESS(ES)

NASA Langley Research Center
Hampton, Virginia 23681-2199

8. PERFORMING ORGANIZATION REPORT NUMBER

9. SPONSORING/MONITORING AGENCY NAME(S) AND ADDRESS(ES)

National Aeronautics and Space Administration
Washington, DC 20546-0001

10. SPONSOR/MONITOR'S ACRONYM(S)

NASA

11. SPONSOR/MONITOR'S REPORT NUMBER(S)

NASA/CR-2011-217323

12. DISTRIBUTION/AVAILABILITY STATEMENT

Unclassified - Unlimited
Subject Category 31
Availability: NASA CASI (443) 757-5802

13. SUPPLEMENTARY NOTES

This report was prepared by Applied Research Associates, Inc., under NASA contract NNL07AA00B with ATK Space Systems, Inc.
Langley Technical Monitor: Ralph D. Buerhle

14. ABSTRACT

Accurate soil models are required for numerical simulations of land landings for the Orion Crew Exploration Vehicle (CEV). This report provides constitutive material models for two soil conditions at Kennedy Space Center (KSC) and four conditions of Mason Sand. The Mason Sand is the test sand for LaRC's drop tests and swing tests of the Orion. The soil models are based on mechanical and compressive behavior observed during geotechnical laboratory testing of remolded soil samples. The test specimens were reconstituted to measured in situ density and moisture content. Tests included: triaxial compression, hydrostatic compression, and uniaxial strain. A fit to the triaxial test results defines the strength envelope. Hydrostatic and uniaxial tests define the compressibility. The constitutive properties are presented in the format of LSDYNA Material Model 5: Soil and Foam. However, the laboratory test data provided can be used to construct other material models. The soil models are intended to be specific to the soil conditions they were tested at. The two KSC models represent two conditions at KSC: low density dry sand and high density in-situ moisture sand. The Mason Sand model was tested at four conditions which encompass measured conditions at LaRC's drop test site.

15. SUBJECT TERMS

Crew Exploration Vehicle; Landing; Orion; Soil

16. SECURITY CLASSIFICATION OF:			17. LIMITATION OF ABSTRACT	18. NUMBER OF PAGES	19a. NAME OF RESPONSIBLE PERSON
a. REPORT	b. ABSTRACT	c. THIS PAGE			STI Help Desk (email: help@sti.nasa.gov)
					19b. TELEPHONE NUMBER *(Include area code)*
U	U	U	UU	128	(443) 757-5802